Studies on Hydrogelation Properties of Functional Pharmaceutical Polymers utilizing Infrared Spectroscopy and Quantum Chemical Calculations

A Thesis for the Degree

of

Doctor of Engineering

Submitted to

School of Science and Technology

Kwansei-Gakuin University by

Tomokazu Tajiri

in October 2011

Contents

List of Abbreviations

AAP: acetaminophen

ATR-IR: attenuated total reflection infrared

CAD: charged aerosol detector

DDS: drug delivery system

DFT: density functional theory

DGDE: diethyleneglycol diethyl ether

DTGS: deuterated tryglycine sulfate

EC: ethyl cellulose

EP: European Pharmacopoeia

FaSSIF : fasted state simulated intestinal fluid

FaSSGF : fasted state simulated gastric fluid

FeSSIF: fed state simulated intestinal fluid

FeSSGF: fed state simulated gastric fluid

FT-IR: fourier transform infrared

HF: Hartree-Fock

HPMC: hydroxypropyl methylcellulose

HPC: hydroxypropyl cellulose

HPLC: high performance liquid chromatography

IDM: indomethacin

IR: infrared

IVIVC: *in vitro/in vivo* correlation

JP: the Japanese Pharmacopoeia

MCT: mercury-cadmium-telluride

MD: molecular dynamics

MRI: magnetic resonance imaging

NMR: nuclear magnetic resonance

PA: propionic acid

PEG: polyethylene glycol

PEO: poly(ethylene oxide)

PMAA: poly(methacrylic acid)

POE: polyoxyethylene

PVP: polyvinylpyrolidone

QCC: quantum chemical calculation

SCF: self-consistent fields

SEC: size-exclusion chromatography

SEDDS: self-emulsifying drug delivery system

SLS: sodium lauryl salfate

USP: the United State Pharmacopeia

UV-VIS: ultraviolet-visible

XRD: X-ray diffraction

General Introduction

1. Scope of This Thesis

The purpose of this thesis is to explore the roles of functional pharmaceutical polymers through the studies on hydrogelation processes of hydrophilic pharmaceutical excipients at the molecular levels. In this thesis, poly(methacrylic acid) (PMAA, Figure 1a) as a enteric-coating agent and poly(ethylene oxide) (PEO, Figure 1b) as a hydrogel forming matrix base were used. The macromolecular structure changes during hydrogelation in PMAA and PEO were studied by using infrared (IR) spectroscopy, X-ray diffraction and quantum chemical calculations (QCCs). Further, a drug-release mechanism from a PEO hydrogel matrix tablet was revealed by using a flow-through cell dissolution apparatus equipped with magnetic resonance imaging (MRI).

In an effort to improve the quality of life among patients, researchers have developed a lot of drug delivery systems (DDS), to control the drug-release in oral administration using a variety of functional polymers such as PMAA and its derivatives for pH-responsive enteric coating agents,[1–3] and hydroxypropyl methylcellulose (HPMC) and PEO for hydrogel matrix controlled-release tablets and capsules.[4–11] pH-responsive polymers are widely used as an enteric coating agent not only for controlling drug-release, but also for protecting an unstable pharmaceutical ingredient like a protein from acidic conditions.[12–16] The pH of digestive juices are changed after a tablet or a capsule moves to the lower part of the gastro intestinal tract, at which time the enteric coating agent is dissolved and then the drug is released. On the other hand, a hydrophilic polymer matrix is a tablet or a capsule containing water-swellable, non-crosslinked hydrophilic polymers. After ingestion, surface polymer molecules

hydrate and swell to form a viscous hydrogel layer (Figure 3). This acts as a barrier controlling the drug-release from a tablet, and as a water introduction base to uptake water into a tablet immediately.[17]

The qualities and efficacies of a variety of DDS technologies have been usually evaluated by *in vivo* and/or *in vitro* studies. Though many dissolution tests described in each Pharmacopoeia are the commonly *in vitro* testings,[18–20] for more complex systems comprised of a number of functional polymeric excipients, thorough comprehension of the drug-release mechanism is difficult using drug-release profiles alone. In particular, hydrogel matrix tablets require a certain amount of time before the testing fluid reaches the tablet core, and subsequently they swell characteristically. Maggi et al.[21] reported that some PEO matrices take approximately eight hours to reach maximum swelling. Such previous findings have lent support to the belief that the kinetics of water ingress into tablets plays an important role in controlling drug-release from hydrogel matrices. Further, water molecules perform a crucial function in creating hydrated structures with PMAA and PEO via hydrogen bonding. However, the structure changes during hydrogelation in polymer chains such as PMAA and PEO in water have not been well investigated, although their dried and hydrated structures have been well-studied. In order to clarify the drug-releasing mechanisms of their controlled drug-release products, better understandings of the drug-release mechanisms from a PMAA coating film and PEO hydrogel matrices require investigations of these compounds' inherent physical properties and their hydrogelation phenomena.

Gel has been widely well-known as a substantially dilute network system, which exhibits no flow when in the steady-state,[22] and hydrogel conforms networks between

hydrophilic moieties in polymer chain and water molecules. Hydrogel, which has high water absorbability and biocompatibility, has been applied to a variety of fields such as chemical, pharmaceutical and medical industries as a functional polymer.

In this study, IR spectroscopy, which can directly provide structural information of PMAA and PEO about hydrogen bonding to each other and with water molecules, further MRI, which can supply information about water mobility in a tablet, have been utilized. The notable features of this study are described as follows: (1) Collecting a large number of IR spectra under the perturbation of water underlies the elucidation of continuous structural changes in the hydrated structures and the hydrogelling behaviors of PMAA and PEO in their hydrogelling process. (2) In order to unravel the complicated spectral variation in the IR region, second derivative processing as well as fourth derivative processing, which is widely applied to improve peak resolution and prevent intensity changes from affecting adjacent large peaks in an ultraviolet-visible study,[23,24] have been utilized. (3) Obtained spectra-structure correlations were examined by conducting QCCs based on the density functional theory (DFT) using short chain models of PMAA and PEO. (4) In order to comprehensively examine the unique drug-release mechanism from a PEO/PEG hydrogel matrix tablets. This study used the combination of the compendial flow-through cell equipped with an MRI device to simultaneously evaluate the cumulative drug-release profiles and internal states of tablets over time in a non-invasive and non-destructive manner.[25–32] (5) The effect of polymeric erosion from a tablet was assessed using size-exclusion chromatography (SEC), which was the most common way to obtain information about the molecular mass distribution of polymers.[25,33,34] In this study, these powerful

experimental and computation methods have made it possible to reveal important findings about the hydrated structures changes of PMAA and PEO, and the conformational changes of PEO during their hydrogelling processes.

2. Characteristic of Poly(methacrylic acid) and Poly(ethylene oxide)

PMAA (Figure 1a) is a water soluble hydrophilic polymer, which has a carboxylic acid group including the acid dissociation constant; pKa of 5-6.[35–37] It and its derivatives are applied in several fields such as chemical, food and pharmaceutical industries. Its sodium salt is widely used in disposable diapers as a high groscopical substance, and its methyl ester, poly methyl methacrylate, is manufactured into plastic. Furthermore, PMAA and its copolymers like poly (methacrylic acid–*co*-ethyl acrylate) (1:1 mol %) and poly (methacrylic acid–*co*-methyl methacrylate) (1:1 and 1:2 mol %), are widely used for pharmaceutical excipients as pH-responsive enteric coating agents, which are a kind of stimulus-responsive DDS,[38,39] to control the drug-releasing and/or to protect pharmaceutical ingredients like proteins from an acid digestive juice.

The carboxylic acid group in PMAA, which has a dissociating proton, plays an important role to dissolving in aqueous solutions. In general, carboxylic acids normally exist in cyclic dimers with strong hydrogen bonds among their carbonyl and hydroxyl groups in their carboxyl groups. Those hydrogen bondings and the interaction between carboxylic acid monomer and water are well reported, especially formic acid, acetic acid and propionic acid (PA) using various equipment; such as Raman,[40–44] IR spectroscopy,[41,45,46] X-ray diffraction,[47] nuclear magnetic resonance (NMR)[48] and QCCs.[49–56] Dong et al., have reported that carboxylic acid groups in PMAA form

several associated conformations via hydrogen bonding as cyclic dimers, side-on dimers and linear open chain oligomers including open dimers,[57,58] and it is well-known that cyclic dimers dominate in the pure liquid or solid states of carboxylic acids.[40–47,59] Hydrated structures of carboxylic acid group have also been studied by using various techniques and QCCs.[55,56,60,61] There has been great attention to the polymeric structures and their changes of hydrogen bonding to each other and with water molecules, however, many of the previous studies on carboxylic acid groups in polymers have dealt almost exclusively with the structures in solid forms and those in aqueous solutions, separately.

PEO (Figure 1b) is a polyether type of water soluble synthetic polymers, in other words, polyoxyethylene (POE) which has the unit of ethylene oxide; $-CH_2-CH_2-O-$. Low molecular weight POE with hydroxyl terminated (i.e. less than 10,000 daltons) is referred to as polyethylene glycol (PEG), while those with higher molecular weights are known as PEO.[62]

PEO is one of the most important polymers in industrial, biotechnical and biomedical fields,[63] and has been also widely used as a biocompatible polymer, because surface modification with hydrophilic polymers such as PEO has been beneficial in improving blood compatibilities.[64] Surface-bound PEO is expected to prevent plasma protein adsorption, platelet adhesion, and bacterial adhesion by steric repulsion. Polymeric materials have several advantages which make them very attractive as biomaterials.[65] Furthermore, PEO, which is highly soluble in water and has high gelability and low toxicity, has been applied in extended drug-release systems, and the *in vivo* and *in vitro* drug-release behaviors from PEO hydrogel matrices have been reported.[8–11]

A large number of experimental studies based on X-ray diffraction,[66,67] IR,[68–71] Raman,[72,73] and nuclear magnetic resonance (NMR) spectroscopies,[74,75] as well as studies involving numerical computations such as QCCs [76,77] and molecular dynamics (MD) [78] have been conducted on PEO, POE and PEG in crystalline or random-coil phases. Several studies have noted a preference for a gauche conformation in the C–C bond of POE in not only the crystalline phase but also in solutions.[66–75] While a trans conformation in the C–O bond has been found to be dominant in dried PEO with a 7/2 helical structure in the crystalline phase (Figure 2),[66] both gauche and trans conformations in the C–O bond have been known to exist in aqueous solutions.[68,69]

Many research groups have investigated the hydrogen bonding interactions between POE and water molecules by experimental[66–70] and computational approaches[76–78] such as a monodentate hydration structure, with only one OH group in a water molecule donating a hydrogen bond to the POE chain, and bidentate ones, with the two OH groups in a water molecule donating two different hydrogen bonds to the first and the second available oxygen atoms from another hydrogen bonding in POE. Wahab et al. [76] have theoretically examined the above-mentioned hydration structures of short chain POE ($CH_3(OCH_2CH_2)_mOCH_3$, m=1 and 2), and demonstrated the bidentate hydration structure where the second available oxygen atoms from another hydrogen bonding in POE is more stable than that where the adjacent ones in the gas phase by QCC. While extensive research has been conducted on the most favorable conformations of POE in the crystalline phase and aqueous solutions, little attention has been focused on the conformational changes of the polymer chain during hydrogelation from a dried state in the crystalline phase to a hydrated state in a swollen gel.

3. Infrared Spectroscopy of Poly(methacrylic acid) and Poly(ethylene oxide)

In order to investigate the molecular interactions among polymer chains, and between polymers and water, vibrational spectroscopy is best suited, as the vibrational bands are assigned to the molecular functional groups with a specific vibrational mode, and the band shape and position are very sensitive to the molecular environment. Furthermore, it allows the simultaneous evaluation of both the structures of the hydrogen-bonded polymer in a solid state and those of the hydrated ones in a gel and a liquid under the same conditions with detection time-resolved structural changes.

PMAA, as mentioned above, has a carboxylic acid group as a characteristic functional group, which forms several associated conformations via hydrogen-bonds. In the 1750-1680 cm^{-1} region, C=O stretching bands of carboxylic acid are detected as the most intensive bands. And the band makes it possible to understand the state of carboxylic acid, whose monomer (non-hydrogen bonded), side-on and cyclic dimeric hydrogen bonded, and linear oligomeric hydrogen bonded exists in that order from a higher wavenumber. In the aqueous solution, the states of carboxylic acid of PMAA are also confirmed by using IR, because when the carboxylic acid groups of PMAA are dissociated, an asymmetric stretching COO^- band is found at around 1550 cm^{-1}.[58]

For PEO, PEG and POE, many fundamental studies have been done using vibrational spectroscopy. Since PEG is a semi-crystalline polymer, its crystal structure has been determined using X-ray diffraction,[66] and additionally, its double helical structure can be seen by scanning electron microscopy.[79] For the semi-crystalline state, infrared and Raman spectroscopies have been used to assign vibrational bands of PEG based on the

symmetry group and normal mode analysis with the help of the derived crystal structure.[72,80] For the solution state, extensive studies using transmission IR spectroscopy have shown that amorphous PEG chains, particularly in water, form some kind of ordered conformation rather than being a random coil.[69,76] The studies on water vapor diffusion into PEG were done by Kitano et al. by using 10-bounce ATR-IR.[69,81] They investigated the water band in PEG, and the diffusion behavior of water vapor. However, they did not discuss the vibrational bands of polymers at all, and based on my observations, it is likely that the polymer does not absorb enough water to totally destroy its crystal structure.

In order to explore time-resolved conformational variations of the PEO chain during the hydrogelling process by using in situ IR transmission spectroscopy. ATR–IR spectroscopy has been widely applied to investigations of the hydration structure of various polymers.[82,83] However, quantitative analysis at the same depth position is difficult in ATR–IR spectroscopy, as the penetration depth of an incident IR beam in a polymer sample depends on the IR vibrational frequency.[84] Here, to avoid this problem, IR transmission spectroscopy was used to examine PEO hydrogelation, as was done in previous investigations involving POE.[70,71]

4. Quantum Chemical Calculations of Poly(methacrylic acid) and Poly(ethylene oxide)

QCCs consist of calculating the normal vibration frequencies of a molecule from information on its structure and internal force field. From such a calculation, I obtained the values of the frequencies and the forms of the vibrations of the molecule which can be observed in IR abdorption and in Raman scattering. By comparing such calculated

frequencies with the observed spectrum, it is possible to evaluate my assumptions concerning the structure and force field of the molecule.

Several QCCs are also applied and reported in studying polymer analysis, semi-empirical (e.g., AM1, PM3, MNDO),[49] *ab initio* (e.g., Hartree-Fock, MP2, CC),[49–52] density functional theory (DFT) (e.g., BLYP, B3LYP, PW91)[53–56] and matrix isolation methods.[61] These sources said that most molecules of carboxylic acids were better-known to exist as cyclic dimer structures, and the longer acryl chain length, the larger the ratio of cyclic dimers.[60] But there are few reports about the hydrating structure changes of carboxyl groups of solid polymers during hydrogellation process. In this study, thus, the hydration process for carboxyl groups of a PMAA film was observed by using FT-IR, and PA was used for DFT calculations as an easy monomeric model of PMAA to predict the solid and the hydrated structures of carboxyl groups. This is particularly useful for a better interpretation of the observed IR spectra. Obtained spectra-structure correlations were examined by conducting QCCs based on DFT using a short chain model of diethyleneglycol diethyl ether (DGDE) instead of a real polymer of PEO.

5. Flow-through Cell *In Vitro* Drug-release Testing Apparatus

All oral pharmaceutical products have been controlled and assured their efficacy and safety by quality control testings. The *in vitro* drug-release characteristics are evaluated by using a dissolution apparatus; such as a basket, paddle and flow-through cell described in the United State Pharmacopeia (USP), European Pharmacopoeia (EP) and the Japanese Pharmacopoeia (JP) (Figure 4a and b). The three dissolution

apparatuses are harmonized with the corresponding texts of the three pharmacopoeia. Basket (USP apparatus 1) and paddle (USP apparatus 2) apparatuses are the same assembly which consist of a 1L glass vessel, a motor, a metallic drive shaft and cylindrical basket or paddle (Figure 4a). The water bath permits holding the temperature inside the vessel at 37 ± 0.5 °C during the test. On the other hand, a flow-through cell (USP apparatus 4) consists of a reservoir and a pump for the dissolution medium, and a flow-through cell and water bath that maintains the medium at 37 ± 0.5 °C in the flow-through cell (Figure 4b).

In general, a basket and a paddle apparatus has been widely applied to *in vitro* drug-releasing tests because of the strict guidelines for immediate release products, which say that "Apparatus 1 and Apparatus 2 should be used unless shown to be unsatisfactory. The *in vitro* dissolution procedures, such as a reciprocating cylinder (USP apparatus 3) and a flow-through cell system (USP apparatus 4) described in the USP, may be considered if needed".[85] Recently, however, the number of poorly water-soluble pharmaceutical compounds has increased, and they should also be evaluated for *in vitro* release behaviors by using a compendial dissolution apparatus. In an *in vitro* drug-releasing study of a pharmaceutical product containing a poorly-water soluble drug, an appropriate dissolution method should be used under sink conditions to evaluate the drug-releasing property precisely. There is still a lot of discussion about sink conditions, where the drug solubility is ten times the total concentration of the drug in the vessel, or at least greater than three to five times,[86–88] though, in general, the sink condition is defined as three times the drug concentration based on the solubility in USP (2011).[18] However, in a dissolution method for a poorly

water-soluble drug using a basket and paddle apparatus (USP apparatus 1 and 2) whose medium volumetric-constraint is 1 L in capacity, it is sometimes difficult to develop the dissolution method under sink conditions due to poor drug solubility.

A flow-through cell apparatus (Figure 4b) allows using an unbounded medium volume. Therefore it has a huge advantage to maintain sink conditions continuously, thus making it possible to select a type of a dissolution medium more flexibly. Hence, it has attracted attention as one of the compendial methods not only from the above-mentioned sink conditions point of view, but also from IVIVC point of view.[91,92] Further, flow-through cell dissolution has a variety of testing options to meet their *in vivo* drug-release characteristics and/or excellent discrimination capability; such as a volumetric medium flow rate, a medium flow speed in a flow-cell using a large or a small cell, single or multi dissolution media, with or without 120 pulse/min. sinusoidal pulsation, and laminar or turbulent hydrodynamic flow[93,94] and open or closed-loop configurations (Figure 4b). As mentioned above, the open-loop configuration is able to consistently supply a fresh medium which helps to maintain sink conditions, while a large medium volume might be required when a long-term dissolution test is performed with high volumetric medium flow rate. On the other hand, closed-loop configuration can apply an arbitrary and an appropriate medium volume due to drug solubility, but a medium containing a cumulated releasing-drug is used in subsequent dissolution tests as the same as the basket or paddle method.

6. Magnetic Resonance Imaging of Hydrogel Matrix Tablets

MRI is a non-invasive technique which can provide cross-sectional images from inside solid materials and living organisms. In a pharmaceutical field, MRI has been used to study internal mechanisms underlying *in vitro* drug-release behaviour in dosage forms,[95–97] to monitor events within pharmaceutical processes, and *in vivo* to investigate the behaviour of drug delivery systems in the body.[98] Hydration underpins the performance of many solid pharmaceutical dosage forms, and most studies have utilised MRI to observe and measure the internal events unfolding as a consequence of solvent penetration. Most reports are *in vitro* investigations of oral modified release devices, particularly hydrophilic matrix systems. As an example, a PEO hydrogel matrix tablet and the MRI picture are shown in Figure 5, and MRI image provides us additional internal information of a tablet like a gelling front. When examined in detail, these are complex dynamic systems that are difficult to model, however, in simple terms, water-soluble drugs appear to undergo a diffusion-controlled release through the gel layer, whereas insoluble drugs are released from the perimeter of the gel by surface erosion during gastro-intestinal transit.[99] Factors that influence either the formation or integrity of the gel such as rates of water transport, polymer swelling, drug dissolution, and matrix erosion, can critically influence the performance of these dosage forms.[17] MRI can be used non-invasively to measure water penetration, concentration, diffusion, and polymer swelling and is therefore particularly suited to probing the gel layer properties that influence the functionality of hydrophilic matrices.

A number of researchers have sought to characterise the formation of the gel layer and determine how its properties might influence drug-release. Rajabi-Siahboomi and

Madhu used MRI to reveal the mobility of water within the gel layer,[100,101] and to determine the spatial distribution of self-diffusion coefficient and T_2 relaxation values for water, drug, and polymer.[101] Rajabi-Siahboomi et al. showed how there was a self-diffusion coefficient gradient with values increasing progressively with the distance from the core, reaching a maximum in the outer parts of the gel layer where water mobility was comparable to free water.[100] Hyde and Gladden have quantified the concentration profile of water and polymer in hydrating PEO discs using one-dimensional NMR imaging.[102] They exploited differences in the T_1 relaxation time of water and polymers, to quantify and spatially resolve the distribution of polymers and water across the hydrating gel layer. They concluded that both water penetration and polymer swelling exhibited the characteristics of diffusion-controlled processes. Kojima et al.[28,103] have studied the influence of cellulose ether type on the mobility and diffusivity of water in the gel layer. One-dimensional maps of T_2 and water self-diffusion coefficient were acquired and used to determine the position of the dry core, gel layer, and aqueous phase. They also observed a pronounced expansion of the tablet core in an axial direction, and showed how the incorporation of drugs resulted in the increased penetration of water and growth of the gel layer in all matrix types. Further, when MRI is combined with a flow-through cell apparatus for use in compendial analysis,[18–20] the physical changes in solid dosage forms can be examined in a dissolution test.[27,104–106] Indeed, Fyfe et al.[27] used such a combined system to assess drug delivery devices and thereby obtained a better understanding of drug delivery systems based on diffusion, dissolution, and osmosis mechanisms. Further, Dorożyński et al.[104] and Kulinowski et al.[105] carried out the compendial flow-through

cell dissolution method for a HPMC matrix using two different solutions; the fasted state simulating gastric fluid (FaSSGF) and the fed state simulating gastric fluid (FeSSGF), under the continuous flow conditions to simulate *in vivo* conditions as closely as possible. However, the integrated investigation of the drug-release mechanism from PEO hydrogel matrix tablets among the cumulative drug-release profiles and the contribution of hydrogel matrix erosion and the conformation changes of the hydrogel under the compendial flow-through cell dissolution method have not been reported.

7. Introduction of Each Chapter

This thesis is organized into four chapters. Chapter 1 described a structure change during the hydration process of a PMAA film, and it was observed by using time-resolved *in situ* ATR-IR spectroscopy. This study has provided new insight into the hydration mechanism of carboxyl groups in the PMAA film. The intra- and inter-side-chain hydrogen-bonds in the PMAA are dissociated and the film is swelled by infiltrating water, subsequently their generated non-hydrogen-bond carboxyl groups instantly hydrate with water molecules and equilibrate to the side-on form which is the most stable structure for the carboxyl groups. The calculated frequencies and the interaction energies by QCCs using a model monomer of PA instead of PMAA have supported my spectral assignment and the structural simulation of the hydrogen-bonded and the hydrated structures of PMAA. It has been concluded from this chapter that the dissociation of hydrogen-bonded and newly created hydrated structures via the carboxyl groups are evident.

In chapter 2, a drastic conformation change in a PEO chain during the hydrogelation process was investigated by IR spectroscopy and QCCs. Time-resolved *in situ* IR spectra of the hydrogelling process of a semi-crystalline PEO solid were measured using a flow-cell. The time-resolved IR study has revealed that C–C bonds with hydrophobic moieties rapidly shift to a random-coil gauche conformation after water penetration, whereas C–O bonds with hydrophilic moieties hydrogel more slowly, with at least half of these bonds changing from trans to gauche conformations after hydration. In addition, two main steps in hydration during PEO hydrogelation were identified: First, the ether oxygen atoms in PEO become hydrated as mono-hydrated structures were created with water molecules following rapid water penetration. Then, they were converted to the bridged hydration form as the most stable structure. The calculated wavenumbers and interaction energies obtained by QCC using a model oligomer of diethyleneglycol diethyl ether (DGDE) instead of an actual PEO chain supported my estimation of the spectra-structure correlation of the hydrated PEO. The C–C gauche structure is important in maintaining a bridged hydrogen bonding network with water molecules. It has been concluded that the hydrogelling behaviors of PEO including the conformation change in the polymer chain and the hydrated structures.

In chapter 3, in order to accurately evaluate the drug-releasing property of a oral pharmaceutical product, the critical factors of a drug-releasing test method by using a flow-through cell apparatus were revealed. In this study, an extended drug-release matrix consisted a solid dispersion of hydrophoic ethylcellulose (EC) and HPMC and contained a poorly water-soluble indomethacin (IDM) was used as a model formulation. The flow-through cell apparatus demonstrated the ability of maintaining

perfect sink conditions, which are defined as the necessary and sufficient condition for the drug-dissolving and the releasing in terms of drug solubility for an extended release matrix formulation containing a poorly water-soluble drug during the *in vitro* dissolution study. This study has discussed an appropriate drug-release test method based on the mechanism.

In chapter 4, a drug-release mechanism from extended-release tablets of hydrogel polymer matrices containing PEO and PEG were achieved using an above-discussed flow-through cell apparatus equipped with MRI. In the light of the critical factors on the flow-through cell apparatus in chapter 3, acetaminophen (AAP) as a water-soluble drug was used to avoid the oversaturation in a flow-cell. The hydrogel forming abilities were observed characteristically and the layer thickness which was corresponding to the diffusion length of a drug had a good correlation with the drug-release profiles. In addition, the polymeric erosion contribution to a drug-releasing from hydrogel matrix tablets was directly quantified using SEC. The matrix erosion profile indicated that the PEG erosion kinetic depends primarily on the composition ratio of PEG to PEO. It has been concluded from this chapter that the drug-release mechanism form PEO/PEG hydrogel matrices due to the drug self-diffusion and matrix erosion was identified.

8. References

1 Tahami, K. A.; Singh, J. *Recent Patents on Drug Deliv & Formul* 2007, 1, 65–71.

2 Lin, S. Y.; Yu, H. L. *J. Polym. Sci. Part A Polym. Chem.* 1999, 37, 2061–2067.

3 Victor, S. P.; Sharma, C. P. *J. Biomaterials Applications* 2002, 17, 125–134.

4 Lin, C. C.; Metters, A. T. *Adv. Drug Deliv. Rev.* 2006, 58, 1379–1408.

5 Ford, J. L.; Rubinstein, M. H.; McCaul, F.; Hogan, J. E.; Edgar, P. J. *Int. J. Pharm.* 1987, 40, 223–234.

6 Rao, K. V. R.; Devi, K. P.; Buri, P. *J. Control. Release* 1990, 12, 133–141.

7 Salomen, J. L.; Doelker, E.; Buri, P. *Pharm. Ind.* 1979, 41, 799–802.

8 Graham, N. B.; McNeill, M. E. *Biomaterials* 1984, 5, 27–36.

9 Kim, C. J. *J. Pharm. Sci.*, 1995, 84, 303–306.

10 Sako, K.; Nakashima, H.; Sawada, T.; Fukui, M. *Pharm. Res.* 1996, 13, 594–598.

11 Kojima, H.; Yoshihara, K.; Sawada, T.; Kondo, H.; Sako, K. *Eur. J. Pharm. Biopharm.* 2008, 70, 556–562.

12 Liu, F.; Lizio, R.; Meier, C.; Petereit, H. U.; Blakey, P.; Basit, A. W. *J. Control. Release* 2009, 133, 119–124.

13 Liu, F.; Basit, A. W. *J. Control. Release* 2010, 147, 242–245.

14 Felton, L. A.; Haase, M. M.; Shah, N. H.; Zhang, G.; Infeld, M. H.; Malick, A. W.; McGinity, J.W. *Int. J. Pharm.* 1995, 113, 17–24.

15 Breitkreutz, J. *J. Control. Release* 2000, 67, 79–88.

16 Liu, F.; Merchant, H. A.; Kulkarni, R. P.; Alkademi, M.; Basit, A. W. *Eur. J. Pharm. Biopharm.* 2011, 78, 151–157.

17 Colombo, P.; Bettini, R.; Santi, P.; Peppas, N. A. *Pharm. Sci. Technol. Today*

2000, 3, 198–204.

18 *The United States Pharmacopeia 34-National Formulary 29*, The United States Pharmacopeial Convention, 2011, 278–285.

19 *European Pharmacopoeia, seventh ed.*, European Directorate for the Quality of Medicines, 2011, 266–275.

20 *The Japanese Pharmacopoeia 16th ed.*, Society of Japanese Pharmacopoeia, 2011, 116–120.

21 Maggi, L.; Bruni, R.; Conte, U. *Int. J. Pharm.* 2000, 195, 229–238.

22 Ferry, J. D. Viscoelastic Properties of Polymers. New York: Wiley, 1980.

23 Fell, A. F.; Jarvie, D. R.; Stewart, M. J. *Clin. Chem.* 1981, 2712, 286–292.

24 Lange, R.; Bec, N.; Mozhaev, V. V.; Frank, *J. Eur. Biophys. J.* 1996, 24, 284–292.

25 Abrahmsén-Alami, S.; Körner, A.; Nilsson, I.; Larsson, A. *Int. J. Pharm.* 2007, 342, 105–114.

26 Baumgartner, S.; Lahajnarb, G.; Sepeb, A.; Kristala, J. *Eur. J of Pharm. and Biopharm.* 2005, 59, 299–306.

27 Fyfe, C. A.; Grondey, H.; Blazek-Welsh, A. I.; Chopra, S. K.; Fahie, B. J. *J. Control. Release* 2000, 68, 73–83.

28 Kojima, M.; Nakagami, H. *Chem. Pharma. Bull.* 2002, 50, 1621–1624.

29 Malaterre, V.; Metz, H.; Ogorka, J.; Gurny, R.; Loggia, N.; Mäder, K. *J. Control. Release* 2009, 133, 31–36.

30 Metz, H.; Mäder, K. *Int. J. Pharm.* 2008, 364, 170–175.

31 Richardson, J. C.; Bowtell, R. W.; Mäder, K., Melia, C. D. *Adv. Drug Deliv. Rev.* 2005, 57, 1191–1209.

32 Strübing, S.; Metz, H.; Mäder K. *J. Control. Release* 2008, 126, 149–155.

33 Kuga, S. *J. Chromatgr.* 1981, 206, 449–461.

34 Laguna, M. T. R.; Medrano, R.; Plana, M. P.; Tarazona, M. P. *J. Chromatogr. A* 2001, 919, 13–19.

35 Nagasawa, M.; Murase, T.; Kondo, K. J. Phys. Chem. 1965, 69, 4005–4012.

36 Kim, B.; Y. Shin, Y.; J. Appl. Polym,. Sci., 2007, 105, 3656–3661.

37 Chao, G. T.; Deng, H. X.; Huang, Q.; Jia, W. J.; Huang, W. X.; Gu., Y. C.; Tan, H. P.; Fan, L. Y.; Liu, C. B.; Huang, A. L.; Lei, K.; Gong, C. Y.; Tu, M. J.; Qian, Z. Y. J. Polym. Res., 2006, 13, 349–355.

38 Gupta, P.; Vermani, K.; Garg, S., *Drug discovery today* 2002, 7, 569–579.

39 Qui, Y.; Park K., *Advanced drug delivery reviews*, 2001, 53, 321–339.

40 Semmler, J.; Irish, D. E. *J. Solution Chem.* 1988, 17, 805–823.

41 Genin, F.; Quiles, F.; Burneau, A. *Phys. Chem. Chem. Phys.* 2001, 3, 932-942.

42 Tanaka, N.; Kitano, H.; Ise, N. *J. Phys. Chem.* 1990, 94, 6290–6292.

43 Nishi, N.; Nakabayashi, T.; Kosugi, K. *J. Phys. Chem. A* 1999, 103, 10851–10858.

44 Nakabayashi, T.; Nishi, N. *J. Phys. Chem. A* 2002, 106, 3491–3500.

45 Flakus, H. T.; Stachowska, B. *Chem. Phys.* 2006, 330, 231–244.

46 Flakus, H. T.; Tyl, A. *Chem. Phys.* 2007, 336, 36–50.

47 Takahashi, O.; Yamanouchi, S.; Yamamoto, K.; Tabayashi, K. *Chem. Phys. Lett.* 2006, 419, 501–505.

48 Asano, A.; Eguchi, M.; Kurotu, T. *J. Polym. sci. Part B* 1999, 37, 2007–2012.

49 Turi, L.; Dannenberg, J. J. *J. Phys. Chem.* 1933, 97, 12197–12204.

50 Brurneau, A.; Genin, F.; Quiles, F. *Phys. Chem. Chem. Phys.* 2000, 2, 5020–5029.

51 Lourderaj, U.; Giri, K.; Sathyamurthy, N. *J. Phys. Chem. A* 2006, 110, 2709–2717.

52 Nakabayashi, T.; Kosugi, K.; Nishi, N. *J. Phys. Chem. A* 1999, 103, 8595–8603.

53 Zhang, R. Q.; Wong, N. B.; Lee, S. T.; Zhu, R. S.; Han, K. L. *Chem. Phys. lett.* 2000, 319, 213–219.

54 Lewandosli, H.; Koglin, E.; Meier, R. J. *Vib. Spectrosc.* 2005, 39, 15–22.

55 Zhou, Z.; Shi, Y.; Zhou, X. *J. Phys. Chem. A* 2004, 108, 813–822.

56 Chuchev, K.; BelBruno, J. J. *J. Mol. Struc.* 2006, 736, 199–204.

57 Dong, J.; Ozaki, Y.; Nakashima, K. *Macromolecules* 1997, 30, 1111–1117.

58 Dong, J.; Tsubara, N.; Fujimoto, Y.; Ozaki, Y.; Nakashima, K. *Appl. Spectrosc.* 2001, 55, 1603–1609.

59 Pettersson, A.; Marino, G.; Pursiheimo, A.; Rosenholm, J. B. *J. Colloid Interface Sci.* 2000, 228, 73–81.

60 Tanaka, N.; Kitano, H.; Ise, N. *J. Phys. Chem.* 1991, 95, 1503–1507.

61 George, L.; Sander, W. *Spectrochim. Acta Part A* 2004, 60, 3225-3232.

62 Bailey, F. E.; Koleske, J. V. Poly(ethylene oxide), *Academic press*, New York, 1976.

63 *Poly(ethylene glycol) Chemistry: Biotechnical and Biomedical Applications*; Harris, J. M., Ed.; Plenum: New York, 1992.

64 Amiji, M.; Park, K. In polymers of Biological and Biomedical Significance, *American Chemical Society*, 1993, Chapter 11, 135–146.

65 Goldberg, E. P.; Nakajima, A. Biomaterial Polymers, Polymeric Materials and

Pharmaceuticals for Biomedical Use. *Academic Press*, New York, 1980.

66 Takahashi, Y.; Tadokoro, H. *Macromolecules*, 1973, 6, 672–675.

67 Brubach, J. B.; Ollivon, M.; Jannin, V.; Mahler, B.; Bourgaux, C.; Lesieur, P.; Roy, P. *J. Phys. Chem. B* 2004, 108, 17721–17729.

68 Shephard, J. J.; Bremer, P. J.; McQuillan, A. J. *J. Phys. Chem. B* 2009, 113, 14229–14238.

69 Begum, R.; Matsuura, H. *J. Chem. Soc., Faraday Trans.* 1997, 93, 3839–3848.

70 Kitano, H.; Ichikawa, K.; Ide, M.; Fukuda, M.; Mizuno, W. *Langmuir* 2001, 17, 1889–1895.

71 Kusanagi, H.; Yukawa, S. *Polymer* 1994, 35, 5637–5640.

72 Yoshihara, T.; Tadokoro, H.; Murahashi, S. *J. Chem. Phys.* 1964, 41, 2902–2911.

73 Maxfield, J; Shepherd, I. W. *Polymer* 1975, 16, 505–509.

74 Inomata, K.; Abe, A. *J.Phys.Chem.* 1992, 96, 7934–7937.

75 Björling, M.; Karlström, G.; Linse, P. *J.Phys.Chem.* 1991, 95, 6706–6709.

76 Wahab, S. A.; Harada, T.; Matsubara, T.; Aida, M. *J. Phys. Chem. A* 2006, 110, 1052–1059.

77 Aray, Y.; Marquez, M.; Rodriguez, J.; Vega, D.; Simón-Manso, Y.; Coll, S.; Gonzalez, C.; Weitz, D. A. *J. Phys. Chem. B* 2004, 108, 2418–2424.

78 Tasaki, K. *J. Am. Chem. Soc.* 1996, 118, 8459–8469.

79 Yang, R.; Yang. X. R.; Evans, D. F.; Hendrickson, W. A.; Baker, J. *J. Phys. Chem.* 1990, 94, 6123–6125.

80 Shimomura, M.; Tanabe, Y.; Watanabe, Y.; Kobayashi, Y. *Polymer* 1990, 31, 1411–1414.

81 Ichikawa, K.; Mori, T.; Kitano, H.; Fukuda, M.; Mochizuki, A.; Tanaka, M. *J. Polym. Sci, B* 2001, 39, 2175–2182.

82 Hajatdoost, S.; Yarwood J. *J. Chem. Soc. Faraday Trans.* 1997, 93, 1613–1620.

83 Morita, S.; Tanaka, M.; Ozaki, Y. *Langmuir* 2007, 23, 3750–3761.

84 Chalmers, J. M.; Griffths, P. R. *Handbook of Vibrational Spectroscopy*, John Wiley & Sons: New York, 2001.

85 Guidance for Industry, Dissolution Testing of Immediate Release Solid Oral Dosage Forms, U.S. Department of Health and Human Services, Food and Drug Administration, Center for Drug Evaluation and Research (CDER), August 1997.

86 Dressman, J. B.; Amidon, G. L.; Reppas, C.; Shah, V. P. *Pharm. Res.*, 1998, 15, 11–22.

87 Langenbucher, F. *J. Pharm. Sci.*, 1969, 58, 1265–1272.

88 Rohrs, B. R. *Diss. Tech.*, 2001, August.

89 Shah, V. P.; Konecny, J. J.; Everett, R. L.; McCullough, B.; Noorizadeh, A. C.; Skelly, J. P. *Pharm. Res.*, 1898, 6, 612–618.

90 Shah, V. P.; Noory, A.; Noory, C.; McCullough, B.; Clarke, S.; Everett, R.; Naviasky, H.; Srinivasan, B. N.; Fortman, D.; Skelly, J. P. *Int. J. Pharm.*, 1995, 125, 99–106.

91 Fang, J. B.; Robertson, V. K.; Rawat, A.; Flick, T.; Tang, Z. J.; Cauchon, N. S.; McElvain, J. S. *Mol. Pharm.*, 2010, 7, 1466–1477.

92 Jantratid, E.; Maio, V. D.; Ronda, E.; Mattavelli, V.; Vertzoni, M.; Dressman, J. B. *Eur. J. Pharm. Sci.*, 2009, 37, 434–441.

93 Kakhi, M. *Int. J. Pharm.*, 2009, 376, 22–40.

94 D'Arcy, D. M.; Liu, B.; Bradley, G.; Healy, A. M.; Corrigan, O. I. *Pharm. Res.*, 2010, 27, 246–258.

95 Ashraf, M.; Iuorno, V. L.; Coffin-Beach, D.; Evans, C. A.; Augsburger, L. L. *Pharm. Res.* 1994, 11, 733–737.

96 Rajabi-Siahboomi, A. R.; Bowtell, R. W.; Mansfield, P.; Henderson, A.; Davies, M. C.; Melia, C. D. *J. Control. Release* 1994,31, 121–128.

97 Bowtell, R.; Sharp, J. C.; Peters, A.; Mansfield, P.; Rajabi-Siahboomi, A. R.; Davies, M. C.; Melia, C. D. *Magn. Reson. Imaging* 1994, 12, 361–364.

98 Steingötter, A.; Weishaupt, D.; Kunz, P.; Mader, K.; Lengsfeld, H.; Thumshirn, M.; Boesiger, P.; Fried, M.; Schwizer, W. *Pharm. Res.* 2003, 20, 2001–2007.

99 Alderman D. *Int. J. Pharm. Technol. Prod. Manuf.* 1984, 5, 1–9.

100 Rajabi-Siahboomi, A. R.; Bowtell, R. W.; Mansfield, P.; Davies, M. C.; Melia, C. D. *Pharm. Res.* 1996, 13, 376–380.

101 Madhu, B.; Hjärtstam, J.; Soussi, B. *J. Control. Release* 1998, 56, 95–104.

102 Hyde, T. M.; Gladden, L. F. *Polymer* 1998, 39, 811–819.

103 Kojima, M.; Ando, S.; Kataoka, K.; Hirota, T.; Aoyagi, K.; Nakagami, H. *Chem. Pharm. Bull.* 1998, 46, 324–328.

104 Dorożyński, P.; Kulinowski, P.; Jachowicz, R.; Jasiński, A. *AAPS PharmSciTech* 2007., 8, art no. 15, E1–E4.

105 Kulinowski, P.; Dorożyński, P.; Jachowicz, R.; Weglarz, W. P. *J. Pharm. Biomed. Aanl.* 2008, 48, 685–693.

106 Nott, K. P. *Eur. J. Pharm. Biopharm.* 2010, 74, 78–83.

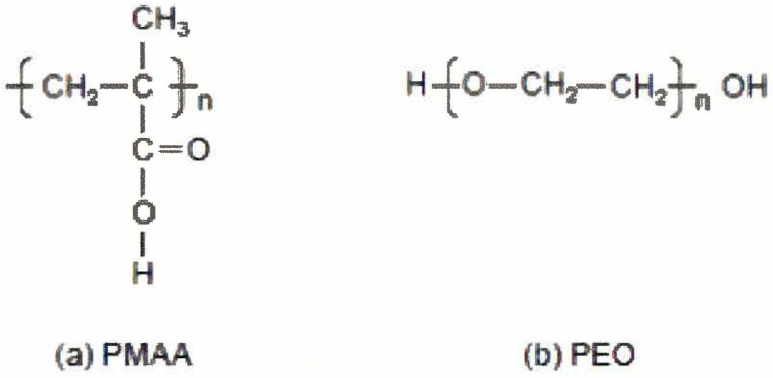

Figure 1. Chemical structural formula of (a) PMAA and (b) PEO.

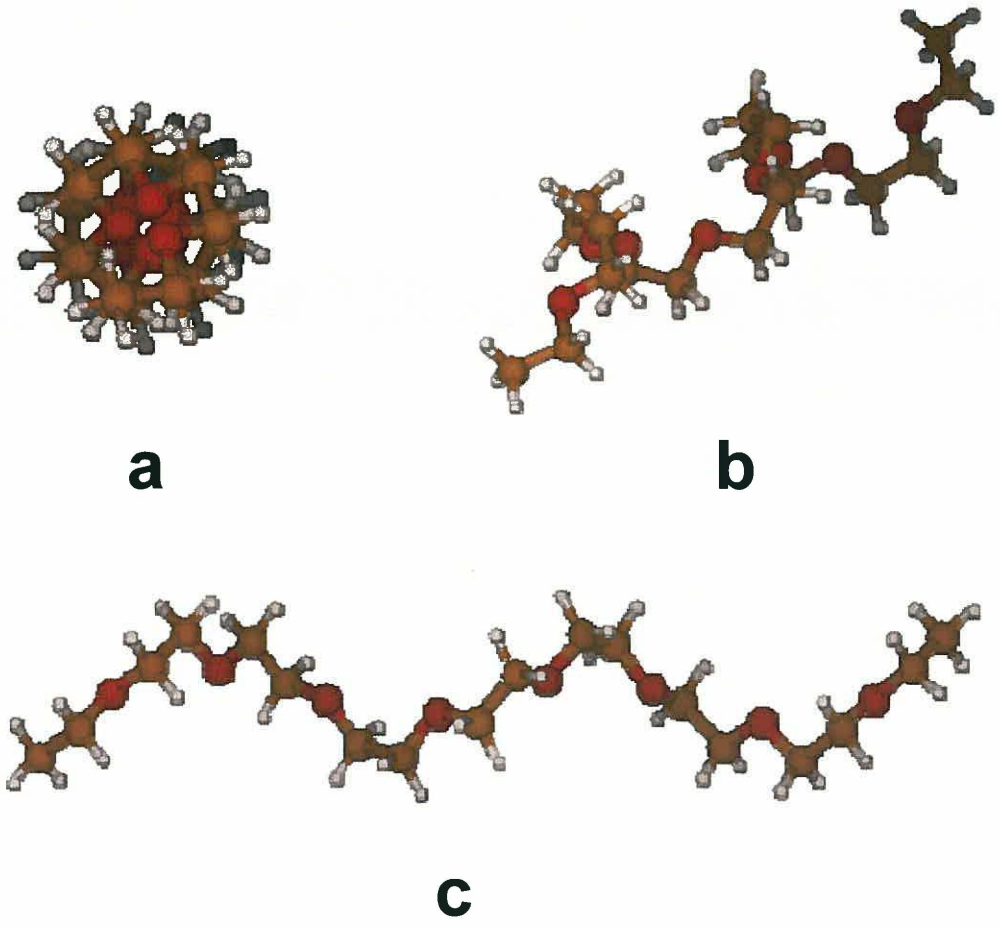

Figure 2 The projection drawing for the crystal structure (helix) of PEO shown from different angles; a: top, b: oblique and c: side views.

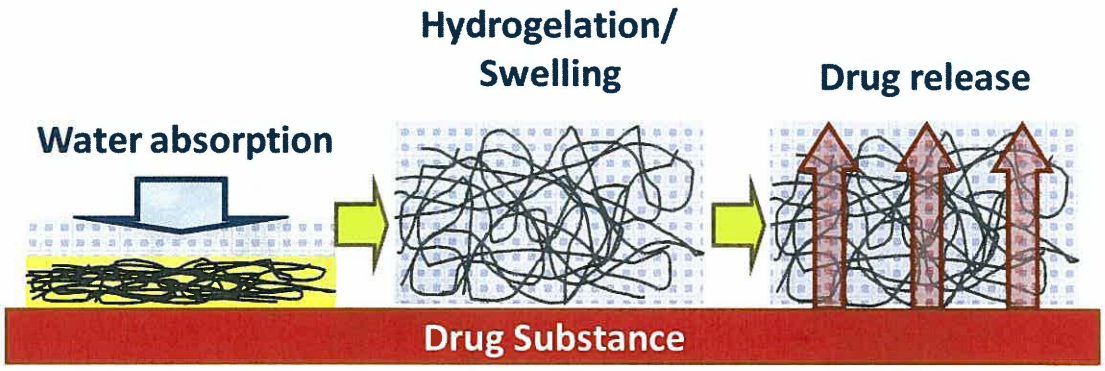

Figure 3 The schematic illustration of a hydrogelling and swelling behavior of a polymer film and a drug-release phenomenon by self-diffusion through a hydrogel layer.

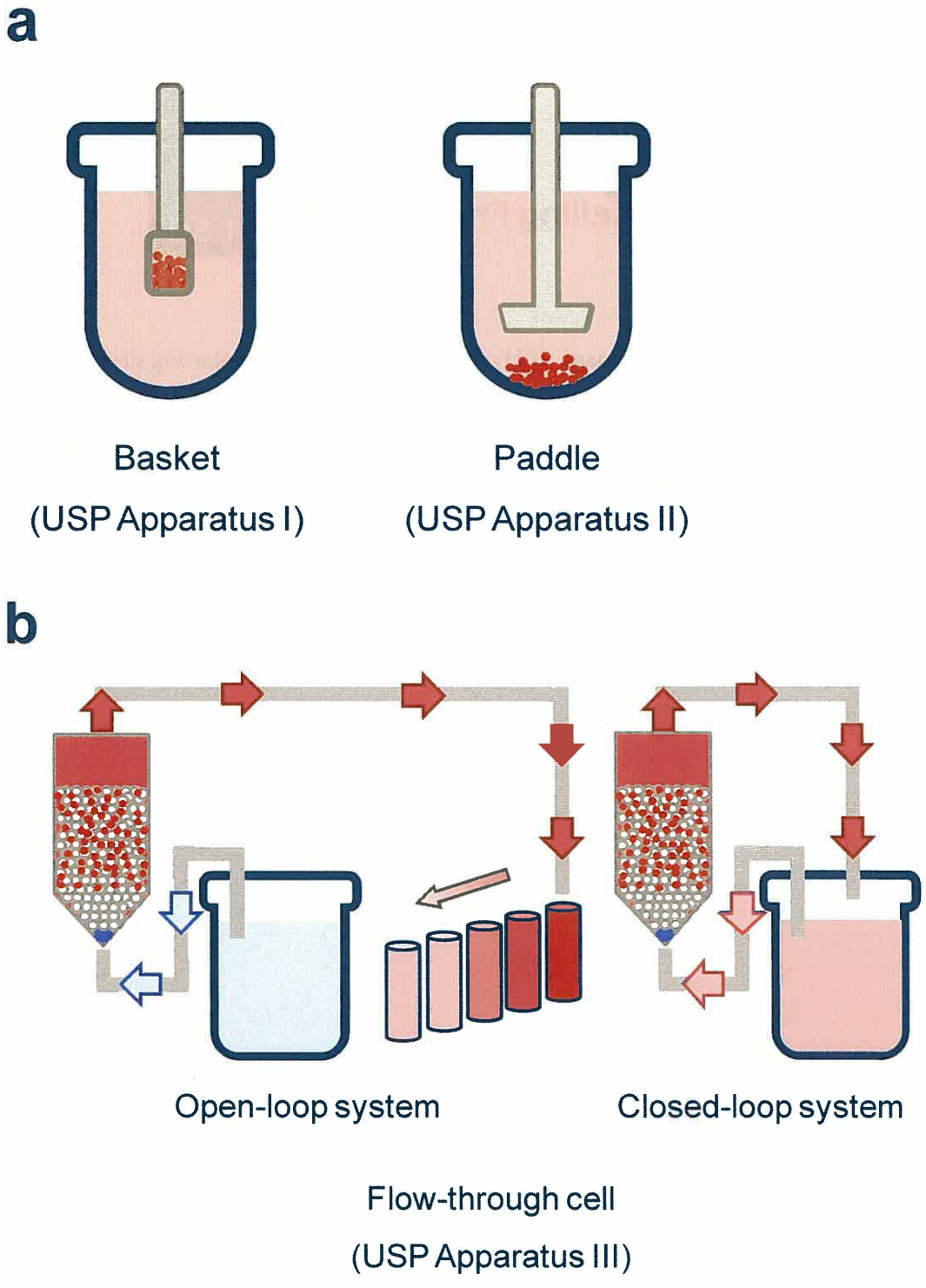

Figure 4 The schematic illustrations of dissolution apparatuses; (a) left; basket and right; paddle, and (b) flow-through cell apparatus, left; open-loop and right; closed-loop configurations.

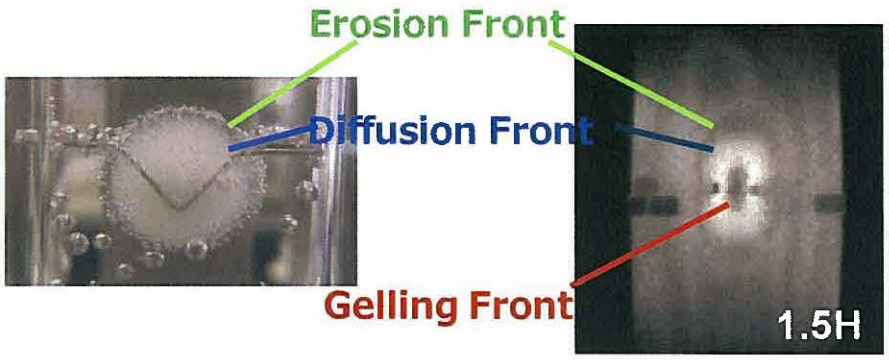

Figure 5 Photo and MRI image of Hydrogel of 1.5 hour after starting dissolution test.

Chapter 1: Hydration Mechanism on a Poly(methacrylic acid) Film Studied by *In Situ* Attenuated Total Reflection Infrared Spectroscopy

Abstract

A drastic structure change during a hydration process of a poly(methacrylic acid) (PMAA) film was observed by time-resolved *in situ* attenuated total reflection infrared (ATR-IR) spectroscopy. Inter- or intra-hydrogen-bonds via side-chain carboxyl groups are formed as cyclic dimers, side-on dimers and linear open chain oligomers including open dimers in a dried PMAA film. By contacting water, the side-chain hydrogen-bonds in PMAA are dissociated instantly, and then the subsequent carboxyl groups which have no hydrogen-bond newly hydrate with water molecules in a side-on form. Quantum chemical calculations (QCCs) using a model monomer of propionic acid (PA) also support the hydrogen-bonded and hydrated structures explored by the ATR-IR spectroscopy. It has been concluded from the present study that the dissociation of hydrogen-bonded and newly created hydrated structures via the carboxyl groups play an important role for the swelling of PMAA in water.

1. Introduction

Poly(methacrylic acid) (PMAA) and its derivatives have widely been applied to pharmaceutical products as a pH-responsive enteric coating agent, a kind of drug delivery systems (DDS), to control the drug-releasing in oral administration.[1-3] The quality of a drug have been usually evaluated about only its active pharmaceutical ingredient by an *in vivo* testing as a blood drug concentration in clinical practice or an *in vitro* dissolution test as a percent drug-releasing ratio from their products following the dissolution tests described in each Pharmacopoeia.[4-6] However, in order to clarify the drug-releasing mechanisms of DDS products, the investigation of inherent physical properties and dissolution mechanisms of pharmaceutical functional excipients in water are of great importance.

There has been a number of studies on dried and hydrated structures of various kinds of polymers and the states of water interacting with the polymers,[7-11] and the structures of water soluble polymer solutions have also been studied.[12] However, little attention has been paid to the hydration and dissolving process of hydrophilic polymers, because it is difficult to monitor their flash structure changes in water. To overcome the difficulty, I have recently applied high-speed scan attenuated total reflection infrared (ATR-IR) spectroscopy equipped with a flow-cell (Figure 1). The flow-cell method allows me to measure a process of water sorption into a polymer film.[7]

Hydrogen-bonded and hydrated structures of carboxylic acids such as formic acid, acetic acid and PA have well been studied by Raman spectroscopy,[13-17] IR spectroscopy,[14,18,19] X-ray diffraction[20] and nuclear magnetic resonance (NMR).[21] Furthermore, several quantum chemical calculations (QCCs) have also been applied

for such studies.[21-28] It has been reported that carboxylic acid groups form several associated conformations via hydrogen-bonds, namely cyclic dimers, side-on dimers and linear open chain oligomers including open dimers,[29,30] and it is well-known that cyclic dimers dominate in the pure liquid or solid states of carboxylic acids.[12-20]

Hydrated structures of carboxylic acid monomers have also been studied by using various techniques and QCCs.[28,31-33] In the field of polymers, there has been a great attention on the structures and their changes of hydrogen-bonded and hydrated poorly water soluble polymers,[34] however, many of previous studies on carboxylic acid groups in polymers have dealt almost exclusively with the structures in solid forms and those in aqueous solutions, separately.

In this study, the hydration process of carboxyl groups in a water soluble hydrophilic PMAA film is explored by using rapid-scan ATR-IR spectroscopy with a flow-cell, because it allows me to evaluate simultaneously both the structures of hydrogen-bonded PMAA in a solid state and those of hydrated one in a gel and a liquid under the same conditions, and furthermore, to detect time-resolved structural changes. Additionally, obtained spectra-structure correlations are examined by QCCs based on density functional theory (DFT) using a model monomer of PA instead of a real polymer of PMAA.

2. Experimental

2.1. Materials

An atactic PMAA was purchased from Polysciences, Inc. (averaged molecular weight of ca. 1.0×10^5). Methanol labeled guaranteed grade was purchased from Kanto Chemical. Water with a resistivity of 18.2 MΩ·cm was prepared by use of a Milli-Q

system.

A PMAA film was deposited on a hemispherical Zinc-Selenium (ZnSe) prism by 150 μL solvent-casting method of 10 mg/mL methanol solution and was dried at 80 °C for 3 hours. A PMAA aqueous solution was prepared by stirring excessive amounts of PMAA in water over night at room temperature.

2.2. Infrared Measurements

All the ATR-IR spectra were measured at a resolution of 4 cm^{-1} by using a Thermo Electron Nexus 470 Fourier-transform IR spectrometer equipped with a Seagull variable angle reflection accessory and a liquid nitrogen cooled HgCdTe detector. A prism with an adhered polymer film was mounted onto a homemade flow-cell shown in Figure 1. More detailed information about the cell was described elsewhere.[7] IR beam was introduced into the prism at an incident angle of 45°, which is larger than the critical angle of ca. 34°. A total of 64 scans were co-added to obtain each spectrum. ATR-IR spectra of liquid samples were measured using the same flow-cell at the prism/liquid interface without a polymer film. Hydration process of a PMAA film was investigated by pouring water into the flow-cell. In order to achieve such high-speed scans, a velocity of the moving mirror in the interferometer of 6.33 cm • s^{-1} (100 kHz) was applied. A total of 2 scans, every 0.20 s from 0 to 30 s, were co-added to obtain each spectrum and a total of 148 spectra were measured. All the ATR-IR spectra were defined in an absorbance unit as

$$A = -\log_{10}\frac{R}{R_0} \tag{1}$$

where R and R_0 are intensities of the ATR-IR light from a sample and a reference,

respectively. All the ATR-IR spectra were not subjected to Kramers-Kronig transformation and ATR correction. Note that a penetration depth of the evanescent wave can be estimated as

$$d_p = \frac{\lambda / n_{prism}}{2\pi\sqrt{sin^2\theta - (n_{sample}/n_{prism})^2}} \quad (2)$$

where λ, n and θ are a wavelength of the near-field light, a refractive index and an incident angle into the prism, respectively.[35] Since the thickness of the film sample of ca. 3 μm is enough thicker than the penetration depth of ca. 0.9 μm at 1700 cm^{-1}, ATR-IR absorption by bulk water contacting with polymer film surface is never detected. The second derivative spectra were calculated by the Savitzky-Golay method[36] using homemade software after the spectra were subjected to Kawata-Minami smoothing.[37] In the present study, the curve-fitting spectra were obtained with software named SPINA 3.0 (Y. Katsumoto, Kwansei Gakuin University).

2.3. Quantum Chemical Calculations

All QCCs were performed based on DFT using a B3LYP function and a 6-31G(d) base set. The calculations of optimized structures, vibrational frequencies, IR intensities and self-consistent fields (SCF) were carried out with the Gaussian 03 program.[38-40] The force fields calculated at the B3LYP/6-31G(d) level were scaled down using a single scale factor of 0.9613, which is accepted to be the best for the level.[41] In order to estimate hydrogen-bonded and hydrated structures of PMAA, a model monomer of PA was used for the QCCs.

All the calculated spectra were constructed assuming a Lorentzian band shape with a 7 cm^{-1} band width. In addition, DFT calculations on the basis of the Onsager reaction field model[42,43] were performed to investigate the effects of hydration of PA on the IR spectra as a simple model of PMAA.

The energy of intermolecular interaction due to hydrogen-bond and hydration is defined as a energy difference before and after separation of each optimized hydrogen-bonded and hydrated structures, respectively. It was calculated using their SCF energies.

2.4. Gravimetric Measurement

A PMAA film was prepared on a cover-glass for microscope by the same method as that of the ATR-IR measurement. After drying, water was cast and held on the PMAA dry film for around 30 seconds. After wiping the superfluous liquid water on the surface of the film, the weight of sample was measured before and after liquid water evaporating.

3 Results and Discussion

3.1. Attenuated Total Reflection Infrared Spectra

Figure 2a shows an ATR-IR spectrum in the 4000-1000 cm^{-1} region of a PMAA film dried by nitrogen gas flow in the cell. A broad feature overlapping with several weak peaks is observed in the 3700-2300 cm^{-1} region. Relatively sharp peaks in the 3000-2700 cm^{-1} region are assigned to C-H stretching modes of PMAA. O-H stretching bands are observed in the 3700-3000 cm^{-1} region.[7-11] A lower wavenumber

bands in the 2700-2300 cm^{-1} region is assigned to overtones and combination of bands near 1391 and 1262 cm^{-1} enhanced by Fermi resonance with the broad O-H stretching band.[29] The most intensive bands in the 1750-1680 cm^{-1} region are identified as C=O stretching bands. The assignments for major IR bands in the 4000-1000 cm^{-1} region are summarized in Table 1. Figure 3 shows a close-up spectrum and curve fitting spectra in the C=O stretching region of the dried PMAA film shown in Fig. 2a. Overlapped C=O peaks are deconvoluted by four curve fitting components corresponding to the non-hydrogen-bonded monoer, cyclic dimer, side-on dimer and linear oligomers of side-chain carboxyl groups in PMAA based on the second derivative result and the previously reported.[29] The four peaks observed and estimated at 1736, 1719, 1695 and 1679 cm^{-1} are assigned to C=O stretching bands of monomer (non-hydrogen bonded), side-on and cyclic dimeric hydrogen bonded, and linear oligomeric hydrogen bonded, respectively (Table 2). The assignments are also confirmed by QCCs for PA, the model compound of PMAA (Table 2).

Figure 2b shows an ATR-IR spectrum in the 4000-1000 cm^{-1} region of bulk water measured from a ZnSe/water interface directly. An intense and broad O-H stretching band in the 3700-3000 cm^{-1} region and an O-H deformation band in the 1750-1550 cm^{-1} region are identified in the ATR-IR spectrum of water.

Figure 2c and d shows an ATR-IR spectrum of a 57.6 $mg \cdot mL^{-1}$ PMAA aqueous solution and a difference spectrum calculated by the subtraction of the spectrum of water from that of the PMAA aqueous solution, respectively. The spectrum of the PMAA aqueous solution is very close to that of bulk water in the whole spectral region except for a few small peaks observed in the finger print region. The assignments for

major IR bands in the spectrum of Fig. 2d are also listed in Table 1. In the aqueous solution, most of the carboxylic acid groups of PMAA are not dissociated, because an asymmetric stretching COO^- band is not detected at around 1550 cm^{-1}.[30]

3.3. Time-Resolved Infreared Spectra

Figures 4a and 4b represent time-resolved *in situ* ATR-IR spectra of a hydration process into a PMAA film collected every 0.20 s intervals and their second derivative spectra in the C=O stretching and finger print regions, respectively. An O-H deformation band of water at 1640 cm^{-1} increases with time, whereas other bands arising from PMAA decrease, due to swelling of the PMAA film by water sorption. Although the O-H deformation band is overlapped with the C=O stretching bands in the 1800-1600 cm^{-1} region, they are clearly distinguished by the second derivative spectra. The second derivative analysis shows that two of the four C=O stretching bands revealed by the curve fitting appear in the time-resolved spectra. A main peak at 1693 cm^{-1} and a higher wavenumber shoulder at 1740 cm^{-1} are assigned to cyclic dimer and free C=O groups of PMAA, respectively.[29] The main peak and the higher wavenumber shoulder shift by ca. 10 cm^{-1} to a higher and lower wavenumber with time, respectively. In the finger print region, peaks located at 1262 and 1242 cm^{-1} assigned to the C-C-O stretching modes show a high wavenumber shift with time. The C-O-H bending and C-O stretching bands at 1185 and 1154 cm^{-1}, respectively, also shift during the water sorption progress. On the other hand, bands assigned to CH_2 and CH_3 groups shift slightly in the hydration process. These results imply that conformational changes due to hydration occur at around the carboxyl groups in

PMAA.

The refractive index changed from about 1.5 to 1.3 due to the changes in the state from a solid film to hydrogel, and then there is a possibility that the absorbance of the peaks is affected. In this study, however, no C-H stretching and bending bands in the 3000-2900 cm^{-1} and 1500-1400 cm^{-1} regions, respectively, shifted in the time resolved spectra in Figure 4b. Thus, there is little effect for band positions by the refractive index changes, and the structure changes of PMAA could be evaluated.

3.4. Quantum Chemical Calculations

Figure 5A shows optimized structures and their simulated spectra of the (a) monomer, (b) cyclic dimer, (c) side-on dimer, (d) linear dimer and (e) linear trimer of PA. The observed vibrational frequencies of PMAA and the calculated ones of its model monomer, PA, in the C=O stretching region are summarized in Table 2. The calculated frequencies are obtained to compare with their observed and estimated C=O stretching bands. Compared with the calculated frequency of the free C=O stretching band of PA monomer (1778 cm^{-1}), the calculated frequencies of the hydrogen-bonds C=O stretching bands of the cyclic dimers, side-on dimers and linear oligomers of PA shift, respectively. With the increase in the PA molecules forming a linear oligomer, the calculated frequency of the C=O stretching band shifts to a lower wavenumber and broadens. And the simulation supports that a overlapped linear oligomers band is broaden. These calculation results are in good agreement with the observed spectrum of the dried PMAA film shown in Figure 2a and 3.

Figure 5B illustrates optimized structures and their simulated spectra of PA hydrated

with (f) the carbonyl group, (g) the hydroxyl group and (h) the carboxyl group like side-on from. These results are also in accord with the observed one shown in Figure 2d. The observed and calculated vibrational frequencies of hydrated PMAA and its hydration model monomer, PA, in the C=O stretching region are also summarized in Table 2. When the carbonyl groups of PA are hydrated (Figure 5B (f) and (h)), the C=O stretching band is shifted to a lower frequency, Moreover, it was shown by their SCF energies that the latter structure is more stable than the former. On the other hand, when the oxygen atoms in hydroxyl groups are hydrated (Figure5B(g)), the C=O stretching band is moved to a higher frequency. Furthermore, Table 2 lists the intermolecular interaction energies of the respective structures. The calculated intermolecular interaction energies indicate that the cyclic dimer of PA is more stable than any other hydrogen-bonded structures of PA per a PA molecule. Thus, the carboxyl groups of dried PMAA film may also form easily the cyclic dimer structures as the most stable structure. However, if the hydrated structures are included, the most stable structure is (h), the PA hydrated with the carboxyl group. Thus, the carboxyl groups of dried PMAA film may also form easily the side-on hydrated structures as the most stable structure after water penetration.

QQC is really useful and a solid investigation tool. However, I have to consider mainly a couple of the other critical parameters for the present calculations to acquire better agreements. One is the difference between the monomer and the polymer, and the other is the effect of environmental conditions. The former is concerned with a steric barrier of the polymer chain, while the latter contains a hydrophobic interaction among hydrophobic groups and a dielectric constant in water environment.

3.5. Hydration Mechanism into Poly(methacrylic acid) Film

Figure 6 shows time-dependent variations in the peak intensities and positions of the C=O stretching bands near 1736 and 1695 cm^{-1} and the O-H deformation band at 1628 cm^{-1} in the time-resolved spectra shown in Figure 4. The discussion regarding the peak intensities and positions are made in the narrow region of 1750 - 1680 cm^{-1} to prevent the effect of penetration depth of evanescent wave. Figure 6a plots the time-dependent peak intensity changes of bands at 1695 and 1628 cm^{-1} due to the C=O stretching modes and the O-H deformation mode,, respectively. These peak intensities begin to change at seven seconds after the water addition, and the intensity changes are almost completed in five seconds. Thus, the speed of the hydration process of the PMAA film is estimated to be ca. 0.18 $\mu m \cdot s^{-1}$. Furthermore, the gravimetric results demonstrate that 16 water molecules exist each methacrylic acid monomer unit in a swelled PMAA film. Consequently, there are a number of free water molecules which are not hydrated with the carboxyl groups in the hydrated PMAA film. Figure 6b shows plots of time-dependent peak shifts of bands at 1736 and 1695 cm^{-1} due to the non-hydrogen-bonded and cyclic dimer C=O stretching modes, respectively. The peak position of cyclic dimer C=O stretching band at 1695 cm^{-1} shifts to a high frequency in parallel with the peak intensity attenuating. The free C=O stretching band at 1736 cm^{-1} also moves to a low frequency in parallel with the peak intensity decrease. Actually, there are some differences in frequencies of observed bands between the solid state and the hydrated samples due to the differences of physical characterization like permittivity and refractive index, however, the PMAA film was swelled and hydrated

quickly after water penetration. Thus these bands could be assigned to each state, separately.

In the hydration process, the most stable cyclic dimer structure in the dried PMAA film is easily dissociated by the water storming and the hydrophobic interaction. Following that, the free carboxyl groups due to the dissociation of the cyclic dimers newly associate with water molecules to form more stable structure; hydrated structure with carboxylic groups of PA like side-on conformation. In other words, the hydration process of the carboxyl groups is induced by the dissociation of the cyclic dimer structure by hydrogen-bonded in the dried state. They are supported by the above QCCs discussion. Thus, the other side-on and linear dimers, and oligomers which have weaker hydrogen-bond are also dissociated in the hydration process, and their non-hydrogen-bonded carboxylic groups newly associate with water molecules to form the same stable hydrated structure. Figure 6 indicates that, the PMAA film is swelling by water absorption, and its carboxyl groups conformation changes from some kinds of hydrogen-bonded structures to entirely-different hydrated one occur in an instant.

4. Summary

A process of hydration into a PMAA film was investigated by time-resolved *in situ* ATR-IR spectroscopy. The present study has provided new insight into the hydration mechanism of carboxyl groups in the PMAA film. The intra- and inter-side-chain hydrogen-bonds in the PMAA are dissociated, and it is swelled by the water storming, and then their generated non-hydrogen-bond carboxyl groups instantly hydrate with water molecules and equilibrate to the side-on form which is the most stable structure

for the carboxyl groups (Figure 7). The calculated frequencies and the interaction energies by QCCs using a model monomer of PA instead of PMAA have supported my spectral assignment and structure simulation of the hydrogen-bonded and the hydrated structures of PMAA.

Rapid-scan ATR-IR spectroscopy with a flow-cell is well suited to investigate hydration mechanisms of coating films using a stimulus-responsive polymer. Eventually, this sort of study may allow me to understand the dissolution mechanisms of pharmaceutical DDS products.

5. References

1 Tahami K. A.; Singh J. *Recent Patents on Drug Deliv & Formul* 2007, 1, 65-71.

2 Lin S. Y.; Yu H. L. *J. Polym. Sci. Part A Polym. Chem.* 1999, 37, 2061-2067.

3 Victor S. P.; Sharma C. P. *J. Biomater. Appl.* 2002, 17, 125.

4 *The United States Pharmacopeia 34-National Formulary 29*, The United States Pharmacopeial Convention, 2011, 278–285.

5 *European Pharmacopoeia, seventh ed.*, European Directorate for the Quality of Medicines, 2011, 266–275.

6 *The Japanese Pharmacopoeia 16th ed.*, Society of Japanese Pharmacopoeia, 2011, 116–120.

7 Morita S.; Tanaka M.; Ozaki Y. *Langmuir* 2007, 23, 3750-3761.

8 Kitano H.; Ichikawa K.; Fukuda M.; Mochizuki A.; Tanaka M. *J. Colloid Interface Sci.* 2001, 242, 133-140.

9 Kitano H.; Ichikawa K.; Ide M.; Fukuda M.; Mizuno W. *Langmuir* 2001, 17, 1889-1895.

10 Kusanagi H.; Yukawa S. *Polymer* 1994, 35, 5637-5640.

11 Hajatdoost S.; Yarwood J. *J. Chem. Soc. Faraday Trans* 1997, 93, 1613-1620.

12 Pettersson A.; Marino G.; Pursiheimo A.; Rosenholm J. B. *J. Colloid Interface Sci.* 2000, 228, 73-81.

13 Semmler J.; Irish D. E. *J. Solution Chem.* 1988, 17, 805-823.

14 Genin F.; Quiles F.; Burneau A. *Phys. Chem. Chem. Phys.* 2001, 3, 932-942.

15 Tanaka N.; Kitano H.; Ise N. *J. Phys. Chem.* 1990, 94, 6290-6292.

16 Nishi N.; Nakabayashi T.; Kosugi K. *J. Phys. Chem. A* 1999, 103, 10851-10858.

17 Nakabayashi T.; Nishi N. *J. Phys. Chem. A* 2002, 106, 3491-3500.

18 Flakus H. T.; Stachowska B. *Chem. Phys.* 2006, 330, 231-244.

19 Flakus H. T.; Tyl A. *Chem. Phys.* 2007, 336, 36-50.

20 Takahashi O.; Yamanouchi S.; Yamamoto K.; Tabayashi K. *Chem. Phys. Lett.* 2006, 419, 501-505.

21 Asano A.; Eguchi M.; Kurotu T. *J. Polymer science Part B Polymer Physics* 1999, 37, 2007-2012.

22 Turi L.; Dannenberg J. J. *J. Phys. Chem.* 1933, 97, 12197-12204.

23 Brurneau A.; Genin F.; Quiles F. *Phys. Chem. Chem. Phys.* 2000, 2, 5020-5029.

24 Lourderaj U.; Giri K., Sathyamurthy N. *J. Phys. Chem. A* 2006, 110, 2709-2717.

25 Nakabayashi T.; Kosugi K.; Nishi N. *J. Phys. Chem. A* 1999, 103, 8595-8603.

26 Zhang R. Q.; Wong N. B.; Lee S. T.; Zhu R. S.; Han K. L. *Chem. Phys. Lett.* 2000, 319, 213-219.

27 Lewandosli H.; Koglin E.; Meier R. J. *Vib. Spectrosc.* 2005, 39, 15-22.

28 Chuchev K.; BelBruno J. J. *J. Mol. Struc.: Theochem.* 2006, 736, 199-204.

29 Dong J.; Ozaki Y.; Nakashima K. *Macromolecules* 1997;30:1111-1117.

30 Dong J.; Tsubara N.; Fujimoto Y.; Ozaki Y.; Nakashima K. *Appl. Spectrosc.* 2001, 55, 1603.

31 Tanaka N.; Kitano H.; Ise N. *J. Phys. Chem.* 1991, 95, 1503-1507 .

32 Zhou Z.; Shi Y.; Zhou X. *J. Phys. Chem. A* 2004, 108, 813-822.

33 George L.; Sander W. *Spectrochim Acta Part A* 2004, 60, 3225-3232.

34 Huang C. F.; Chang F. C. *Polymer* 2003, 44, 2965-2974.

35 Chalmers J. M.; Griffiths P. R. *Handbook of Vibrational Spectroscopy* 2001

36 Savitzky A.; Golay M. J. E. *Anal. Chem.* 1964, 36, 1627-1639.

37 Kawata S.; Minami S. *Appl. Spectrosc.* 1984, 38, 49-58.

38 Becke A. D. *J. Chem. Phys.* 1993, 98, 5648-5652.

39 Johnson B. G.; Frisch M. J. *J. Chem. Phys.* 1994, 100, 7429-7442.

40 Frisch M. J.; Trucks G. W.; Schlegel H. B.; Scuseria G. E.; Robb M. A.; Cheeseman J. R.; Zakrzewski V. G.; Montgomery J. A. J.; Stramann R. M. C.; Burant J. C.; Dapprich S.; Millam J. M.; Daniels A. D.; Kudin K. N.; Strain M. C.; Farkas O.; Tomasi J.; Barone V.; Cossi M.; Cammi R.; Mennucci B.; Pomelli C.; Adamo C.; Clifford S.; Ochterski J.; Petersson G. A.; Ayala P. Y.; Cui Q.; Morokuma K.; Malick D. K.; Rabuck A. D.; Raghavachari K.; Foresman J. B.; Cioslowski J.; Orits J. V.; Stefanov B. B.; Liu F.; Liashenko A.; Piskorz P.; Komaromi I.; Gomperts R.; Martin R. L.; Fox D. J.; Keith T.; Al-Laham M. A.; Peng C. Y.; Nanayakkara A.; Gonzalez C.; Challacombe M.; Gill P. M. W.; Johnson B. G.; Chen W.; Wong M. W.; Andres J. L.; Head-Gordon M.; Replogle E. S.; Pople J. A. *Gaussian 03, Revision B.05*;Gaussian, Inc., Pittsburgh, PA, 2003

41 Bauschlicher C. W. Jr; Partridge H. *J. Chem. Phys.* 1995, 103, 1788-1791.

42 Onsager L. *J. Am. Chem. Soc.* 1938, 58, 1486

43 Wiberg K. B.; Murcko M. A. *J. Phys. Chem.* 1987, 91, 3616

44 Nakashima K.; Fujimoto Y.; Anzai T.; Dong J.; Sato H.; Ozaki Y. *Bull. Chem. Soc. Jpn.* 1999, 72, 1233-1238.

45 Kawaguchi S.; Kitano T.; Ito K. *Macromolecules* 1992, 25, 1294-1299.

46 Tamura T.; Kawauchi S.; Satoh M., Komiyama J. *Polymer* 1997, 38, 2093-2098.

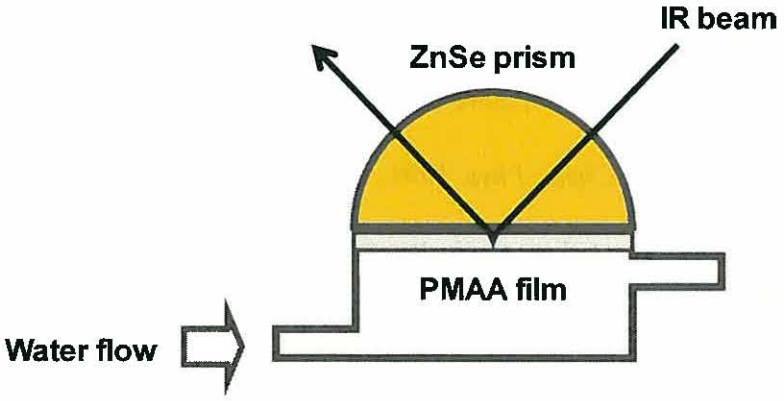

Figure 1 Schematic illustration of the *in situ* ATR-IR flow-cell used.

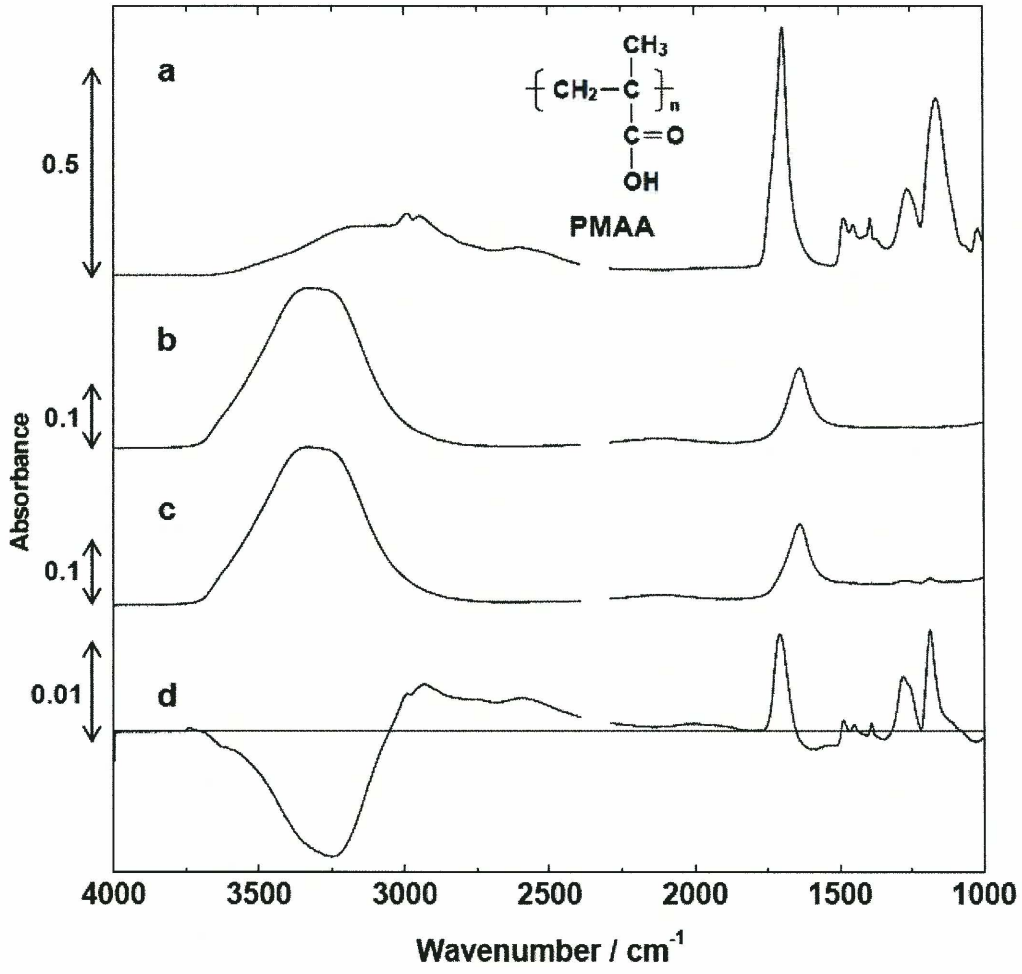

Figure 2 ATR-IR spectra in the 4000-1000 cm^{-1} region of (a) a dried PMAA film, (b) bulk water and (c) a 57.6 $mg \cdot mL^{-1}$ PMAA aqueous solution. (d) Difference spectrum obtained by the subtraction of water spectrum from the spectrum of the PMAA aqueous solution; (c)-(b).

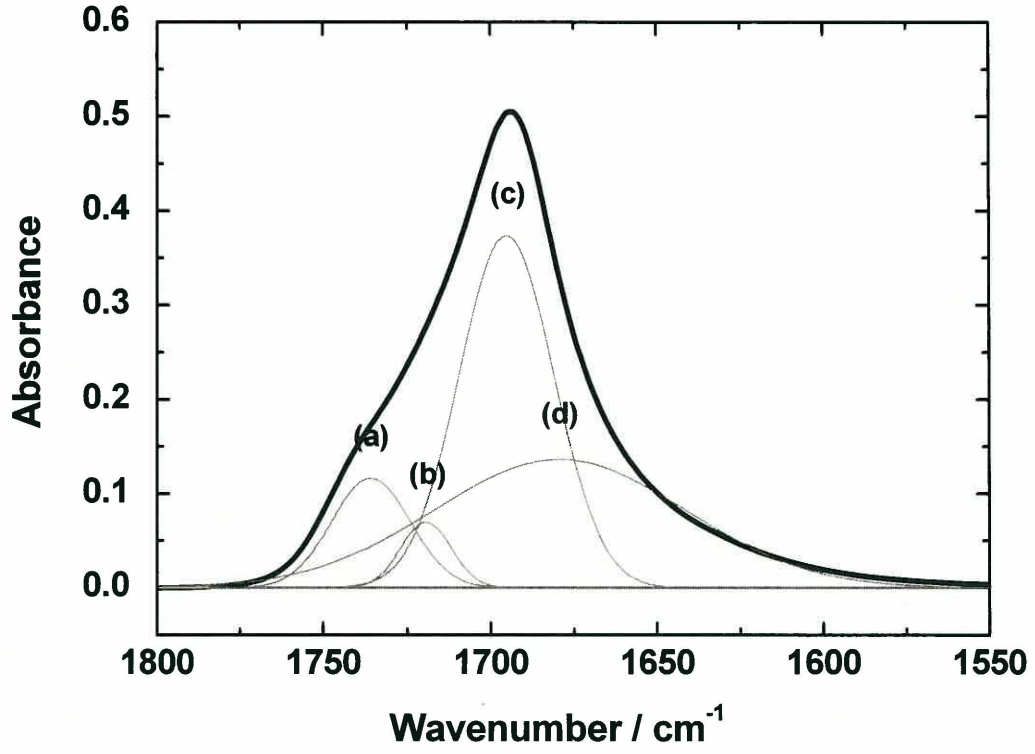

Figure 3 An ATR-IR spectrum (heavy line) and its curve fitting spectra (thin line) of a dried PMAA film in the C=O stretching region. (a) monomer, (b) side-on dimer, (c) cyclic dimer and (d) linear oligomer structures of side-chain carboxyl groups in PMAA.

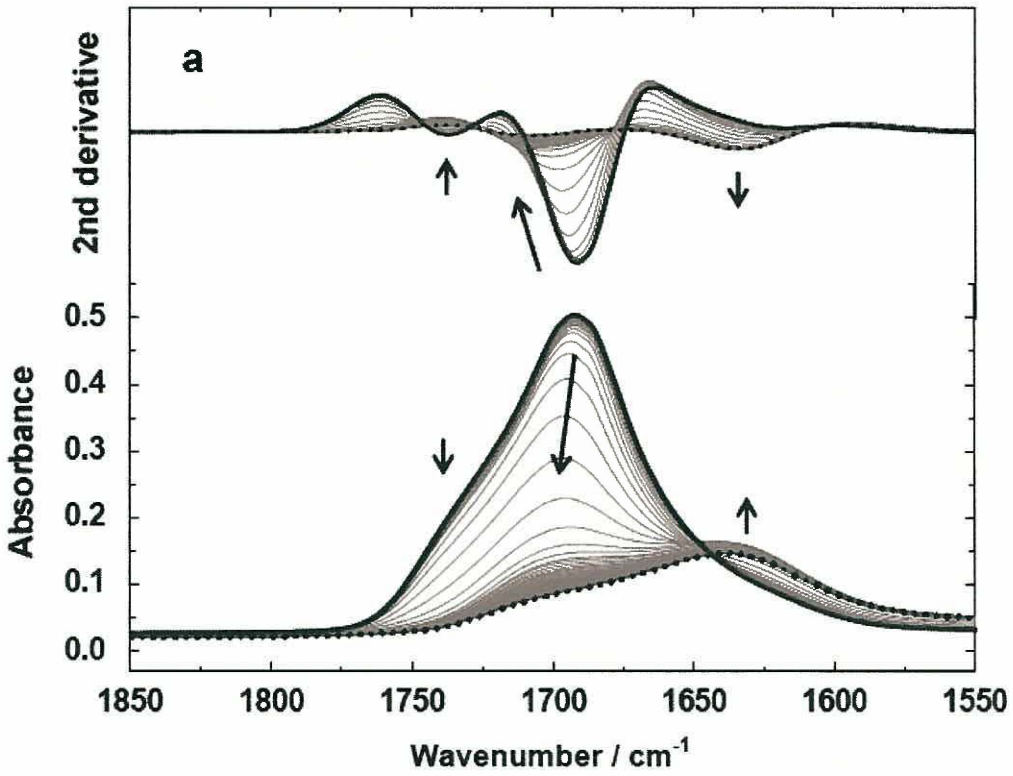
a
2nd derivative
Absorbance
0.5
0.4
0.3
0.2
0.1
0.0
1850
1800
1750
1700
1650
1600
1550
Wavenumber / cm-1

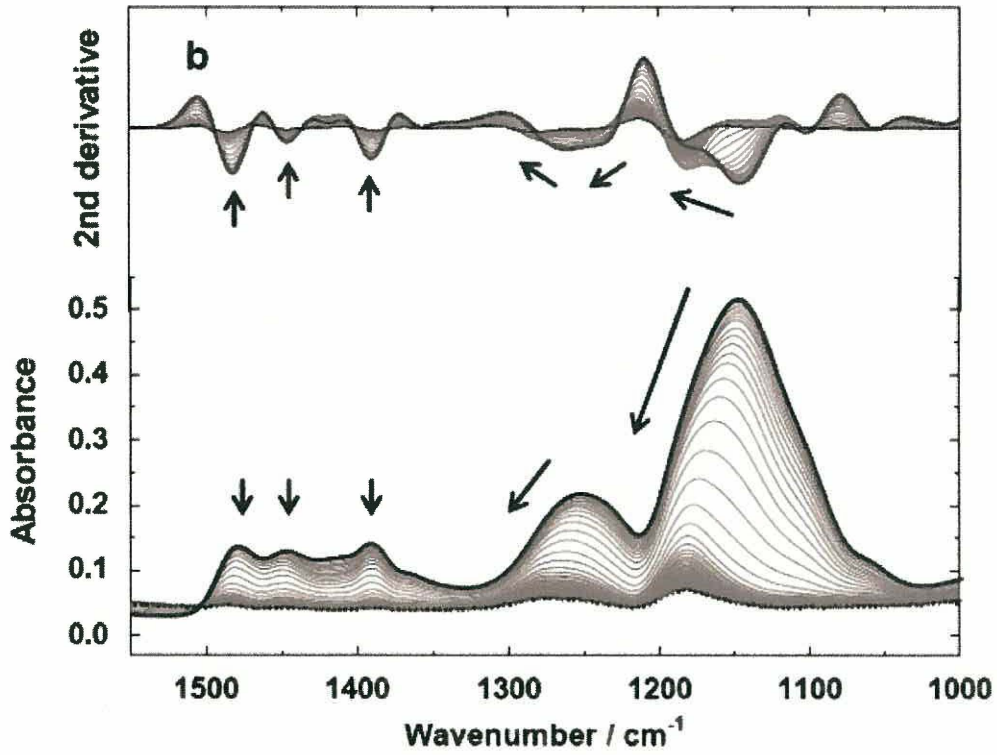
b
2nd derivative
Absorbance
0.5
0.4
0.3
0.2
0.1
0.0
1500
1400
1300
1200
1100
1000
Wavenumber / cm-1

Figure 4 Time-resolved ATR-IR spectra of the hydration process into a PMAA film by water (bottom) and their second derivative spectra (top) every 0.2 s between 0 and 30 s, (a) the C=O stretching and water O-H deformation region, and (b) finger print region, respectively. Before (heavy line) and after hydration (broken line).

A. Hydrogen-bonded structures

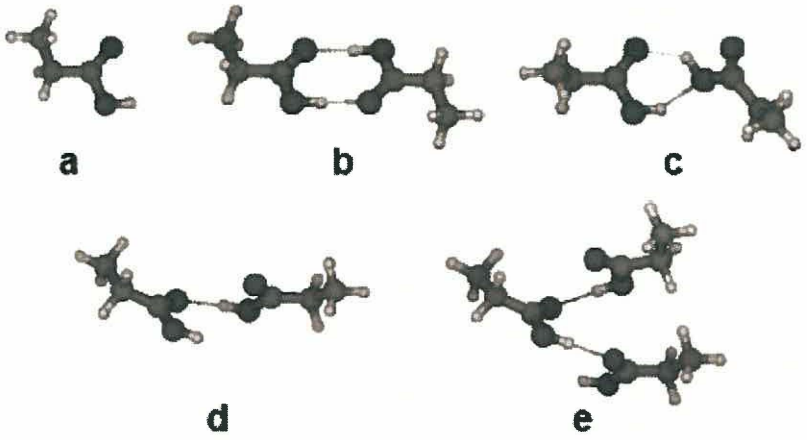

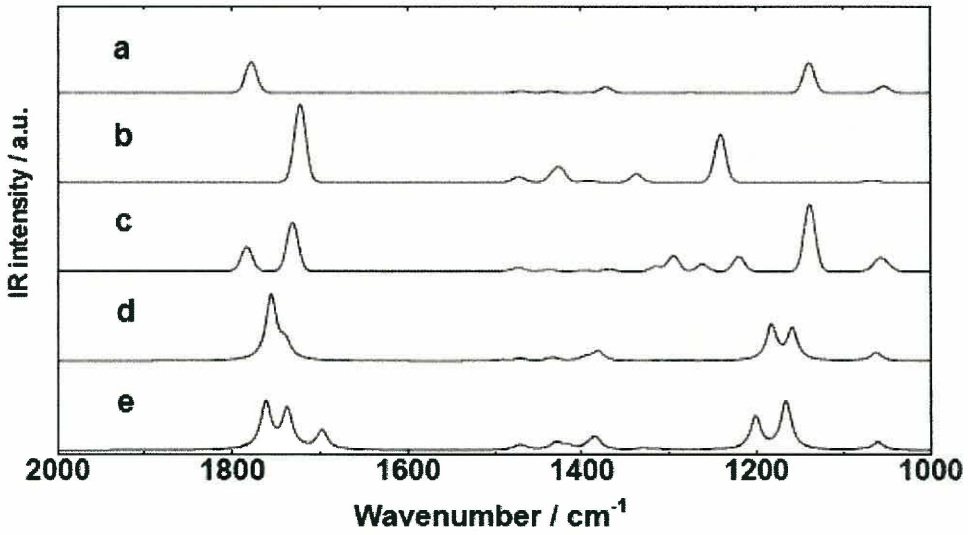

B. Hydrated structures

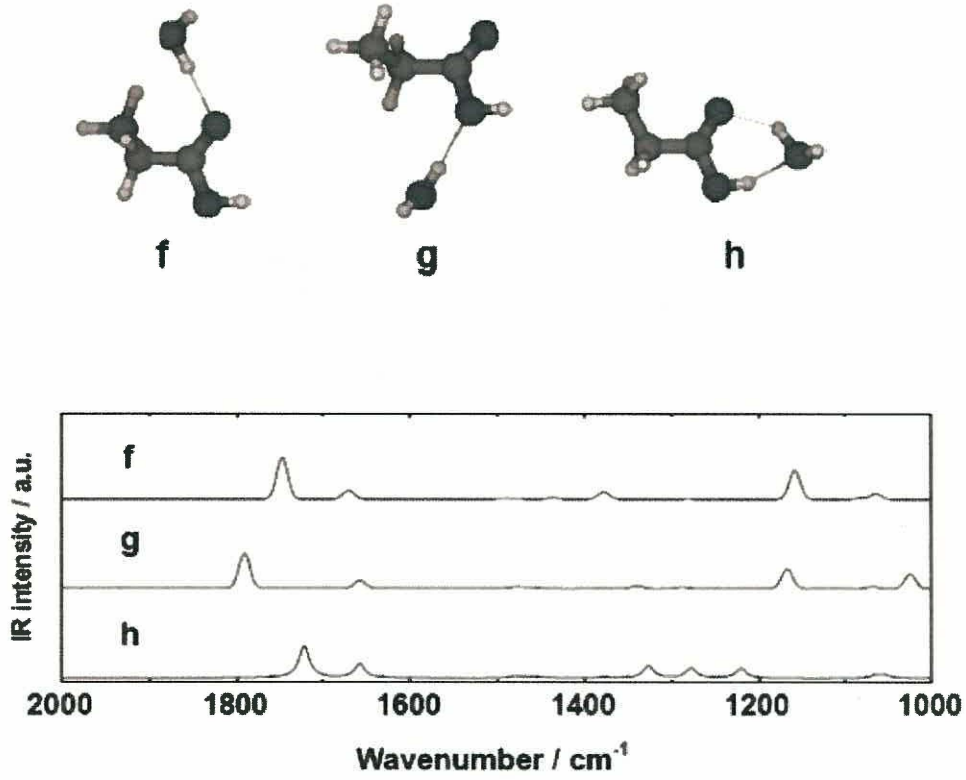

Figure 5 Optimized structures and their simulated spectra obtained by QCCs. (A) Hydrogen-bonded structures; (a) PA monomer, (b) PA cyclic dimer, (c) PA side-on dimer, (d) PA linear dimer and (e) PA linear trimer. (B) Hydrated structures; (f) Hydrated with the carbonyl group, (g) Hydrated with the hydroxyl group and (h) Hydrated with the carboxyl group.

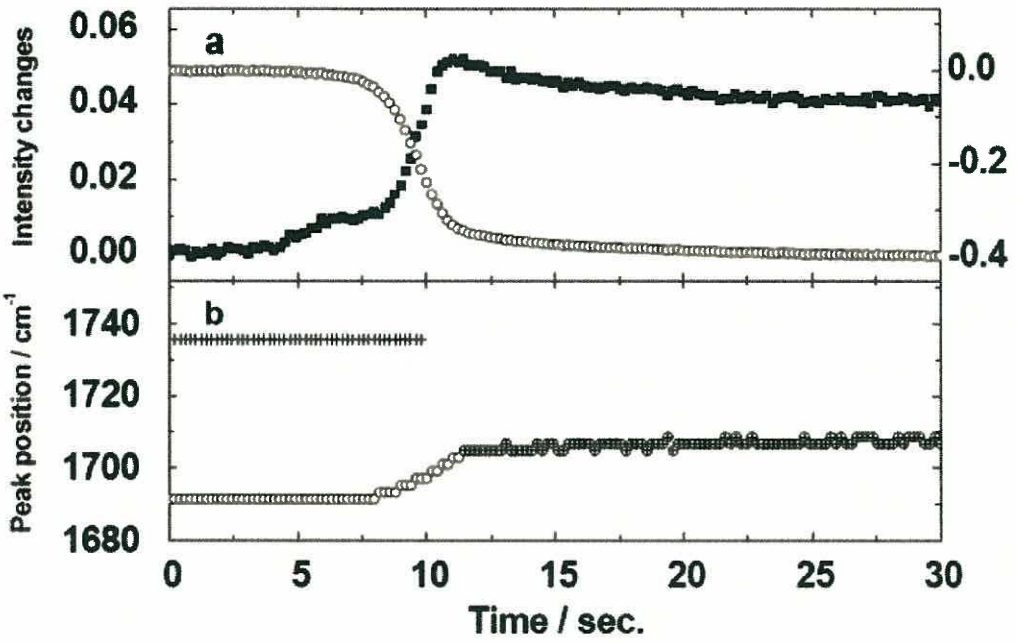

Figure 6 (a) Time-dependent intensity changes in the O-H deformation band at 1628 cm^{-1} (■; on the left-hand scale) and the C=O stretching band at 1695 cm^{-1} of the cyclic dimer (○; on the right-hand scale) versus time. (b) Time-dependent peak shifts of the cyclic dimer C=O stretching band (○) and the non-hydrogen-bonded C=O stretching band at 1736 cm^{-1} (+) in the time-resolved spectra shown in Figure 4.

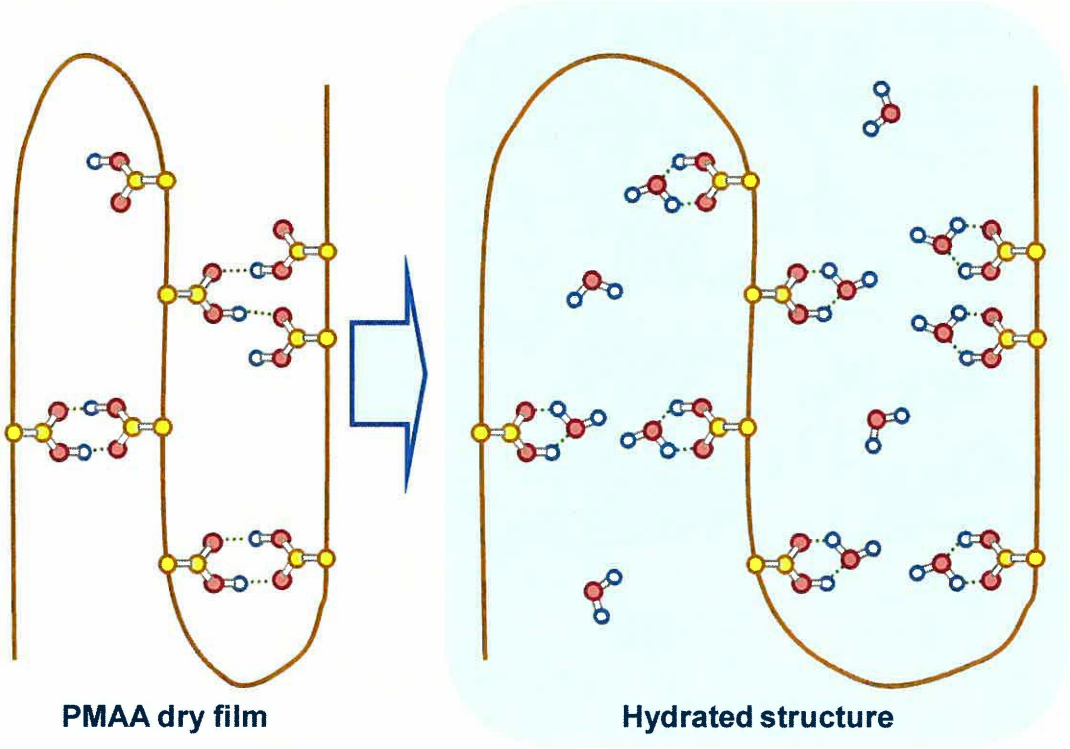

Figure 7 The schematic illustration of the structure changes during hydration process of a PMAA film.

Table 1 Band assignments of IR spectra of a dried PMAA film and an aqueous PMAA solution.

Frequency [ν/cm^{-1}]		Assignments
Dry film	Aqueous solution	
3205 broad	3552	O-H stretching
2995	2997	CH_3 asymmetric stretching
2942	2942	CH_2 antisymmetric stretching
2610	2585	Overtone and combination of bands near 1391 and 1262 cm^{-1} enhanced by Fermi resonance with the broad O-H stretching band
1693	1708	C=O stretching
1483	1486	CH_3 asymmetric bending
1447	1447	CH_2 scissoring
1391	1389	CH_3 symmetric bending
1262	1285	C-C-O stretching
1242	1256	C-C-O stretching
1185	1185	C-O stretching coupled with O-H in-plane bending
1154	1138	C-O stretching

Table 2 Observed frequencies of a C=O stretching band of PMAA and calculated frequencies of a C=O stretching band of PA, and hydrogen-bond energy calculated by QCCs. Indices of (a)-(h) correspond to the optimized structures shown in Figure 5.

		Structures	Observed frequencies of C=O st. of PMAA [cm^{-1}]	Calculated frequencies of C=O st. of PA [cm^{-1}]	Calculated hydrogen-bond/ hydration energy of PA [kcal/mol]
Hydrogen-bonded	a	Monomer	1736	1778	-
structure	b	Cyclic dimer	1695	1722	19.5
	c	Side-on dimer	1719	1783, 1731	9.0
	d	Linear dimer	-	1755, 1741	9.1
	e	Linear trimer	-	1761, 1737, 1698	20.1
	-	Linear oligomer	1679	-	-
Hydration	f	Carbonyl hydrated	-	1748	7.1
structure	g	Hydroxyl hydrated	-	1792	5.7
	h	Carboxylic acid hydrated	1708	1722	14.0

Chapter 2: Time-Resolved Conformational Analysis of Poly(ethylene oxide) during the Hydrogelling Process

Abstract

I investigated a drastic conformation change in a poly(ethylene oxide) (PEO) chain during the hydrogelation process using infrared (IR) spectroscopy and quantum chemical calculations (QCCs). Time-resolved *in situ* IR spectra of the hydrogelling process of a semi-crystalline PEO solid were measured using a flow-cell. It was found from the time-resolved IR study that gauche conformations around the C–C bonds in the crystalline-phase PEO chain maintain their conformations even after hydrogelation, while at least half of the trans conformations around the C–O bonds change into gauche conformations upon hydrogelling. With regard to the phenomena of these conformation changes after contacting water, the destruction and hydrogelation of the crystalline phase around the C–C bonds of the hydrophobic moiety occur prior to changes around the C–O bonds of the hydrophilic moiety. In addition, my QCC confirmed that the stable hydration structure of bridging water, wherein the two hydroxyl groups in a water molecule donate hydrogen bonds to every other ether oxygen atoms in the PEO chain.

1. Introduction

Poly(ethylene oxide) (PEO), $(–OCH_2CH_2–)_n$, is one of the most important polymers in industrial, biotechnical and biomedical fields.[1,2] A large number of structural studies based on X-ray diffraction,[3–7] infrared (IR),[8–11] Raman,[12,13] and nuclear magnetic resonance (NMR) spectroscopies,[14,15] and also numerical computation studies such as quantum chemical calculations (QCCs)[16,17] and molecular dynamics (MD)[18] have been conducted on PEO as well as poly(ethylene glycol) (PEG) and poly(oxyethylene) (POE) in crystalline or random-coil phases. Several studies have noted a preference for a gauche conformation in the C–C bond of POE in not only the crystalline phase but also in solutions.[3–15] While a trans conformation in the C–O bond has been found to be dominant in dried PEO with a 7/2 helical structure in the crystalline phase,[3] both gauche and trans conformations in the C–O bond have been known to exist in aqueous solutions.[8,9]

Recently, PEO, which is highly water-soluble and has high gelability and low toxicity, has been applied in extended drug-release systems as a hydrogel-forming polymer in the pharmaceutical field.[19–22] The hydrogelling phenomena of PEO matrix tablets have been explored using several visualization techniques, such as magnetic resonance imaging (MRI),[23,24] IR imaging,[25] and visible photography.[26] However, macromolecular structure changes in a PEO chain during hydrogelation have not been well investigated. A better understanding of the drug-release mechanism from PEO hydrogel matrices will require the investigation of this compound's inherent physical properties and its hydrogelation phenomena.

Many research groups have investigated the hydrogen bonding interactions between

POE and water molecules by experimental[8–11] and computational approaches[16–18] such as a monodentate hydration structure, with only one OH group in a water molecule donating a hydrogen bond to the POE chain, and bidentate ones, with the two OH groups in a water molecule donating two different hydrogen bonds to the first or the second available oxygen atom from another hydrogen bonding in POE. Kitano et al.[10] and Tasaki[18] have discussed the hydrogen bonding about not only POE–water but water–water by using IR and NMR, respectively. Further, Wahab et al.[16] have theoretically examined for the above all hydration structures of short chain POE ($CH_3(OCH_2CH_2)_mOCH_3$, m=1 and 2), and demonstrated the bidentate hydration structure where the second available oxygen atom from another hydrogen bonding in POE is more stable than that where the adjacent ones in the gas phase by QCC. While extensive research has been conducted on the most favorable conformations of POE in crystalline phase and aqueous solutions, little attention has been focused on the conformational changes of the polymer chain during hydrogelation from a dried state in the crystalline phase to a hydrated state in a swollen gel.

The purpose of the present study is to explore time-resolved conformational variations of the PEO chain during the hydrogelling process by using in situ IR transmission spectroscopy with a newly designed flow-cell. Attenuated total reflection infrared (ATR–IR) spectroscopy has been widely applied in investigations of the hydration structure of various polymers.[27–29] However, quantitative analysis at the same depth position is difficult in ATR–IR spectroscopy, as the penetration depth of an incident IR beam in a polymer sample depends on the IR vibrational frequency.[30] Here, to avoid this problem, I used IR transmission spectroscopy to examine PEO

hydrogelation, as was done in previous investigations involving POE.[10,11] A flow-cell for the IR transmission spectroscopy with a headrace groove for water supply was newly designed for this experiment (Figure 1). There are a few studies that obtained IR spectra are treated with fourth derivatives to acquire reliable peak resolution of overlapped bands,[31,32] although high-ordered derivative spectra are not generally used for understanding IR spectra. In an ultraviolet-visible study, however, the fourth derivative processing is widely applied to improve their peak resolutions and prevent the intensity changes from affecting adjacent large peaks.[33,34] Therefore, in this study, both second and fourth derivative processing were also applied. Further, obtained spectra-structure correlations were examined by conducting QCCs based on density functional theory (DFT) using a short chain model of PEO.

2. Experimental

2.1. Materials

PEO (average molecular weight: 7.0×10^6 g·mol^{-1}; Polyox WSR 303) was obtained from Dow Chemical. I used high-molecular-weight PEO in the present study to minimize against effects of the terminal OH group on the hydration structure. Ultrapure water with a resistivity of 18.2 MΩ·cm was prepared using a Milli-Q system (Milli-Q gradient A10; Millipore). All other chemicals used were of reagent grade. I prepared 10 mg·mL^{-1} of PEO aqueous and dichloromethane solutions by stirring for 3 days at room temperature.

2.2. Infrared Measurements

To obtain IR spectra of the hydrated polymer and penetrated water solely excluding

bulk water, I specially constructed a homemade flow-cell for *in situ* IR transmission spectroscopy. The cell was designed with a groove to facilitate smooth medium penetration despite the wafer-thin distance between the two crystal plates, as shown in Figure 1. The PEO film was sandwiched between two barium fluoride (BaF_2) crystal plates with a 15-μm thick teflon spacer. The sample in the cell was dried at 40 °C under vacuum (Vacuum Drying Oven DP23; Yamato Scientific) for a day using dry silica gel. All IR spectra were measured at a spectral resolution of 2 cm^{-1} using a Fourier transform IR spectrometer (NEXUS 870; Thermo Fisher Scientific) equipped with a deuterated triglycine sulfate detector. The IR flow-cell with dried PEO film was placed in a sample room of the IR spectrometer under a low-humidity environment purged by nitrogen gas. A total of 64 scans were co-added to obtain each spectrum. IR spectra of liquid samples, including bulk water, were also measured using the same flow-cell with a 6-μm thick spacer. Hydrogelation of the PEO film was examined by flowing water into the flow-cell. Time-dependent spectra were obtained every 5 min. All IR spectra were defined in absorbance units as $A = -\log_{10}(I/I_0)$, where I and I_0 represent the intensities of IR light with and without the PEO sample in the flow-cell, respectively.

The second derivatives of the IR spectra obtained were calculated by the 9-point Savitzky-Golay method[35] using specially developed software after the spectra were subjected to 7-point Kawata-Minami smoothing,[36] and the fourth derivatives were obtained by repeating the second derivative processing twice.

2.3. Synchrotron X-ray Diffraction

To obtain XRD data of hydrogelled PEO, a synchrotron XRD with strong beam intensity was applied. For this experiment, a disk-shaped tablet 8-mm in diameter and approximately 1-mm thick was prepared by compressing 50 mg of PEO powder. Synchrotron XRD data were obtained at the beamline BL32B2 using a Debye-Scherrer camera equipped with a curved image plate detector at the SPring-8 synchrotron facility. The PEO tablet was fixed in a tablet holder before and after hydration and set on the tablet measurement system (SAI). XRD data were recorded using a wavelength of 1.24 Å and a data collection time of 3 min.

2.4. Quantum Chemical Calculations

Diethyleneglycol diethyl ether ($CH_3CH_2(OCH_2CH_2)_2OCH_2CH_3$, DGDE) was used as a short chain model of PEO, and it and its hydration structures were optimized their structures and calculated their vibrational wavenumbers, IR intensities, and self-consistent fields (SCF). In this study, not only a combinations of a DGDE and a water molecules but also those of a DGDE and multi-water molecules, and those of two DGDEs and multi-water molecules were applied to the computational simulation. All QCCs were carried out based on DFT using a B3LYP function and a 6-31G(d) base set by the Gaussian 03 program.[37–39] The force fields calculated at the B3LYP/6-31G(d) level were scaled down using a single scale factor of 0.9613. The bonding energy via hydrogen bonds with a water molecule, defined as the energy difference before and after separation of each optimized free and hydrated structure, was calculated using their SCF energies.

2.5. Gravimetric Measurement.

PEO tablets 8-mm in diameter and approximately 4-mm thick was prepared by compressing 200 mg of PEO powder. The hydrogelling properties of the tablet was evaluated via the flow-cell apparatus (DZ70; Pharma-Test AG, Hainburg, Germany) at a flow rate of 4 mL/min in a closed loop circuit containing 900 mL of water at 37 °C following a pharmacopoeia. A metal clip was used to hold the tablet in the original position. Every four hours, the tablet was taken out from the flow-cell and the amount of water was weighed before and after water evaporation.

3 Results and Discussion

3.1. Infrared Spectra of Poly(ethylene oxide)

Figures 2a, 2b, and 2c show IR spectra in the 4000-900 cm^{-1} region of a dried PEO film, a hydrated PEO film and liquid water, respectively. Further, their second or fourth derivatives are also shown at the bottom of each figure. The IR spectrum of the PEO dried film (Figure 2a) is completely consistent with that of the PEO tablet reported in my previous study.[24] The O-H stretching band located at approximately 3350-3300 cm^{-1} was barely detected in the dried PEO film, because of the small molar fraction of the terminal OH groups (ca. 1.3×10^{-3} %) in a PEO chain compared with the ethylene glycol units.

Relatively sharp peaks in the 3000-2700 cm^{-1} region are due to the C–H stretching of PEO, and the most intense band in the 1200-1000 cm^{-1} region is assigned to the C–O–C stretching.[8,9] Detailed assignments for major IR bands of crystalline and random-coil phases PEO are summarized in Table 1. Further, an intense and saturated

O–H stretching band in the 3700–3000 cm^{-1} region and an O–H deformation band in the 1750–1550 cm^{-1} region are identified in the IR spectra of the hydrated PEO film and water. The bands assigned to water in the spectrum of the hydrogel (Figure 2b) are much more intense than those assigned to PEO (Figure 2a), implying the presence of a large number of water molecules in the hydrogel which are more or less similar to those for bulk water (Figure 2c), though the O–H stretching band is saturated. These results demonstrate the difficulty in differentiating the hydration structure of PEO from the bands assigned to water in the spectrum of the equilibrium-swelled hydrogel, as bulk-like water molecules co-exist in the hydrogel.

Figures 3a and 3b represent close-up spectra in the CH_2 wagging and twisting bands (A: 1400-1250 cm^{-1}) and the C–O–C stretching band (B: 1200-1000 cm^{-1}) regions of the dried and hydrated PEO films shown in Figures 2a and 2b, respectively. The spectra shown in Figures 3c and 3d are difference spectra calculated by subtracting the spectra of water and dichloromethane from those of PEO aqueous and dichloromethane solutions, respectively. The CH_2 wagging and twisting bands of the crystalline PEO associated with the C–C gauche and C–O trans conformations are located at 1343 and 1280 cm^{-1}, respectively, whereas those of the random-coil-associated bands are indentified at 1350 and 1288 cm^{-1}, respectively.[9] These observations demonstrate that the bands arising from the crystalline phase PEO have lower wavenumbers than those from the random-coil phase PEO, due to effects of crystal packing as well as other polymers.[40,41] Further, CH_2 wagging and twisting bands associated with the C–C trans and the C–O gauche conformations are also detected in the random-coil state, at 1329 and 1305 cm^{-1}, respectively.

The observed ratios of the band intensities at 1350 and 1329 cm^{-1}, and at 1305 and 1288 cm^{-1}, arising from the gauche/trans conformations of the C–C and C–O bonds of the POE solution are almost identical to those reported by Begum and Matsuura.[9] The CH_2 wagging and twisting bands of the PEO hydrogel and the aqueous solution (Figure 3b and 3c) are located at the same wavenumbers as those of the PEO dichloromethane solution (Figure 3d), suggesting that those bands are not affected and shifted by forming a hydrogen bonding with hydroxyl groups in water molecules, as dichloromethane has no hydroxyl group in its structure.

The C–O–C asymmetric stretching band of PEO for the aqueous solution and the hydrogel observed at 1112 cm^{-1} shifts to a position approximately 30 cm^{-1} lower than that for the crystalline phase, while the corresponding band of the dichloromethane solution shows only a small shift. These findings indicate that this band position shift is indeed caused by the hydrogen bond between the ether oxygen atom in PEO and the OH group in water or in another PEO, as reported previously.[3–10,16,18,24] In this study, however, the small molar fraction of the terminal OH groups compared with the ethylene glycol units enables me to focus only on the hydrogen-bonding interaction with water. In other words, regarding high-molecular-weight PEO, the hydrogen-bond interaction of terminal-OH in PEO is negligible.

3.2. Crystallographic Structure of Poly(ethylene oxide) Hydrogel

Figures 4a and 4b depict XRD patterns of a PEO tablet after and before hydrogellation. The XRD patterns showed two intensive and sharp diffractions at 2 θ = 19.2° and 23.4° and other ones at 2 θ = 26.4° and 27.1° which are characteristic

diffractions of a 7/2 helix PEO crystalline structure.[5–7] These characteristic crystalline peaks were observed for the dried PEO tablet but not for the hydrogel, in which I observed only a broad XRD pattern. These results suggest that the crystalline phase in the dried PEO was completely altered to a random-coil phase by hydration.

As described above, I noted evidence of helical conformation in the crystalline phase on examining the IR spectrum of the dried PEO film, given the presence of the C–O–C stretching band at 1061 cm^{-1} (Figure 3a) which was absent from the spectra of the hydrogel and the aqueous solution (Figures 3b and 3c). These results demonstrate that water penetration into the film disrupts the crystalline structure in the PEO chain,[24] a notion also supported by XRD findings. Further, as discussed above, the similarities between the IR spectra of the PEO dried film and the tablet indicate that the crystallographic structures of the dried film and the tablet are also the same, because absorption profiles of the parallel bands have been reported to change with crystal morphology.[42,43]

3.3. Time-resolved Infrared Spectra

Enlarged time-resolved *in situ* IR spectra and their second or fourth derivative ones of the PEO film hydration process for the 1400-1250 and 1200-1000 cm^{-1} regions are shown in Figures 5A and 5B, respectively. Those overlapped bands were seen more clearly in the second or fourth derivatives of the spectra. Intensities of the bands located at 1343 and 1323 cm^{-1} (C–C gauche and trans conformations in the crystalline phase, respectively) decreased with time, whereas those at 1350 and 1329 cm^{-1} (C–C gauche and trans conformations in the random-coil phase, respectively) increased. The

band at 1280 cm^{-1} (C–O trans conformation in the crystalline phase) decreased, while those at 1305 and 1288 cm^{-1} (C–O gauche and trans conformations in the random-coil phase, respectively) grew more intense. The C–O–C asymmetric stretching band located at 1112 cm^{-1} shifted to an approximately 30 cm^{-1} lower wavenumber over time, due to hydration of the ether moiety. The C–O–C symmetric stretching band located at 1061 cm^{-1} arising from helical conformation of the chain in the crystalline phase[4] disappeared during hydrogelation.

3.4. Hydration Structure Analysis by Quantum Chemical Calculation

Figure 6 illustrates optimized structures for hydration by a monodentate, with only one OH group in a water molecule donating a hydrogen bond to the DGDE chain in type I, and ones for hydration by a bidentate, with the two OH groups in a water molecule donating two different hydrogen bonds to the DGDE chains; the O3 and O6 oxygen atoms in DGDE are hydrated in type II, whereas O3 and O9 are hydrated in type III structures. Table 2 shows their calculated vibrational wavenumbers, IR intensities, and self-consistent fields (SCF). Numerous conformations are possibly available for DGDE, though, in view of the experimental results and previous studies, I will discuss a portion of these cases consistent with the IR and XRD results for the helical ($TT\underline{G}^{+}TT\underline{G}^{+}TT$) and random-coil conformations ($TT\underline{G}^{+}G^{+}S^{-}\underline{G}^{-}TT$) of DGDE using QCCs, with T, G^{+}, G^{-}, and S^{-} denoting the trans, clockwise and counterclockwise gauche, and counterclockwise skew (anticlinal) conformations, respectively, with the underlined conformation originating at the C–C bond.

Calculated vibrational wavenumbers of optimized DGDEs in the C–O–C stretching

region are summarized in Table 2. The calculated wavenumbers of C–O–C stretching for hydrated DGDEs with random-coil structures in type I and III are shifted approximately 14 and 22 cm^{-1} lower, respectively, than those for non-hydrated DGDE with a helical structure. The hydration structure of Type II is somewhat unstable, and as a result, optimized to that of Type III under the base set. An approximately 30 cm^{-1} downwards band shift for the C–O–C stretching at 1112 cm^{-1} was observed during hydration, implying that the hydration structure of type III dominates over other types. The SCF findings demonstrate that the hydration structure of type III has the strongest hydrogen bonding energy of all assumed structures and further support the notion that the type III structure is the most favorable for the actual hydrated PEO chain (Table 2). In addition, the observations here regarding optimized hydration structure indicate that the dominant structure in a random-coil PEO involves a skew conformation, which has been reported in previous polyethylene studies.[44–46] Further, every oxygen atom in PEO and water is able to have up to two hydrogen bondings as a proton acceptor. Optimized structures of a several combinations of DGDEs and multi-water molecules are depicted in Figure 7. Figure 7 g and h illustrate optimized structures for additionally-hydration by a monodentate to at O6 and O9 of hydrated DGDE in the type III conformation. After optimization, however, the former hydrogen bonding at O6 is dissociated and newly created another hydrogen bonding with an oxygen atom in a water molecule because of its more stable form. A hydrogen bonding between an ether oxygen atom at O6 and a water molecule is formed after two protons in a water molecule are taken by other hydrogen bondings (Figure 7i). Further, Figure 7 j and k shows the optimized conformations of intra-polymers networks via water molecules.

Calculated vibrational wavenumbers of optimized DGDEs in the C–O–C stretching region and their SCF energies are summarized in Table 3. The calculated wavenumbers of C–O–C stretching for hydrated DGDEs and observed broaden IR band suggest that some types of hydrogen bonding structure must be created in a hydrogel. Further, the SCF energies indicate that the Figure 7i conformation is much stably existed via strong hydrogen bondings.

Although QQC is a very useful and solid investigation tool, the experimental portion of the present study has enabled selection of several favorable structures. Further, two other parameters critical for calculations must be considered for the final estimation of the hydration structure: the difference between the oligomer and polymer, and the effect of environmental conditions. The former accounts for the steric barrier of the polymer chain, while the latter concerns hydrophobic interactions among hydrophobic moieties and the dielectric constant of water. In this study, however, the QCC study helped me not only to assign the IR bands of PEO, but also to estimate the optimal hydration structure.

3.5. Crystal Destruction and Hydrogelling Behaviors

In order to obtain reliable peak resolution of overlapped bands and prevent the intensity changes from affecting adjacent large peaks, second or fourth derivative processing[31–34] was applied to the obtained IR spectra. Further, to compare spectral intensity variations as a function of time, normalized intensity of derivative spectra from 0 to 600 min was employed as $I_{\text{t-normalized}} = | (I_t - I_0)/(I_{max} - I_{min})|$, where I_t and I_0 are the intensities of IR light at times t and 0, respectively, and I_{max} and I_{min} are the

maximum and minimum intensities of each IR band during hydrogellation, respectively.

Normalized intensities of the fourth derivative of the associated C–C bands (CH_2 wagging bands) at 1350, 1343, 1329 and 1323 cm^{-1} as a function of time are shown in Figure 8Aa, while intensities of the second derivative of the associated C–O bands (CH_2 twisting bands) at 1305, 1288 and 1280 cm^{-1} are shown in Figure 8Ab. The less the PEO crystal was destructed, the greater the increase in number of PEO random-coils due to CH_2 wagging and twisting bands. Normalized intensities of the fourth derivative of the C–O–C stretching bands at 1112, 1080 and 1061 cm^{-1} are shown in Figure 8Ac. These findings show a lack of correlation among behaviors of the three bands.

I also evaluated the behavior of the PEO hydrogelation from an alternate point of view, and Figure 8Ba and 8Bb shows the normalized intensity changes of the crystal destruction and hydrogelation of PEO about the C–O and the C–C bands plotted in Figure 8A. I found that the normalized intensity variations around the C–C moiety change prior to those about the C–O moiety, indicating that water molecules interact with the C–C moiety before the C–O moiety in the PEO chain. Further, although the crystal C–O–C band at 1112 cm^{-1} is destructed together with the C–C band at 1343 cm^{-1} (Figure 8Ba), my observation that the hydrated C–O–C band at 1080 cm^{-1} behaves differently from the others (Figure 8Bb) indicates that the hydration/hydrogellation process of PEO is comprised of several steps. In contrast to the crystal C–O–C band at 1112 cm^{-1}, another crystal C–O–C band at 1061 cm^{-1} corresponding to the helical conformation changed as fast as the crystal C–O band at

1280 cm^{-1}.

Figure 9 illustrates the IR intensity ratio changes of random-coil C–O trans and gauche bands at 1288 and 1305 cm^{-1}. A large majority of random-coil trans conformations gradually transition to gauche ones at an early stage, and the speed of this conformation change increases with enhancing flexibility of PEO molecules in the hydrogel. in accordance with swelling and hydrogelling, until eventually, nearly three quarters of C–O trans conformations are shifted to gauche ones, which structure transition behavior corresponds approximately to the intensity changes of the hydrated C–O–C band at 1080 cm^{-1}, particularly in the second stage (120 to 240 min). The multiple-step hydrogelling behavior will be discussed below.

3.6. Hydrogellation Mechanism

The hydrogelation process of PEO solid with crystal destruction is likely to be composed of several steps. After water penetration, the hydrophobic ethylene unit ($–CH_2–CH_2–$) and hydrophilic ether oxygen atom (–O–) seek out conformations more stable than the crystal packed state and adopt a stable, hydrated random-coil form with water molecules via hydrogen bonding. The hydrophobic units rapidly shift to random-coil gauche conformations as water molecules approach the PEO molecule (see Figures 8B), whereas hydrophilic units hydrogel more slowly and shift from crystal trans conformations to random-coil gauche, trans, or skew conformations. In addition, during the hydration of the ether oxygen atoms, mono-hydrated structures like the type I form in figure 6 are first quickly created with water molecules following the water penetration, and after acquiring mobility as a hydrogel, the every other

oxygen atoms combine bridged and bi-hydrated conformations like type III form to form an even more stable structure. Further, the bridged and bi-hydrated water molecules must be create two other hydrogen bonds with other water molecules.

Furthermore, the gravimetric result after soaking a tablet in water for 4, 8 and 12 hours are shown in Figure 10. The finding demonstrates that a large number of water molecules are absorbed each ethylene oxide unit in a PEO hydrogel tablet, indicating that there are a lot of free water molecules which are not hydrated with the ether oxygen atoms in the hydrated PEO and create hydrogen bondings with other water molecules. Consequently, the majority of water molecules create hydrogen bondings among them and make water clusters like bulk water.

4. Summary

In this investigation into the process of hydrogelation of a PEO film using time-resolved *in situ* IR spectroscopy, new insights into the hydrogelation behavior of a semicrystalline PEO solid have been provided. The time-resolved IR study has revealed that C–C bonds with hydrophobic moieties rapidly shift to a random-coil gauche conformation after water penetration, whereas C–O bonds with hydrophilic moieties hydrogel more slowly, with at least half of these bonds changing from trans to gauche conformations after hydration. In addition, I identified two main steps in hydration during PEO hydrogelation: First, the ether oxygen atoms in PEO become hydrated as mono-hydrated structures are created with water molecules following rapid water penetration. Then, they convert to the bridged hydration form as the most stable structure.

The calculated wavenumbers and interaction energies obtained by QCC using a model oligomer of DGDE instead of an actual PEO chain supported my estimation of the spectra-structure correlation of the hydrated PEO. The C–C gauche structure is important in maintaining a bridged hydrogen bonding network with water molecules. IR spectroscopy with a flow-cell is well suited to investigating hydration mechanisms of PEO hydrogel matrix tablets. Conducting such a study as performed here may eventually allow me to understand the physical properties of pharmaceutical drug delivery products in water.

5. References

1 *Poly(ethylene glycol) Chemistry: Biotechnical and Biomedical Applications*; Harris, J. M., Ed.; Plenum: New York, 1992.

2 *Poly(ethylene glycol): Chemistry and Biological Applications*; Harris, J. M.; Zalipsky, S., Eds.; American Chemical Society: Washington DC, 1997.

3 Takahashi, Y.; Tadokoro, H. *Macromolecules*, 1973, 6, 672–675.

4 Brubach, J. B.; Ollivon, M.; Jannin, V.; Mahler, B.; Bourgaux, C.; Lesieur, P.; Roy, P. *J. Phys. Chem. B* 2004, 108, 17721–17729.

5 Vasanthan, N.; Shin, I. D.; Tonelli, A.E. *Macromol.* 1996, 29, 263–267.

6 Tanaka, S.; Ogura, A.; Kaneko, T.; Murata, Y.; Akashi, M. *Macromol.* 2004, 37, 1370–1377.

7 Choi, Y. W.; Park, J.; Park, Y.; Kim, K.; Lee, Y.; Sohn, D. *J. Phys. Chem. B* 2007, 111, 12959–12963.

8 Shephard, J. J.; Bremer, P. J.; McQuillan, A. J. *J. Phys. Chem. B* 2009, 113, 14229–14238.

9 Begum, R.; Matsuura, H. *J. Chem. Soc., Faraday Trans.* 1997, 93, 3839–3848.

10 Kitano, H.; Ichikawa, K.; Ide, M.; Fukuda, M.; Mizuno, W. *Langmuir* 2001, 17, 1889–1895.

11 Kusanagi, H.; Yukawa, S. *Polymer* 1994, 35, 5637–5640.

12 Yoshihara, T.; Tadokoro, H.; Murahashi, S. *J. Chem. Phys.* 1964, 41, 2902–2911.

13 Maxfield, J; Shepherd, I. W. *Polymer* 1975, 16, 505–509.

14 Inomata, K.; Abe, A. *J.Phys.Chem.* 1992, 96, 7934–7937.

15 Björling, M.; Karlström, G.; Linse, P. *J.Phys.Chem.* 1991, 95, 6706–6709.

16 Wahab, S.A.; Harada, T.; Matsubara, T.; Aida, M. *J. Phys. Chem. A* 2006, 110, 1052–1059.

17 Aray, Y.; Marquez, M.; Rodriguez, J.; Vega, D.; Simón-Manso, Y.; Coll, S.; Gonzalez, C.; Weitz, D. A. *J. Phys. Chem. B* 2004, 108, 2418–2424.

18 Tasaki, K. *J. Am. Chem. Soc.* 1996, 118, 8459–8469.

19 Graham, N. B.; McNeill, M.E. *Biomaterials 1984, 5*, 27–36.

20 Kim, C. J. *J. Pharm. Sci.*, 1995, 84, 303–306.

21 Sako, K.; Nakashima, H.; Sawada, T.; Fukui, M. *Pharm. Res.* 1996, 13, 594–598.

22 Kojima, H.; Yoshihara, K.; Sawada, T.; Kondo, H.; Sako, K. *Eur. J. Pharm. Biopharm.* 2008, 70, 556–562.

23 Abrahmsén-Alami, S.; Körner, A.; Nilsson, I.; Larsson, A. *Int. J. Pharm.* 2007, 342, 105–114.

24 Tajiri, T.; Morita, S.; Sakamoto, R.; Suzuki, M.; Yamanashi, S.; Ozaki, Y., Kitamura, S. *Int. J. Pharm.* 2010, 395, 147–153.

25 Coutts-Lendon, C. A.; Wright, N. A.; Mieso, E. V.; Koenig, J. L. *J. Control. Release* 2003, 93, 223–248.

26 Wu, N.; Wang, L. S.; Tan, D. C. W.; Moochhala, S. M.; Yang, Y. Y. *J Control. Release* 2005, 102, 569–581.

27 Hajatdoost, S.; Yarwood J. *J. Chem. Soc. Faraday Trans.* 1997, 93, 1613–1620.

28 Morita, S.; Tanaka, M.; Ozaki, Y. *Langmuir* 2007, 23, 3750–3761.

29 Tajiri, T.; Morita, S.; Ozaki, Y. *Polymer* 2009, 50, 5765–5770.

30 Chalmers, J. M.; Griffths, P. R. *Handbook of Vibrational Spectroscopy*, John

Wiley & Sons: New York, 2001.

31 Fleissner, G.; Hallbrucker, A.; Mayer, E. *J. Chem. Soc., Faraday Trans.* 1996, 92, 23–28.

32 Fleissner, G.; Hage, W.; Mayer, E. *Appl. Spec.* 1996, 50, 1235–1245.

33 Fell, A. F.; Jarvie, D. R.; Stewart, M. J. *Clin. Chem.* 1981, 2712, 286-292.

34 Lange, R.; Bec, N.; Mozhaev, V. V.; Frank, *J. Eur. Biophys. J.* 1996, 24, 284-292.

35 Savitzky A, Golay M. J. E. *Anal. Chem.* 1964, 36, 1627–1639.

36 Kawata S, Minami S. *Appl. Spectrosc.* 1984, 38, 49–58.

37 Becke, A. D. *J. Chem. Phys.* 1993, 98, 5648–5652.

38 Johnson, B. G.; Frisch, M. J. *J. Chem. Phys.* 1994, 100, 7429–7442.

39 Frisch, M. J.; Trucks, G. W.; Schlegel, H. B.; Scuseria, G. E.; Robb, M. A.; Cheeseman, J. R.; Zakrzewski, V. G.; Montgomery, J. A. J.; Stramann, R. M. C.; Burant, J. C.; Dapprich, S.; Millam, J. M.; Daniels, A. D.; Kudin, K. N.; Strain, M. C.; Farkas, O.; Tomasi, J.; Barone, V.; Cossi, M.; Cammi, R.; Mennucci, B.; Pomelli, C.; Adamo, C.; Clifford, S.; Ochterski, J.; Petersson, G. A.; Ayala, P. Y.; Cui, Q.; Morokuma, K.; Malick, D. K.; Rabuck, A. D.; Raghavachari, K.; Foresman, J.B.; Cioslowski, J.; Orits, J.V.; Stefanov, B.B.; Liu, F.; Liashenko, A.; Piskorz, P.; Komaromi, I.; Gomperts, R.; Martin, R. L.; Fox, D. J.; Keith, T.; Al-Laham, M. A.; Peng, C. Y.; Nanayakkara, A.; Gonzalez, C.; Challacombe, M.; Gill, P. M. W.; Johnson, B. G.; Chen, W.; Wong, M. W.; Andres, J. L.; Head-Gordon, M.; Replogle, E. S.; Pople, J. A. *Gaussian 03, Revision B.05*;Gaussian, Inc., Pittsburgh, PA, 2003.

40 Sato, H.; Ando, Y.; Dybal, J.; Iwata, T.; Noda, I.; Ozaki, Y. *Macromolecules* 2008, 41, 4305–4312.

41 Zhang, J.; Tsuji, H.; Noda, I.; Ozaki, *Y. J. Phys. Chem. B* 2004, 108, 11514–11520.

42 Kobayashi, M.; Sakashita, M. *J.Chem. Phys.* 1992, 96, 748–760.

43 Tanabe, Y.; Shimomura, M. *Macromolecules* 1990, 23, 5031–5034.

44 Schilling, F. C.; Amundson, K. R. *Macromolecules* 1994, 27, 6498–6502.

45 Fuson, M. M.; Klei, B. R. *Macromolecules* 1996, 29, 5223–5227.

46 Smith, G. D.; Paul, W. *J. Phys. Chem. A* 1998, 102, 1200–1208.

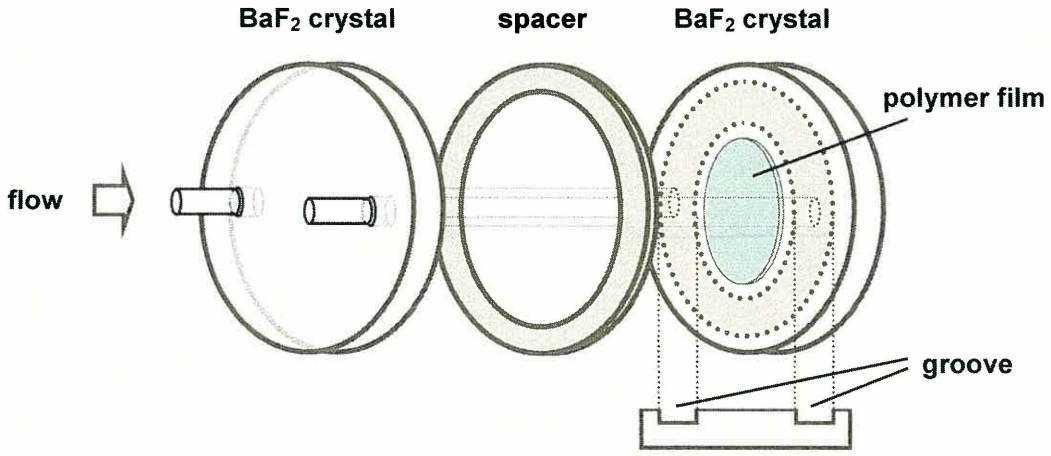

Figure 1. Schematic illustration of *in situ* transmittance IR flow-cell used in the present study

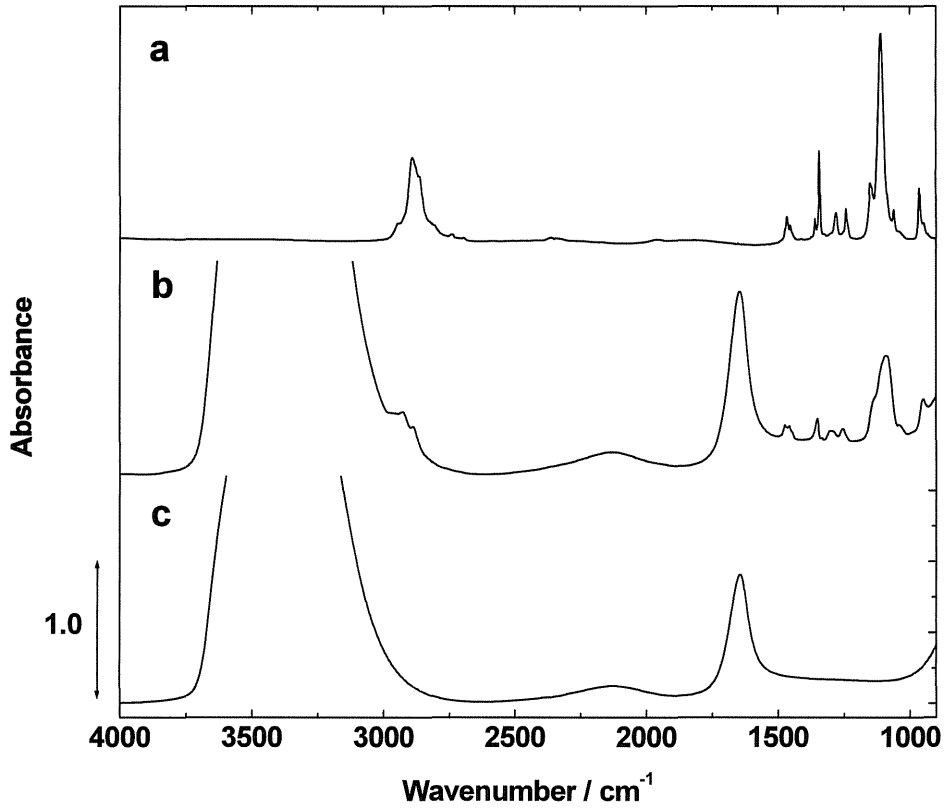

Figure 2. IR spectra in the 4000-900 cm^{-1} region of (a) dried PEO film, (b) hydrated PEO film, and (c) liquid water.

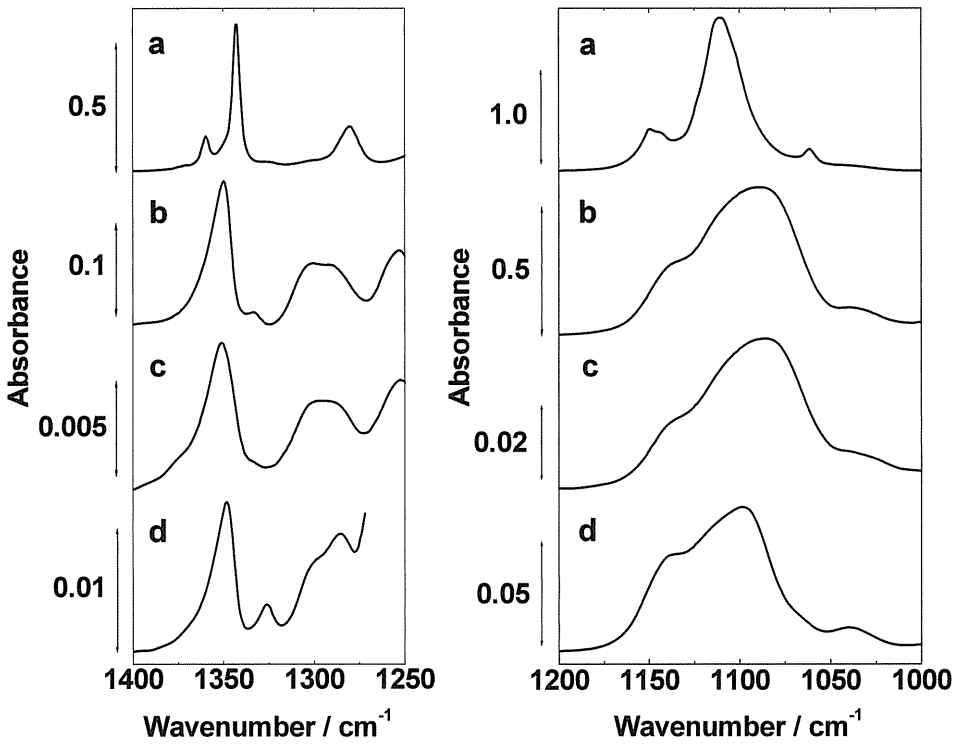

Figure 3. IR spectra of (a) dried PEO film, (b) hydrated PEO film, (c) PEO aqueous solution, and (d) PEO dichloromethane solution in the CH_2 wagging and twisting band region (1400-1200 cm^{-1}); left and the C–O–C stretching band region (1200-1000 cm^{-1}); right, respectively.

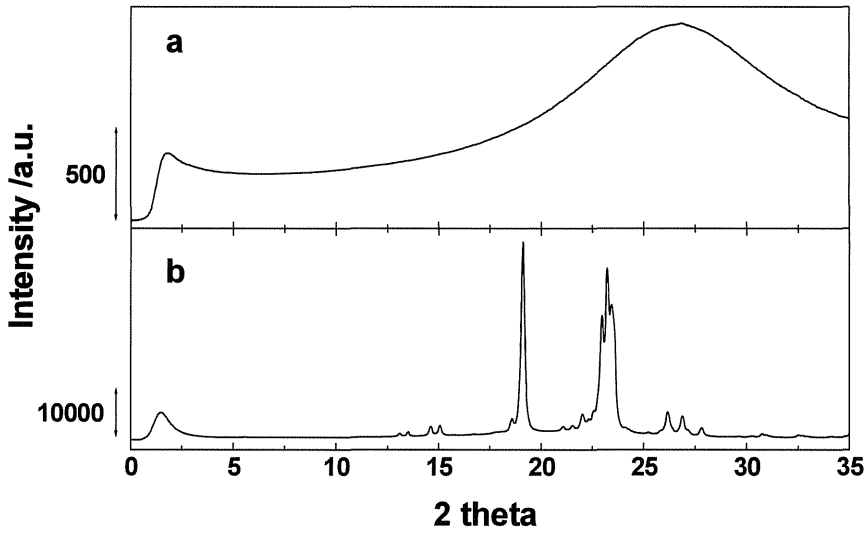

Figure 4. XRD patterns of dried and hydrated PEO tablets.

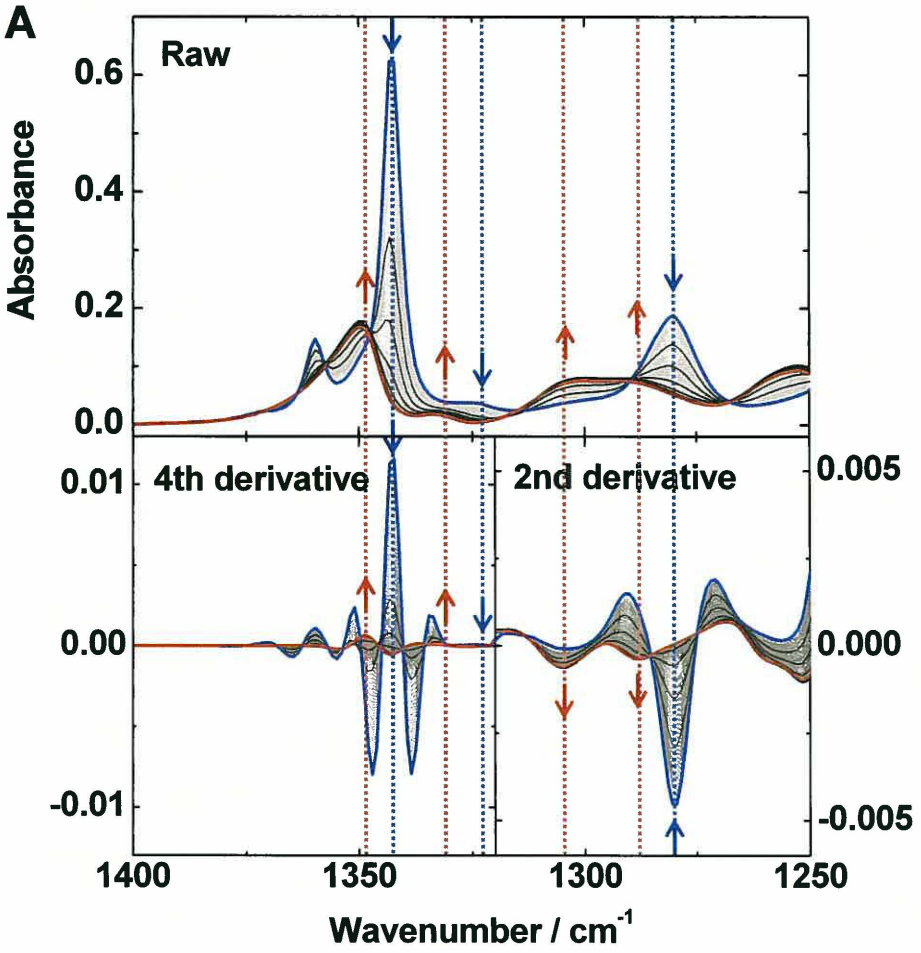
A
Raw
Absorbance
0.6
0.4
0.2
0.0
4th derivative
2nd derivative
0.01
0.00
-0.01
0.005
0.000
-0.005
1400
1350
1300
1250
Wavenumber / cm-1

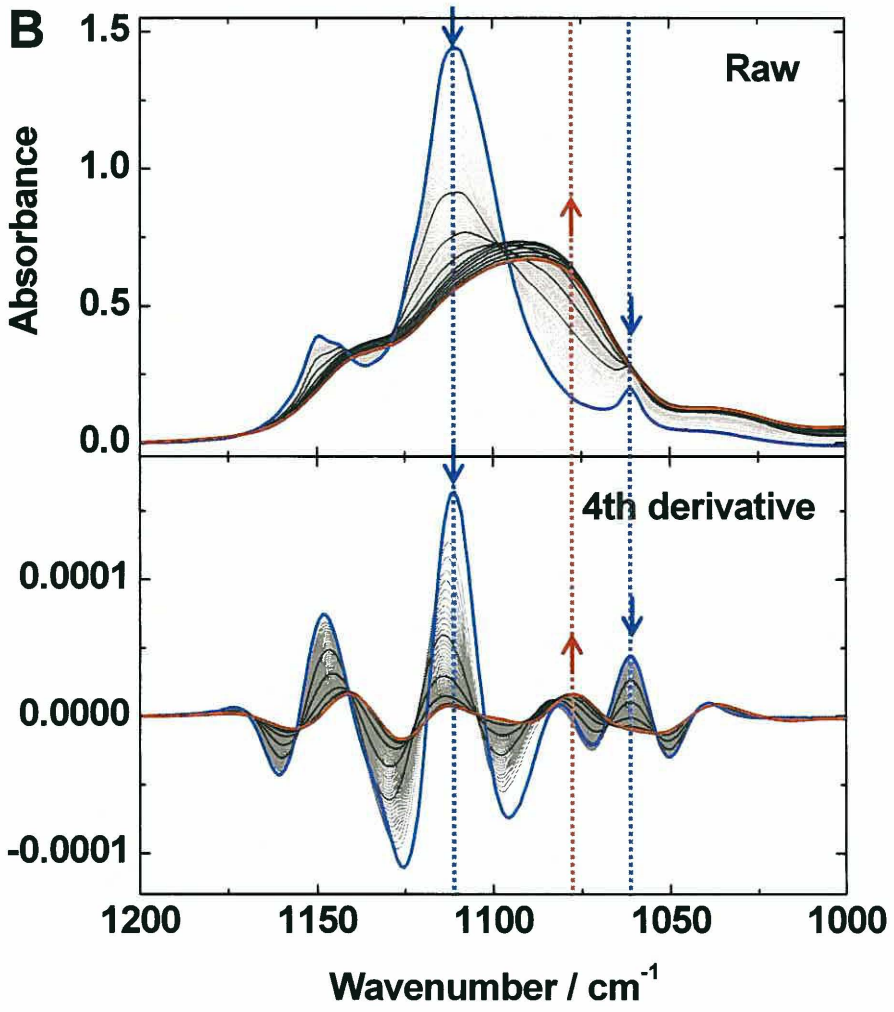

Figure 5. Time-resolved IR spectra and their second and fourth derivative ones of PEO film hydration, taken every 5 min from 0 to 600 min after initiation, in (A) the CH_2 wagging and twisting band region (1400-1200 cm^{-1}) and (B) C–O–C stretching band region (1200-1000 cm^{-1}), respectively. Before (blue line) and after hydration (red line), and every 60 min (black line).

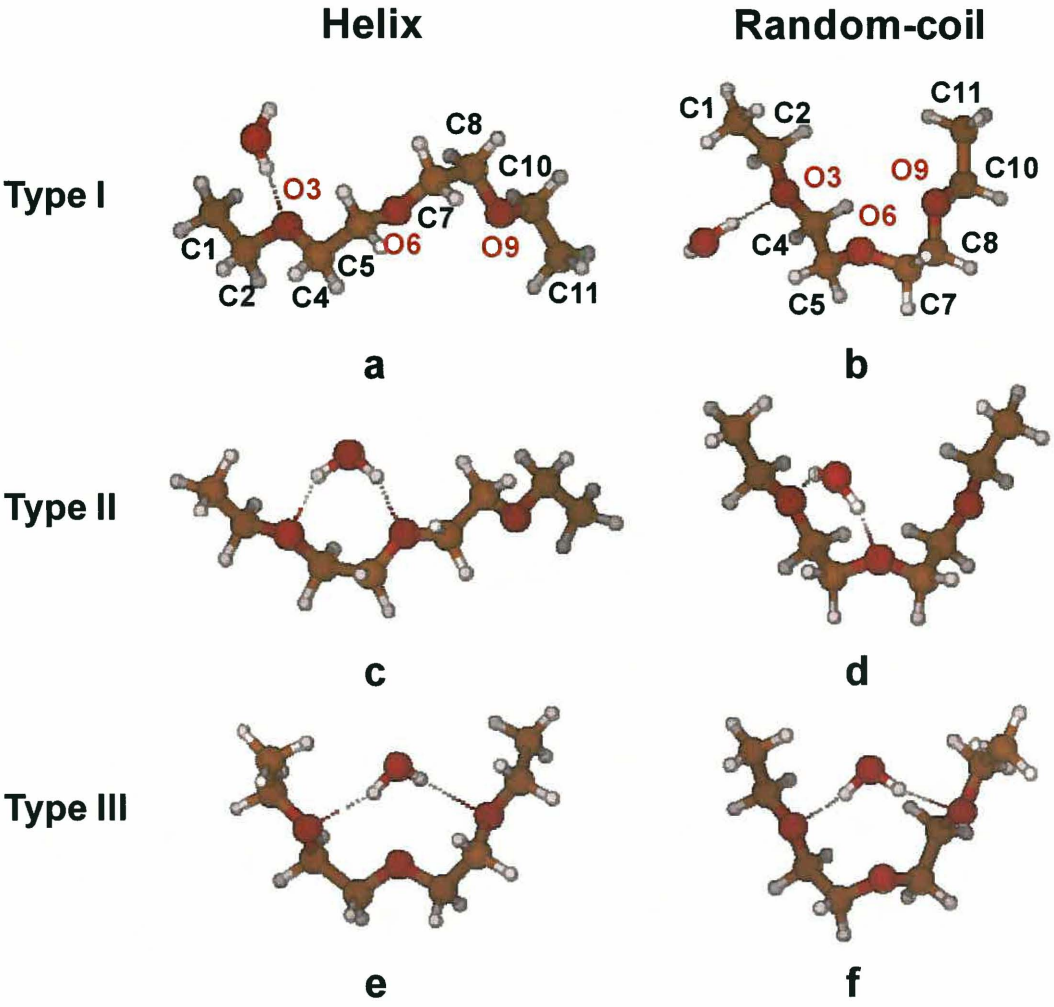

Figure 6. Schematic illustrations of helical and random-coil diethyleneglycol diethyl ether ($CH_3CH_2(OCH_2CH_2)_2OCH_2CH_3$; DGDE) structures. Type I, mono-hydrated DGDE at the O3-position; type II, bi-hydrated DGDE at the O3,O6-position; type III, bi-hydrated DGDE at the O3,O9-position. Helical structure: $TT\underline{G^+}TT\underline{G^+}TT$; random-coil structure: $TT\underline{G^+}G^+S^-\underline{G^-}TT$, where T, G^+, G^- and S^- denote the trans, clockwise and counterclockwise gauche and counterclockwise skew (anticlinal) conformations, respectively, and the underlined conformation originates at the C–C bond.

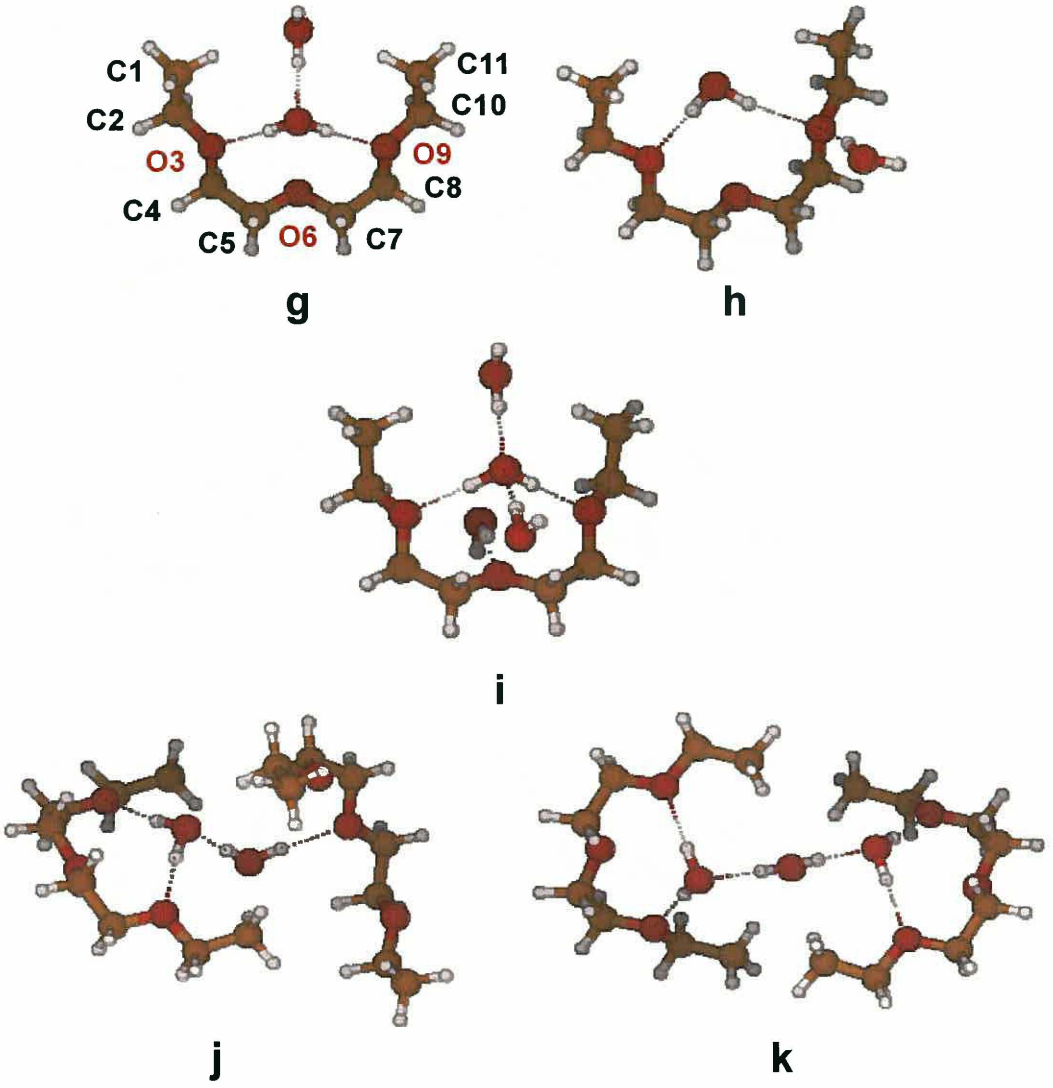

Figure 7. Schematic illustrations of hydrogen bonding structures between random-coil diethyleneglycol diethyl ether and water molecules. (g) bi-hydrated DGDE of one bridged form at the O3,O9-position and another water hydrogen bonding network, (h) tri-hydrated DGDE of one bridged form at the O3,O9-position and another hydration at O9-position, (i) tri-hydrated DGDE of one bridged form at the O3,O9-position and another hydration at O6-position and two water hydrogen bonding network, (j) two DGDE and two water molecules hydration network, (i) two DGDE and three water molecules hydration network.

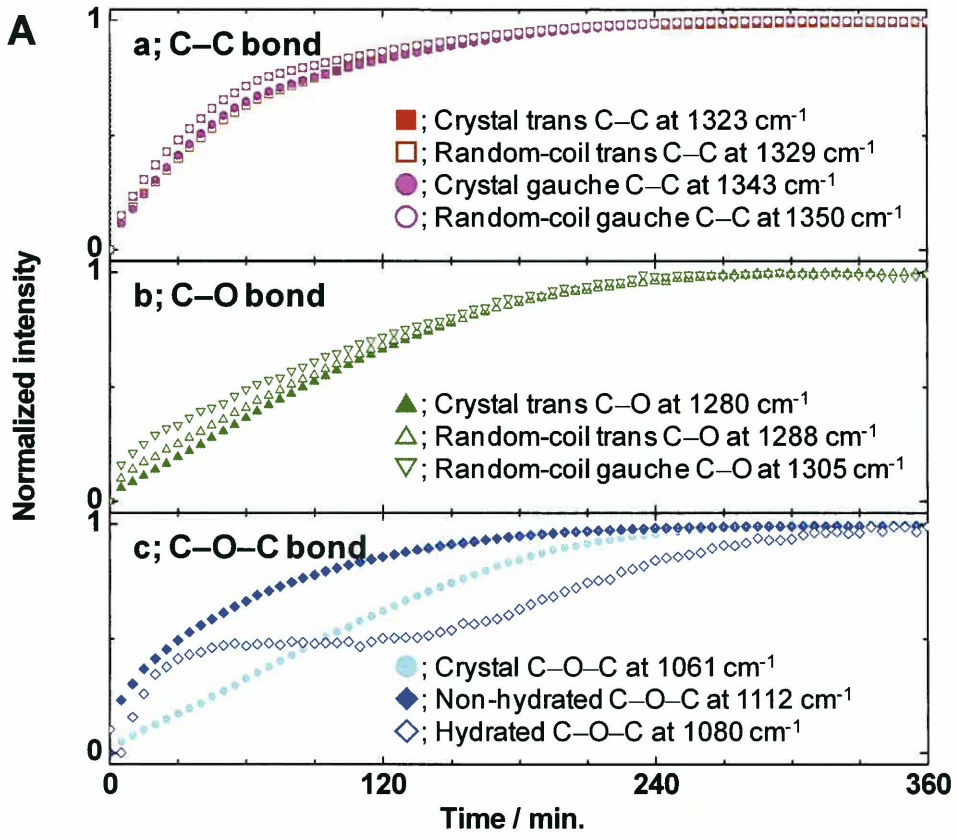
A
a; C–C bond
■; Crystal trans C–C at 1323 cm-1
□; Random-coil trans C–C at 1329 cm-1
●; Crystal gauche C–C at 1343 cm-1
○; Random-coil gauche C–C at 1350 cm-1
b; C–O bond
▲; Crystal trans C–O at 1280 cm-1
△; Random-coil trans C–O at 1288 cm-1
▽; Random-coil gauche C–O at 1305 cm-1
c; C–O–C bond
; Crystal C–O–C at 1061 cm-1
◆; Non-hydrated C–O–C at 1112 cm-1
◇; Hydrated C–O–C at 1080 cm-1
Normalized intensity
1
0
0
120
240
360
Time / min.

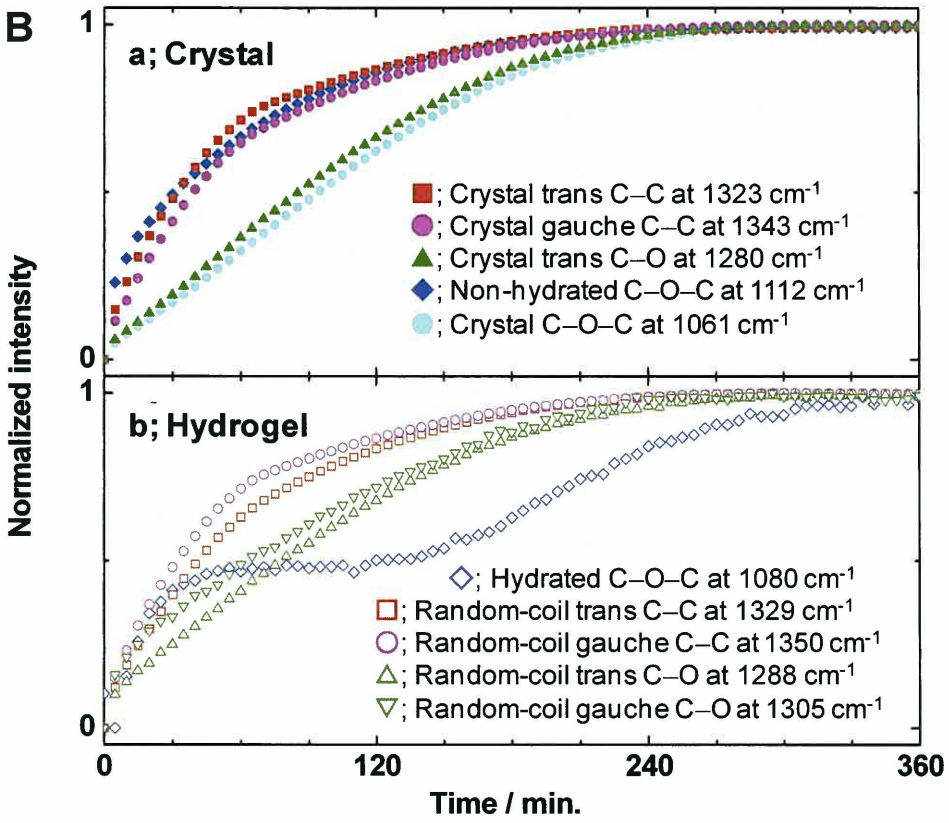

Figure 8. A; Time-dependent normalized intensity changes of (a) the CH_2 wagging bands, (b) the CH_2 twisting bands, and (c) the C–O–C stretching bands in Figure 5. B; Time-dependent normalized intensity changes of (a) crystal and (b) hydrogel conformation change behaviors. ■, crystalline trans C–C bond due to the CH_2 wagging band at 1323 cm^{-1}; □, random-coil trans C–C bond due to the CH_2 wagging band at 1329 cm^{-1}; ●, crystalline gauche C–C bond due to the CH_2 wagging band at 1343 cm^{-1}; ○, random-coil gauche C–C bond due to the CH_2 wagging band at 1350 cm^{-1}; ▲, crystalline trans C–O bond due to the CH_2 twisting band at 1280 cm^{-1}; △, random-coil trans C–O bond due to the CH_2 twisting band at 1288 cm^{-1}; ▽, random-coil gauche C–O bond due to the CH_2

twisting band at 1305 cm^{-1}; ●, crystalline C–O–C symmetric stretching band at 1061 cm^{-1}; ◆, crystalline C–O–C asymmetric stretching band at 1112 cm^{-1}; and ◇, hydrated C–O–C asymmetric stretching band at 1080 cm^{-1}.

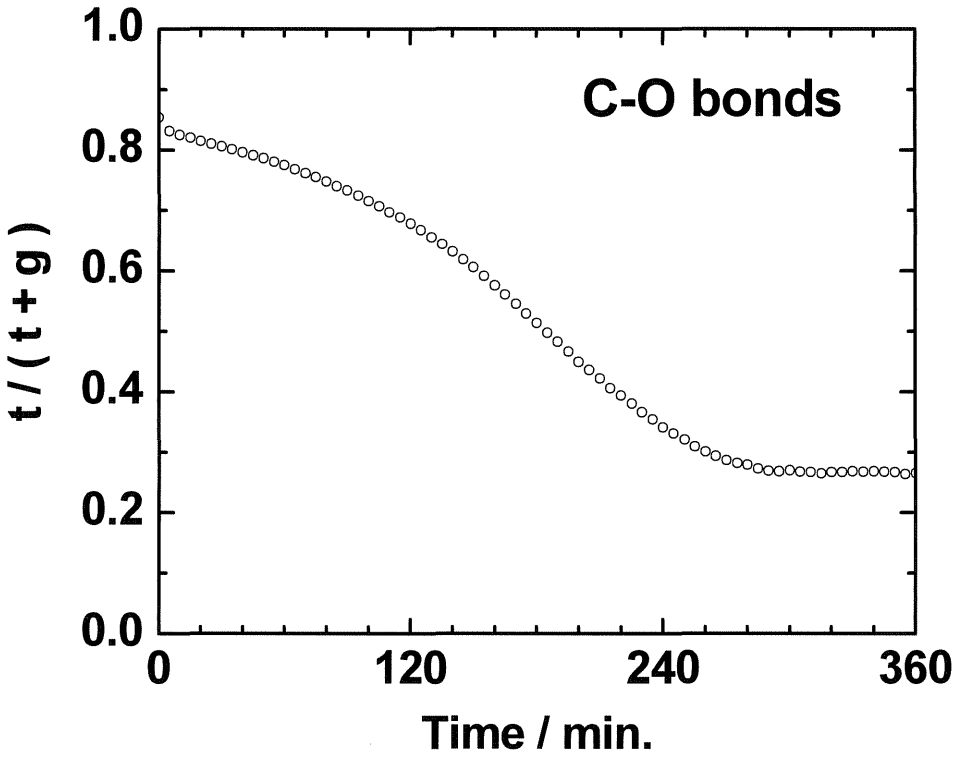

Figure 9. Time-dependent intensity ratio changes of random-coil C–O trans and gauche bands at 1288 and 1305 cm^{-1} in Figure 5, where t and g denote the trans and gauche conformations, respectively.

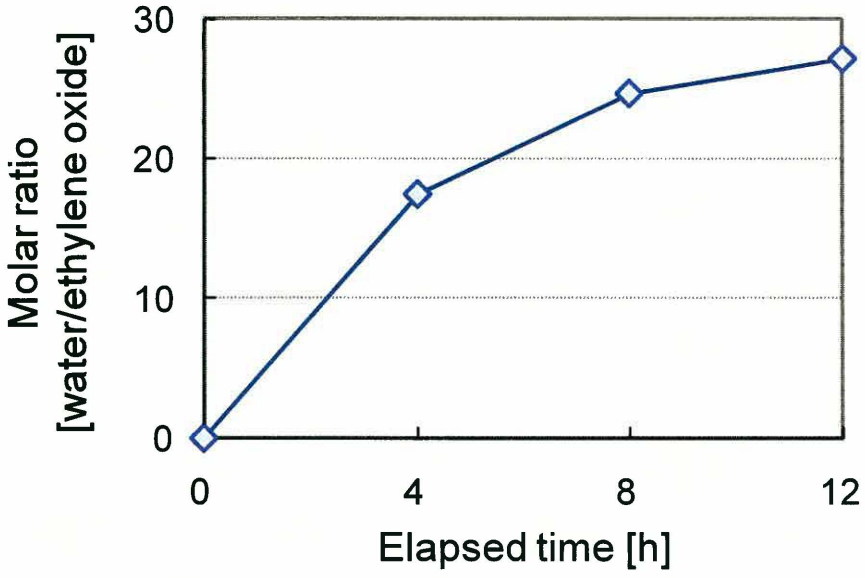

Figure 10 Molar ratio of water molecules compared with ethylene oxide units in PEO.

Table 1. Band assignments of infrared spectra of poly(ethylene oxide) with different conditions.

Wavenumbers [cm^{-1}]			**Assignments**
Dry film	Hydrated film/ Aqueous solution	Dichloromethane solution	
1467	1473	1473	CH_2 asymmetric bending
1451	1455	1455	CH_2 symmetric bending
1343	1350/1349	1350	CH_2 wagging [8,9]
1323	1329	1329	CH_2 wagging [8,9]
-	1305	1305	CH_2 twisting [8,9]
1280	1288	1288	CH_2 twisting [8,9]
1150	1142	1140	C–C stretching[8]
1112	1080	1093	C–O–C asymmetric stretching[8]
1061	-	-	C–O–C symmetric stretching[4]

Table 2. Calculated wavenumbers of a C–O–C stretching band of DGDE, and hydrogen-bond energy calculated by QCC. Indices of (a)-(f) correspond to the optimized structures shown in Figure 6. *s*, strong intensity band; *w*, weak intensity band.

	DGDE Structures		Calculated wavenumbers of C–O–C stretching. (cm^{-1})	Calculated SCF energy (kcal/mol)	Calculated hydrogen bonding energy (DGDE and water) (kcal/mol)
–	Non-hydrated DGDE	Helix	1119 *s*	-339565.5	–
–		Random coil	1133 *s*	-339562.3	–
(a)	Mono-hydrated DGDE at O3	Helix	1105 *s*, 1120 *w*	-387504.6	-8.8
(b)	(Type I)	Random coil	1090 *w*, 1105 *s*, 1123 *w*	-387500.2	-7.5
(c)	Di-hydrated DGDE at O3 and O6	Helix	–	–	–
(d)	(Type II)	Random coil	–	–	–
(e)	Di-hydrated DGDE at O3 and O9	Helix	1099 *s*, 1113 *w*	-387507.7	-11.9
(f)	(Type III)	Random coil	1071 *w*, 1097 *s*, 1117 *w*	-387506.5	-13.8

Table 3. Calculated wavenumbers of a C–O–C stretching band of DGDE, and hydrogen-bond energy calculated by QCC. Indices of (g)-(k) correspond to the optimized structures shown in Figure 7. *s*, strong intensity band.

	Number of molecules		Number of	Calculated wavenumbers	Calculated SCF	Calculated hydrogen bonding
	DGDE	Water	Hydrogen bonds	of C–O–C stretching (cm^{-1})	Energy (kcal/mol)	energy (DGDE and water) (kcal/mol)
–	1	–	–	1133 *s*	-339562.3	–
(g)	1	2	3	1108 *s*	-435453.8	-28.2
(h)	1	2	3	1109 *s*	-435446.3	-20.7
(i)	1	4	5	1193 *s*	-531335.2	-48.9
(j)	2	2	4	1112 *s*	-775026.1	-35.8
(k)	2	3	6	1118 *s*	-822972.9	-52.1

Chapter 3: Design of *In Vitro* Dissolution Test for Extended Drug-release Matrix containing Poorly-water Soluble Indomethacin utilizing Flow-through Cell Apparatus under Perfect Sink Condition

Abstract

The objective of this study was to develop an appropriate *in vitro* dissolution method for an extended drug-release matrix containing a poorly water-soluble drug under the perfect sink conditions, which are defined as the necessary and sufficient conditions for the drug-dissolving and releasing in terms of the drug solubility. The present study demonstrated that flow-through cell dissolution, one of the compendial *in vitro* dissolution methods, enables to maintain the perfect sink conditions for an extended release matrix formulation containing a poorly water-soluble indomethacin (IDM) during the *in vitro* dissolution study. The open-loop configuration should be paid attention to maintain the perfect sink conditions in a flow-cell, which is the drug-dissolving and releasing field, during dissolution test. On the other hand, the closed-loop configuration should be considered not only for the regional but also for the overall perfect sink conditions. In order to discuss the appropriate testing conditions, the drug-release mechanism from the extended-release matrix formulation combined hydrophobic and hydrophilic polymers was also investigated, and since hydrophilic hydroxypropyl methylcellulose (HPMC) showed its ability to enhance the solubility of IDM in water, the contribution of HPMC-releasing to the drug-solubility was quantified using size-exclusion chromatography (SEC). It has confirmed that the flow-through cell should be well-suited to be applied to an *in vitro* dissolution method for an extended release matrix containing a poorly water-soluble drug.

1. Introduction

Recently, with the increase in the number of poorly water-soluble pharmaceutical compounds, formulational technologies such as solid dispersion, nanoparticle and self-emulsifying drug delivery systems (SEDDSs) play increasingly important roles to improve their bioavailability.[1–7] Solid dispersion technologies where an active pharmaceutical ingredient is amorphized using a variety of carrier polymers like polyethylene glycol (PEG), polyvinylpyrrolidone (PVP), hydroxypropylcellulose (HPC) and hydroxypropyl methylcellulose (HPMC) have been widely investigated to enhance the solubility and the oral absorption.[1,4,7] Further, in an effort to improve quality of life among patients, a lot of extended-release technologies of water-insoluble coatings/matrices using hydrophobic polymers like ethylcellulose (EC) and poly(ethyl acrylate-*co*-methyl methacrylate-*co*-trimethylammonioethyl methacrylate chloride)[8–10] and hydrogel forming matrices using hydrophilic polymers such as HPMC and polyethylene oxide (PEO)[11–14] have been reported, and they were also evaluated in terms of their *in vitro* release behaviors using a compendial paddle dissolution apparatus.

In an *in vitro* drug-releasing study of a pharmaceutical product containing a poorly water-soluble drug, an appropriate dissolution method should be developed under the sink conditions to evaluate the drug-releasing property precisely. There are still a lot of discussion about the sink conditions, where is the drug solubility be ten times the total concentration of drug in the vessel, or at least greater than three or five times,[15–17] though, in general, the sink conditions are defined three times the drug concentration based on the solubility in The United States Pharmacopeia (USP).[18]

However, in a dissolution method for a poorly water-soluble drug by using a basket and paddle apparatus (USP apparatus 1 and 2) whose medium volumetric-constraint is 1 L in the capacity of the vessel, it is sometimes difficult to develop the dissolution test under the sink conditions due to a poor drug solubility. Further, the perfect sink conditions, which are defined as the necessary and sufficient conditions for the drug-dissolving and releasing in terms of the drug solubility, may not be coincided with the sink conditions described in USP. In order to improve their solubilities and then to achieve the perfect sink conditions during an *in vitro* dissolution test, some kinds of surfactants such as polysorbate 80 and sodium lauryl sulfate (SLS) may be necessary to be applied,[19,20] however, the use of a surfactant must diminish the drug-release discrimination due to its exceeded solubility, and also sometimes make it difficult to achieve the *in vitro/in vivo correlation* (IVIVC).

A flow-through cell apparatus, which has been described in USP and European Pharmacopoeia (EP) in 1990, and The Japanese Pharmacopoeia (JP) in 1996, allows using an unbounded medium volume. Therefore, it has a huge advantage to maintain the perfect sink conditions during a test, and then it makes possible to select a type of dissolution media more flexibly. In general, the relation between the solubility and the dissolution rate of a drug has been given by the Noyes-Wyitney equation (1),[21]

$$\frac{dM}{dt} = \frac{AD(C_s - C_t)}{h} \qquad (1),$$

where dM/dt is the dissolution rate, A is the specific surface area of the drug particles, D is the dissolution coefficient, h is the diffusion layer thickness, C_s is the saturation solubility and C_t is the drug concentration of a dissolution medium at time

t. However, the open-loop configuration, which is constantly-delivered a fresh dissolution medium, is able to eliminate an influence of an cumulating drug concentration in a medium C_t, and the Noyes-Wyitney equation could be revised as follows;

$$\frac{dM}{dt} = \frac{ADC_s}{h} \quad (2),$$

It has attracted attention as one of the compendial methods due to not only above-mentioned maintainable the sink conditions for any poorly water-soluble drugs with a large medium volume, but also its flexibility to many kinds of dosage forms and easily media changeable, which allowed to apply biorelevant medium set of fasted simulated small intestinal fluid (FaSSIF) and fed state simulated intestinal fluid (FeSSIF) for IVIVC studies.[22,23] Further, the flow-through cell dissolution has a variety of testing options to adjust their *in vivo* drug-release characteristics and/or excellent discrimination capability; a volumetric medium flow rate, medium flow speed in a flow-cell using a large or a small cell, single or multi dissolution media, with or without 120 pulse/min sinusoidal pulsation, and laminar or turbulent hydrodynamic flow[24,25] and open or closed-loop configurations. The open-loop configuration, which is one way medium sending, is able to consistently supply a fresh medium which helps to maintain the perfect sink conditions, while the large medium volume must be necessary when a long-term dissolution test is performed with a large volumetric medium flow rate. On the other hand, closed-loop configuration, which is circulating medium sending, is able to apply an arbitrary and an appropriate medium volume due to a drug solubility, even though a medium containing released drug is used a subsequent dissolution test as the same as basket

or paddle method.

There have been some reports on the sink condtion on flow-through cell dissolution. Langenbucher[16] has concluded only two apparatuses parameter are essential to the dissolution process, i.e. the liquid velocity and the mass specific area, which are defined by the volumetric flow rate and the cell diameter, respectively. Futher Posti and Speiser[26] have pointed out the effect of the active surface area. However they did not focus on regional medium conditions in a flow-cell from the solubility point of view. Here, in order to design of an appropriate dissolution method by using a compendial flow-through cell apparatus with open and closed-loop configurations under the perfect sink conditions, in this study, an extended drug-release matrix consisted a solid dispersion of hydrophoic EC and hydrophilic HPMC and contained a poorly water-soluble indomethacin (IDM) was used as a model formulation. Ohara et al.[28] reported that water-insoluble polymer kept its three-dimensional matrix structure during the dissolution test, while the water-soluble polymer in the matrix dissolved and diffused quickly into dissolution medium. Further, as reported by Ozeki et al.,[29] the behavior of water-soluble polymer during dissolution test has a key factor in the drug-release mechanism from a solid dispersion prepared with water-insoluble and water-soluble polymers. Hence, in order to comprehensively examine and reveal the unique drug-release mechanism from EC hydrophobic matrix, the release behavior of hydrophilic HPMC was also assessed using size-exclusion chromatography (SEC), which was the most common way to obtain information about the molecular mass distribution of polymers.[30–32]

2. Experimental

2.1 Materials

IDM was purchased from Wako chemical (Osaka, Japan). HPMC (TC-5E) with average viscosity of 3 mPa·s was obtained from Shinetsu Chemical Industry (Tokyo, Japan), EC (ETHOCEL STD 10FP) was purchased from Dow Chemical (MI, USA). All other chemicals used were of reagent grade.

2.2 Preparation of solid dispersion

Solid dispersion consisting of IDM, EC and HPMC (1:1:1, weight ratio) were prepared the solvent evaporation method[1] as follows. IDM of 5 g, EC of 5 g and HPMC of 5 g were dissolved in a mixture of ethanol and dichloromethane (1:1) of 200 mL, and then the solvents were evaporated under reduced pressure using a rotary evaporator at 30 °C. Solid dispersion was dried for three nights under vacuum at 40 °C, and then milled and sieved with three particle size fractions; A, 75–150 μm; B, 150–250 μm; C, 250–355 μm. After being dried in a desiccator, the solid dispersions were used for the following studies.

2.3 Solubility study

The solubilities of IDM in water and HPMC solutions were determined at 37±0.5 °C using a paddle apparatus (NTR-6100, Toyama, Osaka, Japan).[18,33,34] The paddle rotation speed was 200 rpm. An excess of active ingredient, equivalent to approximately 100 mg of IDM, as a γ-crystalline powder, an amorphous solution in methanol (10 mg·mL^{-1}) and the solid dispersion described in section 2.2 were added

to 500 mL of water, and 0.5 and 2 mg·mL^{-1} HPMC solutions. 10 mL of each media was taken at 1, 2, 3, 6, 24 and 48 hours, and filtered using 0.2 μm membrane filter (DISMIC-25HP, 0.2 μm; ADVANTEC, Tokyo, Japan) and discarding the first 5 mL. The drug concentration of each fraction was measured by using ultraviolet-visible (UV-VIS) spectroscopy at 265 nm (UV-2400PC; Shimadzu, Kyoto, Japan) after added to the same amount of ethanol. In this study, the concentration of IDM after 48 hours was used as the solubility of the drug.

2.4 Dissolution test

The *in vitro* drug-release properties of the solid dispersion granules were evaluated via a flow-through cell apparatus (DZ70; Pharma-Test AG, Hainburg, Germany) at a flow rate of 4, 12, 16 and 24 mL·min^{-1} in an open-loop configuration and 16 mL·min^{-1} in a closed-loop configuration. A flow-through cell was filled with 1-mm glass beads, and sample granules were mixed with them to avid the aggregation, and applied a glass microfiber filter (GF/F, 0.7 μm; Whatman, Kent, UK). Water at 37±0.5 °C was used as the dissolution medium after degassed by heating at 47 °C before use. In the open-loop configuration, their effluent media were collected every five minutes in the first one hour, and then every 30 minutes until six hours. On the other hand, in the closed-loop configuration, the circulated medium was collected at 1, 2, 3, 5, 8 and 20 hours containing 600, 1,200, 1,800 and 3,000 mL of water. The drug concentration of each fraction was measured by using UV-VIS spectroscopy at 265 nm. In addition, the amounts of HPMC released from the matrix were quantified by SEC,[31] with a high performance liquid chromatography (HPLC) system (1200

series; Agilent Technologies, CA, USA) equipped with a charged aerosol detector (CAD, Corona; ESA Biosciences, MA, USA) and a SEC column (TSK-GEL Alpha-3000; Tosoh, Tokyo, Japan; 7.8 mm i.d. × 30 cm, 7 μm). Purified water was used as a mobile phase for HPLC analysis, and the flow rate was 1 mL·min^{-1}.

2.5 X-ray powder diffraction

X-ray diffraction patterns of γ-IDM crystal, EC, HPMC and the solid dispersion described in section 2.2 were collected by using a X-ray powder diffraction system (RINT-TTR III; Rigaku, Tokyo, Japan). The radiation was generated by Cu·K at 50 kV and 300 mA. The instruments was operated in the continuous scan mode with the scanning speed at 2°·min^{-1}.

2.6 Fourier transform infrared spectroscopy

All infrared (IR) spectra of each raw material and the solid dispersion were measured at a resolution of 4 cm^{-1} using a Fourier transform-IR (FT-IR) spectrometer (NICOLET 6700; Thermo Fisher Scientific, MA, USA) equipped with a diamond-attenuated total reflection (ATR) accessory and a deuterated triglycine sulfate detector. A total of 64 scans were co-added, and all of the IR spectra were defined in absorbance units as

$$A = -\log_{10}\frac{R}{R_0} \quad (3),$$

where R and R_0 are the intensities of IR light from a sample and a reference compound, respectively. The second derivatives of the obtained IR spectra were calculated by the Savitzky-Golay method[35] after Kawata-Minami smoothing.[36]

3 Results and Discussion

3.1 Solubility of indomethacin

Solubilities of IDM in some dissolution media were shown in Table 1, and the change of IDM concentration in each medium was illustrated in Figure 1. Solubilities of IDM added by crystalline and amorphous states in water were approximately 9.1 and 15.6 $\mu g \cdot mL^{-1}$, respectively, as almost the same as previous solubility studies by Higuchi and Connors method.[37,38] Therefore the sink conditions, which needed three times the drug concentration based on the solubility, requires approximately 6,577 mL and 3,837 mL of water for 20 mg of IDM, respectively (Table 1), indicating that it is difficult to develop a dissolution method under the sink conditions by using a basket or a paddle apparatus with 1L of the volumetric-constraint, when water is used as a dissolution medium. However, the solubility of IDM from the solid dispersion in water was much improved, and it was approximately 35.8 $\mu g \cdot mL^{-1}$. Further, the higher concentration of HPMC in the media, the higher solubilities of crystalline and amorphous-IDM, indicating that HPMC has an ability to improve the IDM solubility in water, as the same as previous studies which have been reported that HPMC showed its ability not only to enhance the water-solubility of poorly water-soluble drugs but also to prevent ones from recrystallizing in aqueous dissolution media.[39–41] Furthermore, the amount of HPMC in 0.5 $mg \cdot mL^{-1}$ HPMC solution is almost the same as that in water after dissolving all HPMC from the solid dispersion though, the solubility of IDM from solid dispersion showed much higher than the others, indicating that HPMC has an

ability not only to enhance the drug solubility, but also to keep the stable structure of IDM in water after releasing. The finding suggests that the state of IDM in a medium plays an important role of the solubility depending on the added state of IDM; crystal, amorphous solution and solid dispersion (Table 1). Therefore, the molecular structure of IDM in the solid dispersion will be discussed below. Here, in order to develop a dissolution method for this formulation, the value of IDM solubility can be applied to 35.8 $\mu g \cdot mL^{-1}$ as the solubility of IDM from the solid dispersion in water.

3.2 Crystal and molecular structure of indomethacin in the solid dispersion

XRD patterns of γ-form IDM and the solid dispersion are depicted in Figure 2. Characteristic γ-form crystalline peaks were observed in the diffraction patterns of IDM drug substance but not for the solid dispersion, in which a broaden pattern was observed, suggesting that IDM in the solid dispersion was completely altered to an amorphous phase. IDM has been well-known consisting of cyclic dimer structure of a pair of carboxylic acid groups in the γ-form, whereas benzoyl carbonyl group does not create hydrogen bonding with another IDM molecule.[42] Further, their ATR-IR spectra in the 1800-1550 cm^{-1} region (the C=O stretching band region) are illustrated in Figure 3. Two peaks observed for γ-form IDM observed at 1713 and 1689 cm^{-1} are assigned to C=O stretching bands of a cyclic dimer in carboxylic acids and benzoyl, respectively.[42,43] Detailed assignment for carbonyl IR bands of IDM at γ-crystalline and the solid dispersion state are summarized in Table 1. In the IR spectrum of IDM in the solid dispersion, a band with similar intensity of cyclic

dimer of IDM is detected at 1716 cm^{-1}, but another weak band at 1732 cm^{-1} is also observed, indicating that most IDM molecules keep their cyclic dimer structures in the solid dispersion, but the blue-shifted band indicates that some cyclic dimers between IDM molecules are dissociated and newly created another structure. Further, the benzoyl C=O stretching band at 1691 cm^{-1} is shifted to 1680 cm^{-1}, suggesting that non-hydrogen bonding benzoyl C=O group also forms another structure in the solid dispersion. Since a cyclic dimer structure of carboxylic acid group is generally a much stable form, and it has been well-known to dominate in a pure liquid or a solid state of carboxylic acid.[44–46] My previous study demonstrated IR-frequency shifts of carboxylic acid of propionic acid due to the hydrogen bonds by using a quantum chemical calculation in chapter 1. The calculated wavenumber of C=O stretching band in carboxylic acid via two hydrogen bonds as a cyclic dimer was shifted approximately 56 cm^{-1} compared to free C=O band. The blue-shift was much larger than that of carboxylic acid via one hydrogen bond with hydroxyl group from another carboxylic acid or water.[47] Therefore, the computational simulation supports the assignment of C=O stretching band at 1732 and 1680 cm^{-1}, which are formed hydrogen bonding between carbonyl groups of carboxylic acid/benzoyl and the hydroxyl groups in IDM or EC or HPMC (Table 2). These results find that the crystal lattice of IDM in solid dispersion was destroyed, even though most IDM molecules still maintain cyclic dimer structure in the solid dispersion. However, certain cyclic dimmers of IDM are dissociated, and then the free carboxylic acid and benzoyl carbonyl groups create new hydrogen bondings with hydroxyl groups from another IDM or EC or HPMC in the solid dispersion.

3.3 Dissolution study by a flow-through cell

In the open-loop configuration, cumulated percent drug-release profiles and time-resolved drug concentration changes of the effluent are shown in Figure 4a and 4b, respectively. When the volumetric medium flow rate is not more than 16mL·min^{-1}, the larger volumetric medium flow rate, the faster drug-releasing (Figure 4a). On the other hand, the drug-releasing behavior at the volumetric medium flow rate of 24 mL·min^{-1} demonstrated that it is the same as that at 16 mL·min^{-1} (Figure 4a). Since the larger volumetric medium flow rate, the larger hydrodynamics effect, the polymeric erosion behavior will be discussed below. In the early stage of dissolution, approximately 10 % of the drug was released within the first 30 min, and the first effluent included much high drug concentrations, especially when small medium flow made the highest concentration of 45.4 μg·mL^{-1} at the 4 mL·min^{-1} volumetric medium flow rate (Figure 4b). When the solubility of IDM from the solid dispersion is applied 35.8μg·mL^{-1} (Table 1), supersaturation in a flow-cell must occur at only 4 mL·min^{-1} of volumetric medium flow rate, and with 24 mL·min^{-1} of volumetric medium flow rate enables to maintain the sink conditions in a flow-cell during the dissolution test. However, as above-discussed, HPMC was actually released from the solid dispersion, and enhanced the solubility of IDM. Hence, in order to comprehensively examine the unique drug-release mechanism from EC hydrophobic matrix, the release behavior of hydrophilic HPMC was also evaluated. The cumulated percent release profiles and time-resolved HPMC concentration changes of the effluent are shown in Figure 5a and 5b, respectively. As in the case of the

release behavior of IDM, the larger volumetric medium flow rate, the faster HPMC releases (Figure 5a). Moreover, the release phenomenon of HPMC at 24 $mL \cdot min^{-1}$ showed the same one at 16 $mL \cdot min^{-1}$ (Figure 5a), suggesting that the release kinetic of HPMC from the solid dispersion plays an important role in the release behavior of IDM. However, whole HPMC containing the solid dispersion was released within the first 30 min regardless of volumetric medium flow rate, and approximately 500 $\mu g \cdot mL^{-1}$ of HPMC existed in a flow-cell at the 4 $mL \cdot min^{-1}$ of the volumetric medium flow rate (Figure 5b). Therefore, even if the solubility of IDM in 0.5 $mg \cdot mL^{-1}$ of HPMC solution is applied as 37.7 $\mu g \cdot mL^{-1}$ (Ttable 1), supersaturation in a flow-cell at the smallest volumetric medium flow rate must be inevitable.

On the other hand, in the closed-loop configuration, cumulated percent drug-release profiles with 600, 1,200, 1,800 and 3,000 mL of dissolution media are shown in Figure 6. The drug-release behaviors of closed-loop configuration at 16 $mL \cdot min^{-1}$ are the same one of open-loop configuration at the same volumetric medium flow rate until 50 % of the drug-releasing (Figure 4a and 6). HPMC concentration in each dissolution medium on the closed-loop configuration after released whole HPMC is 33.3, 16.7, 11.1 and 6.7 $\mu g \cdot mL^{-1}$, respectively. It indicates that there is little enhancing effect of the drug solubility by HPMC according to an above solubility study.

All release curves were almost the same, indicating that the whole medium volume does not affect drug-releasing behavior until 20 hours, even though 25 % of 20 mg of IDM in the solid dispersion was not still released. 600 mL of the medium volume may not be satisfied to release the drug completely after 20 hours, because of the

solubility. However, for the 50 % of the drug, the finding indicates that 600 mL of the medium volume is enough to the drug-release behavior from the drug solubility perspective. Therefore, 1,200 mL of the medium volume may be enough for 60 mg of the solid dispersion containing 20 mg of IDM, and 1,800 mL of the medium volume, which is the almost sink conditions, must be a sufficient medium volume.

The flow-through cell could minimize the effect of cumulated dissolved drug concentration; *Ct* in the Noyes-Wyitney equation (1),[21] but it could not be zero in the flow-cell. Therefore, the equation (1) should be also applied to open-configuration on flow-through cell.

3.4 Release mechanism of indomethacin from the extended release matrix

Most oral pharmaceutical formulations control the drug-releasing by the matrix erosion and/or self-diffusion. Hence, in order to estimate the contribution from the hydrodynamic effect to IDM and HPMC releasing in a flow-cell, large and small cells whose inside diameter were 22.6 and 12 mm, respectively, could be used. The small cell has an almost half diameter and then creates approximately four times faster medium flow speed in the flow-cell. Therefore, the combination of small cell and 4 $mL \cdot min^{-1}$ of volumetric medium flow rate makes almost the same hydrodynamic force applied for per unit of area as that of large cell and 16 $mL \cdot min^{-1}$ of volumetric medium flow rate. Further, four times larger volumetric medium flow rate also makes the four times faster flow speed in a flow-cell, as the same size flow-cell is used. The comparison results among a pair of large cell and 4 $mL \cdot min^{-1}$ flow volume whose medium flow speed in the flow-cell is 8 $mm \cdot min^{-1}$, that of small

cell and 4 mL·min^{-1} flow volume whose medium flow speed in the flow-cell is 28 mm·min^{-1}, and that of large cell and 16 mL·min^{-1} flow volume whose medium flow speed in the flow-cell is 32 mm·min^{-1} are shown in Figure 8. As above-discussed, there is little effect of hydrodynamics not only on HPMC dispersion but also on IDM releasing, indicating that the hydrophilic EC matrix could drown out the effect of the fluid dynamics. Therefore, from a comprehensive standpoint including above-discussed medium concentration in a flow-cell, the drug-release was controlled by volumetric medium flow rate. Here, the perfect sink conditions on the flow-through cell, which is defined as the necessary and sufficient conditions for the drug-dissolving and the releasing in terms of the drug solubility, will be discussed below.

Further, the drug-releasing behaviors of the present study indicate that drug-releasing is mainly dominated by two rate-limiting steps as the same as the previous report.[28] In the early stage, release of HPMC occurs when the testing solution begins to penetrate into the matrix. As mentioned above, the contribution of HPMC releasing to the drug-releasing is revealed by using HPLC-SEC, and the drug-release mechanism from the extended-release matrix is strongly controlled by the dispersion of hydrophilic HPMC in the early stage (Figure 4b and 5b). In contrast, in the late stage; after released whole HPMC in the solid dispersion, the drug-releasing is dominated by the self-diffusion of IDM through the hydrophobic EC matrix. Further, the release curves for the matrices of individual particle size fractions; A, 75–150 μm; B, 150–250 μm; C, 250–355 μm, are shown in Figure 7. The smaller the particle size of the matrix granule, the faster drug-releasing,

suggesting that the drug-release behavior from the EC matrix depends on the particle size, in other words, surface area of the matrix and drug diffusion length following the Noyes-Wyitney equation (1).[21]

3.5 Perfect sink condition on a flow-through cell

A schematic illustration of the critical factors in open and closed-loop configurations on flow-through cell was illustrated in Figure 9. In the open-loop configuration, the medium concentration in the flow-cell affects the drug-releasing behaviors. Therefore, sufficient medium volume should be delivered to the flow-cell during the dissolution test to prevent the effluent from supersaturation, even though open-loop configuration which keeps supplying medium without cumulated drug to a flow-cell. For this solid dispersion, 16 $mL \cdot min^{-1}$ of the volumetric medium flow rate is enough for the drug-releasing. In the closed-loop configuration, on the other hand, enough medium volume must be required in the flow-cell as in the case of the open-loop configuration. However, not only volumetric medium flow rate but also overall medium volume circulated should be also paid attention and be kept sufficient medium volume, because the drug concentration increases over time in the closed-loop configuration. In this study, those finding indicates that 1,800 mL of the dissolution medium which satisfies the sink conditions for 20 mg IDM from the solid dispersion, must be enough for the drug-releasing of the solid dispersion.

4. Summary

Here, in order to develop an appropriate *in vitro* dissolution test method for an

extended release matrix containing a poorly-water soluble drug under the perfect sink conditions, the drug-release mechanism should be shed light on firstly. Further, sometimes understanding the release behaviors of not only a drug but also excipients is really important to design a desirable *in vitro* dissolution method, because some excipients have an ability like enhancing a drug solubility. In this study, HPMC showed the abilities of not only keeping the drug in amorphous state in the solid dispersion but also prompting to the drug-releasing with its dispersion and improving the drug solubility.

The key factors for the *in vitro* dissolution method by using a flow-through cell apparatus are described below. In open-loop configuration, "enough medium volume in a flow-cell during the test" must be paid attention to evaluate the drug-release ability accurately. On the other hand, in closed-loop configuration, not only "enough medium volume in a flow-cell during the test" but also "Enough medium volume in a flow-through cell system during the test" should be considered.

The flow-through cell could achieve *in vitro* drug-release test under the perfect sink conditions, even though a basket and paddle apparatus (USP apparatus 1 and 2) could not use sufficient dissolution medium due to the 1 L of volumetric-constraint. Therefore, the flow-through cell is well suited to evaluate the drug-release characteristic of oral pharmaceutical products, especially including a poorly-water soluble drug.

5. References

1 Chiou, W.L.; Riegelman, S. *J. Pharm. Sci.*, 1971, 60, 1281–1302.

2 Jia, L. *Curr. Nanosci.*, 2005, 1, 237–243.

3 Kipp, J.E. *Int. J. Pharm.*, 2004, 284, 109–122.

4 Leuner. C.; Dressman, J. *Eur. J. Pharm. Biopharm.*, 2000, 50, 47–60.

5 Pouton, C.W. *Adv. Drug Del. Rev.*, 1997, 25, 47–58.

6 Tang, B.; Cheng, G.; Gu, J.C.; Xu, C.H. *Drug Discov. Today*, 2008, 13, 606–612.

7 Vasconcelos, T.; Sarmento, B.; Costa, P. *Drug Discov. Today*, 2007, 12, 1068–1075.

8 Crowley, M. M.; Schroeder, B.; Fredersdorf, A.; Obara, S.; Talarico, M.; Kucera, S.; McGinity, J. W. *Int. J. Pharm.*, 2004, 269, 509–522.

9 Mizuno, M.; Hirakura, Y.; Yamane, I.; Miyanishi, H.; Yokota, S.; Hattori, M.; Kajiyama, A. *Int. J. Pharm.*, 2005, 305, 37–51.

10 Siepmann, F.; Siepmann, J.; Walther, M.; MacRae, R. J.; Bodmeier, R. *J. Control. Release*, 2008, 125, 1–15.

11 Ford, J.L.; Rubinstein, M.H.; McCaul, F.; Hogan, J.E.; Edgar, P.J. *Int. J. Pharm.*, 1987, 40, 223–234.

12 Kim, C.J. *J. Pharm. Sci.*, 1995, 84, 303–306.

13 Sako, K.; Nakashima, H.; Sawada, T.; Fukui, M. *Pharm. Res.*, 1996, 13, 594-598.

14 Salomen, J. L.; Doelker, E.; Buri, P. *Pharm. Ind.*, 1979, 41, 799–802.

15 Dressman, J. B.; Amidon, G. L.; Reppas, C.; Shah, V. P. *Pharm. Res.*, 1998,

15, 11–22.

16 Langenbucher, F. *J. Pharm. Sci.*, 1969, 58, 1265–1272.

17 Rohrs, B. R. *Diss. Tech.*, 2001, August.

18 The United States Pharmacopeia 34-National Formulary 29, 2011. The United States Pharmacopeial Convention.

19 Shah, V. P.; Konecny, J. J.; Everett, R. L.; McCullough, B.; Noorizadeh, A. C.; Skelly, J. P. *Pharm. Res.*, 1898, 6, 612–618.

20 Shah, V. P.; Noory, A.; Noory, C.; McCullough, B.; Clarke, S.; Everett, R.; Naviasky, H.; Srinivasan, B. N.; Fortman, D.; Skelly, J. P. *Int. J. Pharm.*, 1995, 125, 99–106.

21 Noyes, A. A.; Whitney, W. R. *J. Am. Chem. Soc.* 1897, 19, 930–934.

22 Fang, J. B.; Robertson, V. K.; Rawat, A.; Flick, T.; Tang, Z. J.; Cauchon, N. S.; McElvain, J. S. *Mol. Pharm.*, 2010, 7, 1466–1477.

23 Jantratid, E.; Maio, V. D.; Ronda, E.; Mattavelli, V.; Vertzoni, M.; Dressman, J. B. *Eur. J. Pharm. Sci.*, 2009, 37, 434–441.

24 Kakhi, M. *Int. J. Pharm.*, 2009, 376, 22–40.

25 D'Arcy, D. M.; Liu, B.; Bradley, G.; Healy, A. M.; Corrigan, O. I. *Pharm. Res.*, 2010, 27, 246–258.

26 Posti, J.; Speiser, P. P. *Int. J. Pharm.*, 1980, 5, 101–107.

27 Klose, D.; Delplace, C.; Siepmann, J. *Int. J. Pharm.*, 2011, 404, 75–82.

28 Ohara, T.; Kitamura, S.; Kitagawa, T.; Terada, K. *Int. J. Pharm.*, 2005, 302, 95–102.

29 Ozeki, T.; Yuasa, H.; Kanaya Y.; Oishi K. *Chem. Pharm. Bull.*, 1995, 43,

1574–1579.

30 Kuga, S. *J. Chromatgr.* 1981, 206, 449-461.

31 Laguna, M. T. R.; Medrano, R.; Plana, M. P.; Tarazona, M. P. *J. Chromatogr. A*, 2001, 919, 13-19.

32 Tajiri, T.; Morita, S.; Sakamoto, R.; Suzuki, M.; Yamanashi, S.; Ozaki, Y.; Kitamura, S. *Int. J. Pharm.*, 2010, 395, 147–153.

33 European Pharmacopoeia seventh ed., 2011. European Directorate for the Quality of Medicines.

34 The Japanese Pharmacopoeia 16th ed., 2011. Society of Japanese Pharmacopoeia.

35 Savitzky, A.; Golay, M. J. E. *Anal. Chem.*, 1964, 36, 1627–1639.

36 Kawata, S.; Minami, S. *Appl. Spectrosc.*, 1984, 38, 49–58.

37 Casella, R.; Williams, D. A.; Jambhekar, S. S. *Int. J. Pharm.*, 1998, 165, 15–22.

38 Sharma, P. K.; Bhatia, S. R. *Int. J. Pharm.*, 2004, 278, 361–377.

39 Kohri, N.; Yamayoshi, Y.; Xin, H.; Iseki, K.; Sato, N.; Todo, S.; Miyazaki, K. *J. Pharm. Pharmacol.*, 1999, 51, 159–164.

40 Suzuki, H.; Sunada, H. *Chem. Pharm. Bull.*, 1998, 46, 482–487.

41 Yamashita, K.; Nakate, T.; Okimoto, K.; Ohike, A.; Tokunaga, Y.; Ibuki, R.; Higaki, K.; Kimura, T. *Int. J. Pharm.*, 2003, 267, 79–91.

42 Towler, C. S.; Taylor, L. S. *Cryst. Growth Des.*, 2007, 7, 633–638.

43 Taylor, L. S.; Zografi, G. *Pharm. Res.*, 1997, 14, 1691–1698.

44 Flakus, H. T.; Tyl, A. *Chem. Phys.*, 2007, 336, 36–50.

45 Nakabayashi, T.; Nishi, N. *J. Phys. Chem. A*, 2002, 106, 3491–3500.

46 Semmler, J.; Irish, D. E. *J. Solution Chem.*, 1988, 17, 805–823.

47 Tajiri, T.; Morita, S.; Ozaki, Y. *Polymer*, 2009, 50, 5765–5770.

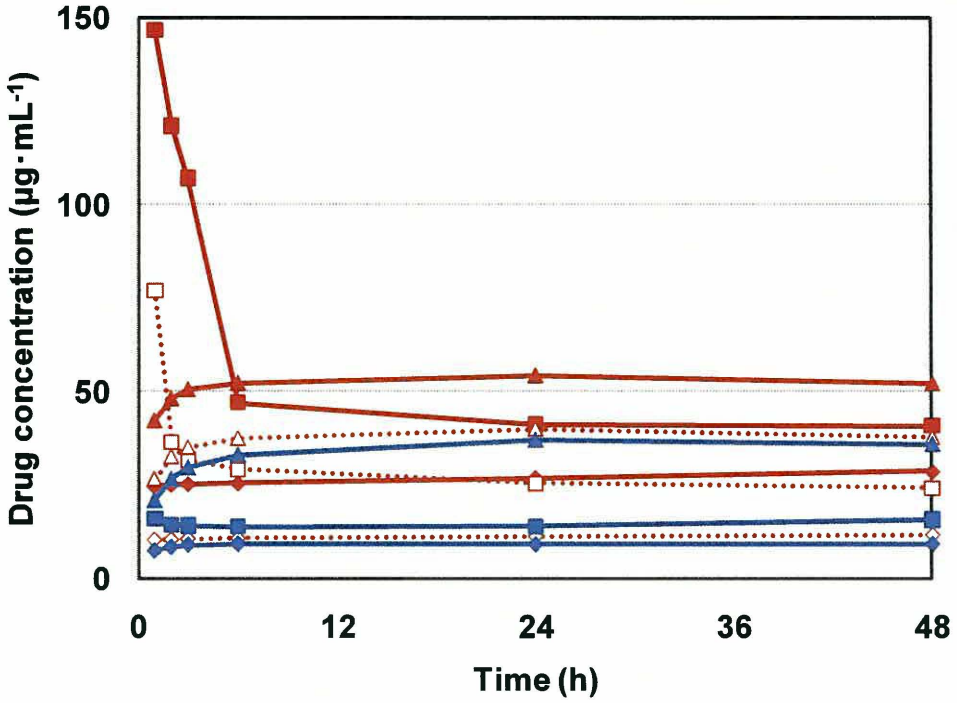

Figure 1. Saturated drug concentration changes with time; Added sample state is diamond: γ crystal power, square: ethanol solution and triangle: solid dispersion. Solvent type is solid blue line: water, dotted red line: 0.5 mg·mL^{-1} and solid red line: 2.0 mg·mL^{-1} HPMC solutions.

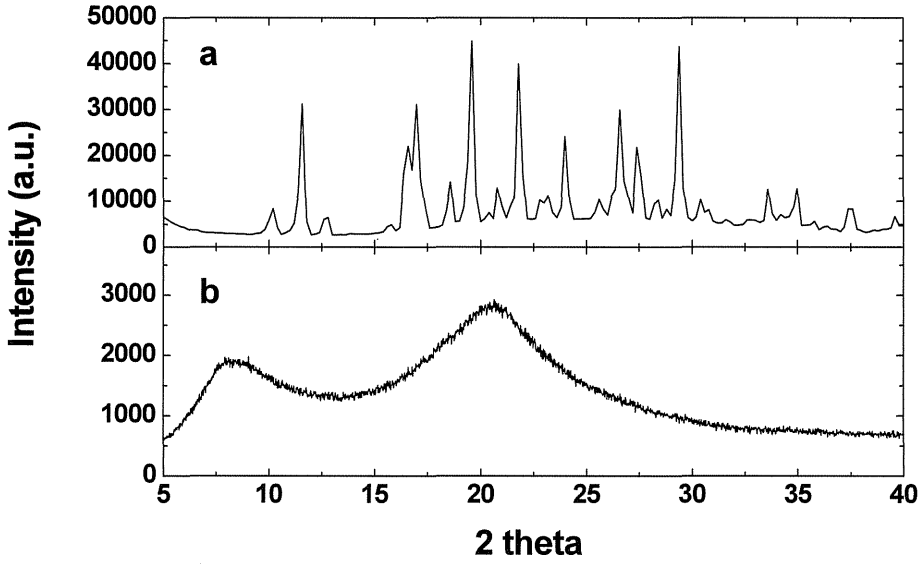

Figure 2. X-ray diffraction patterns of a; γ-form indomethacin and b; the solid dispersion.

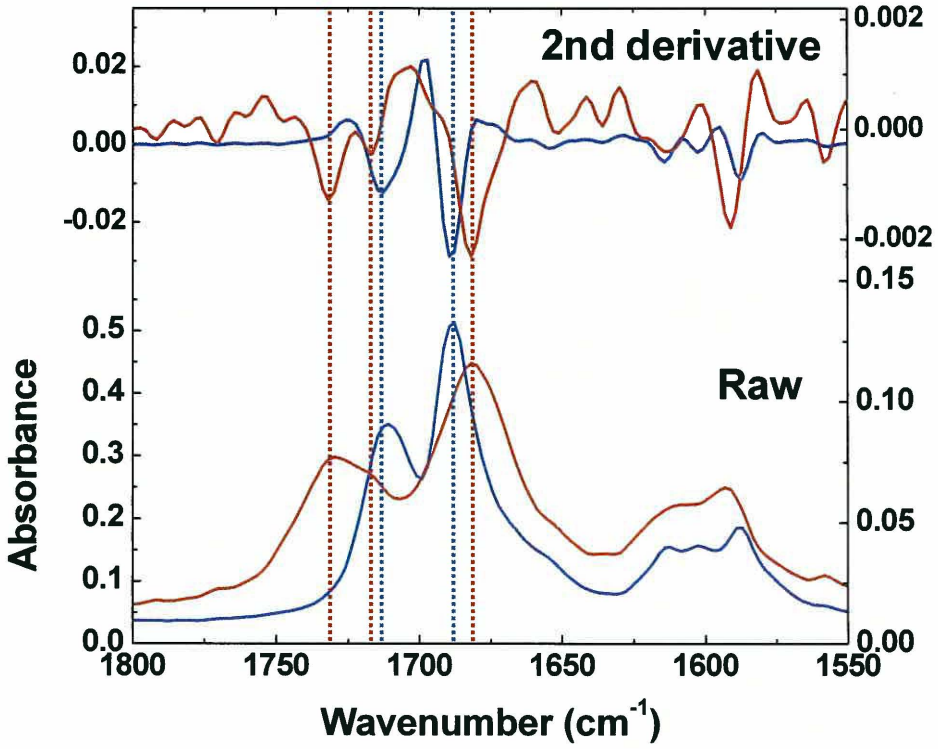

Figure 3. ATR-IR spectra (bottom) and their second derivatives (upper) of γ-crystalline indomethacin (blue line) and amorphous one in a solid dispersion (red line) in the C=O stretching region.

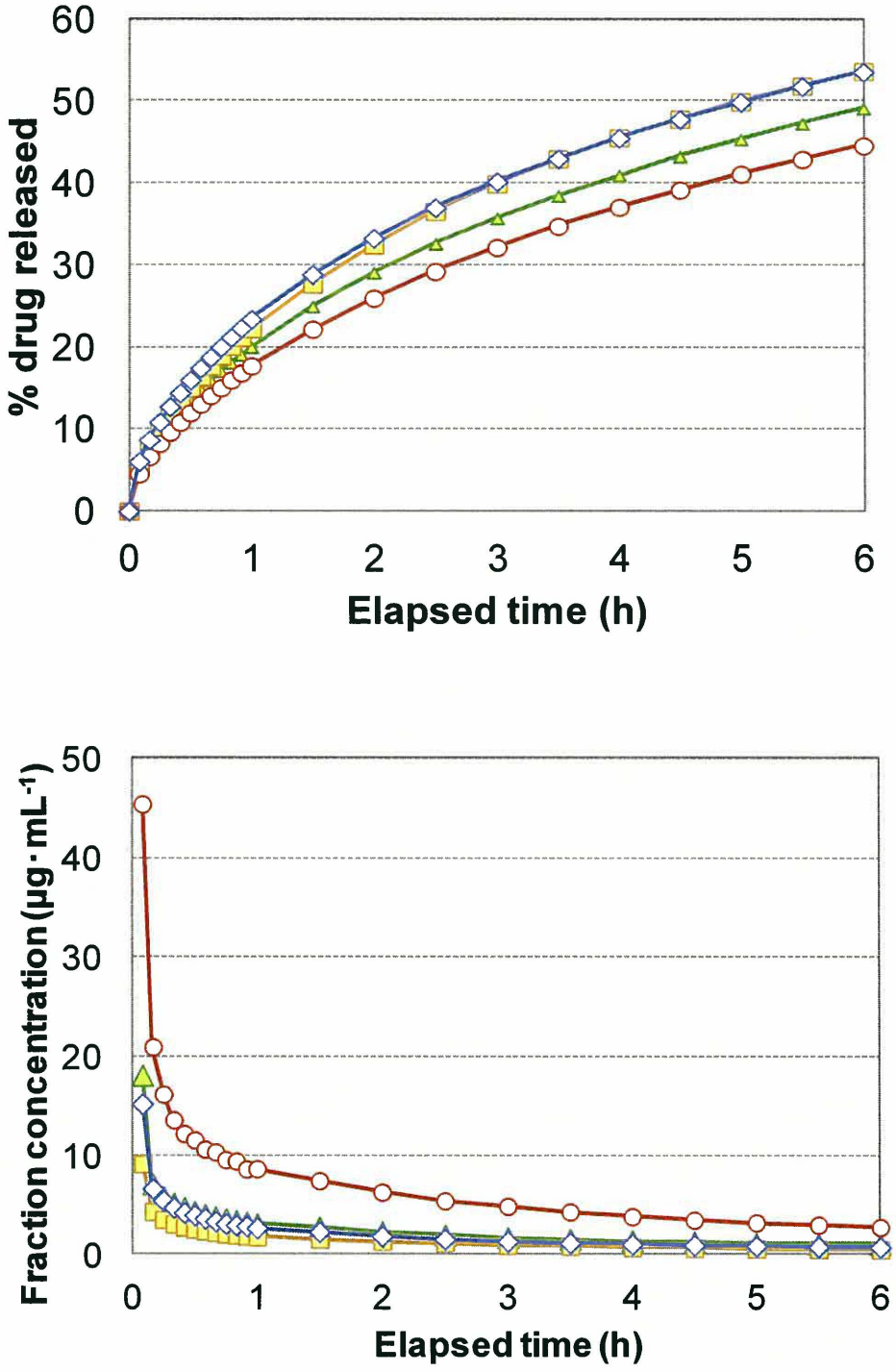

Figure 4. Accumulated percent drug-release profiles; (A), Effluent fraction concentration changes of indomethacin; (B), Medium flow rate is ○: 4 mL·min^{-1}, Δ: 12 mL·min^{-1}, ◇: 16 mL·min^{-1}, □: 24 mL·min^{-1}.

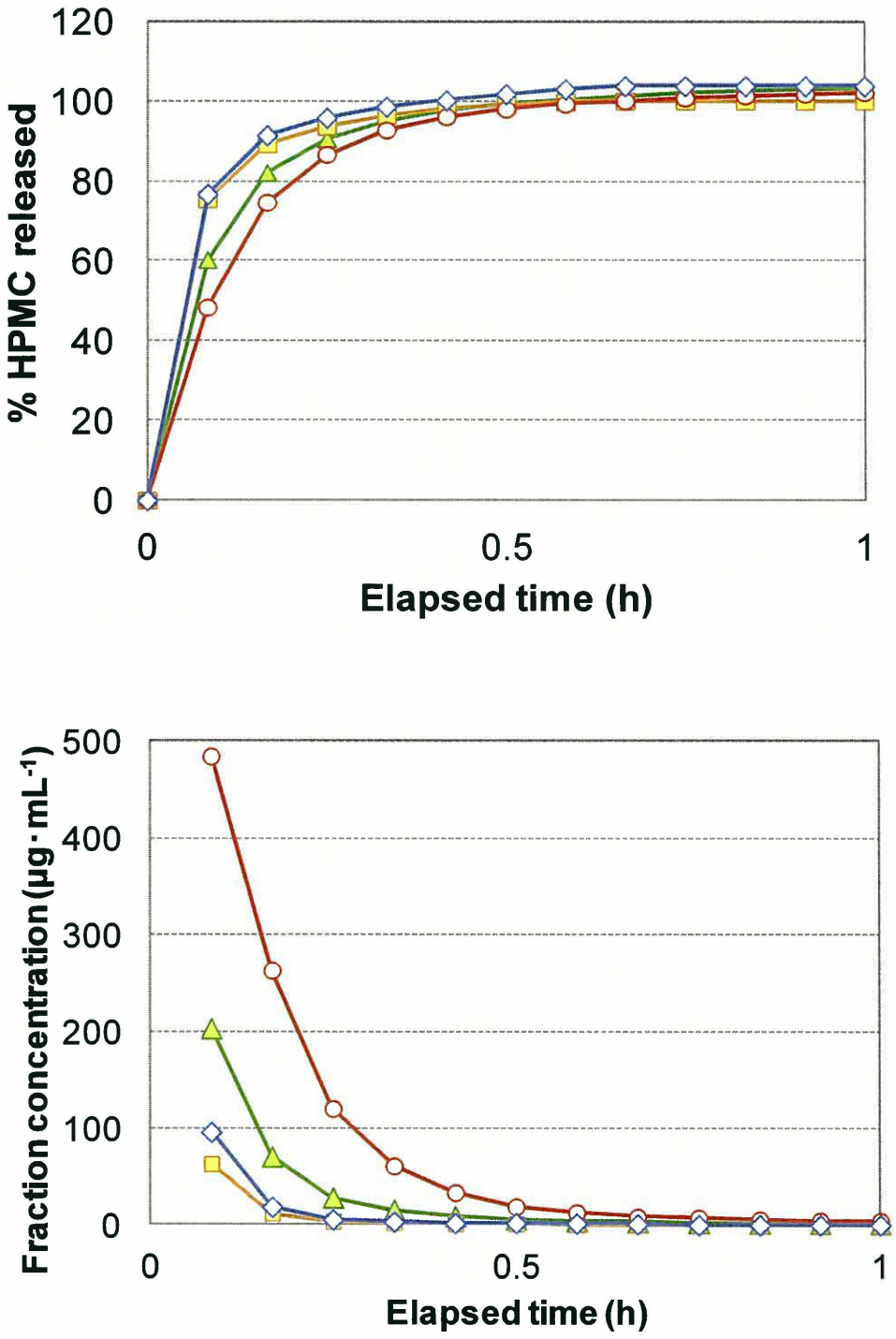

Figure 5. Accumulated percent HPMC-release profiles; (A), Effluent fraction concentration changes of HPMC; (B). Medium flow rate is ○: 4 mL·min^{-1}, Δ: 12 mL·min^{-1}, ◇: 16 mL·min^{-1}, □: 24 mL·min^{-1}.

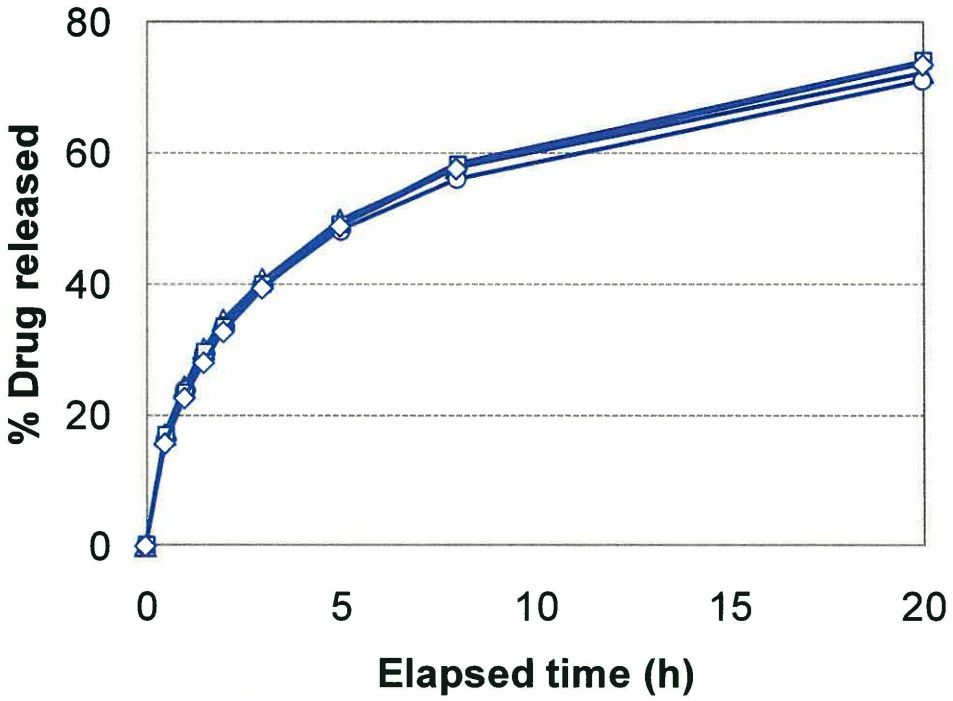

Figure 6. Accumulated percent drug-release profiles on closed-loop configuration.

Medium volume is ○: 600 mL, Δ: 1,200 mL, ◇: 1,800 mL, □: 3,000 mL.

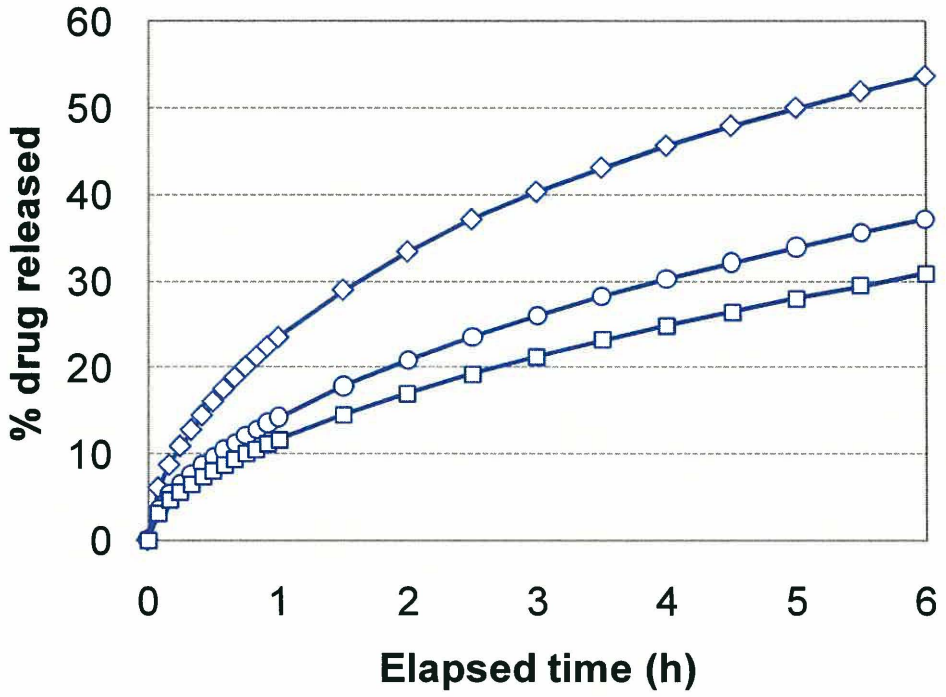

Figure 7. Accumulated percent drug-release profiles. Particle size is ○: 75-150 μm, ◇: 150-250 μm, □: 250-355 μm.

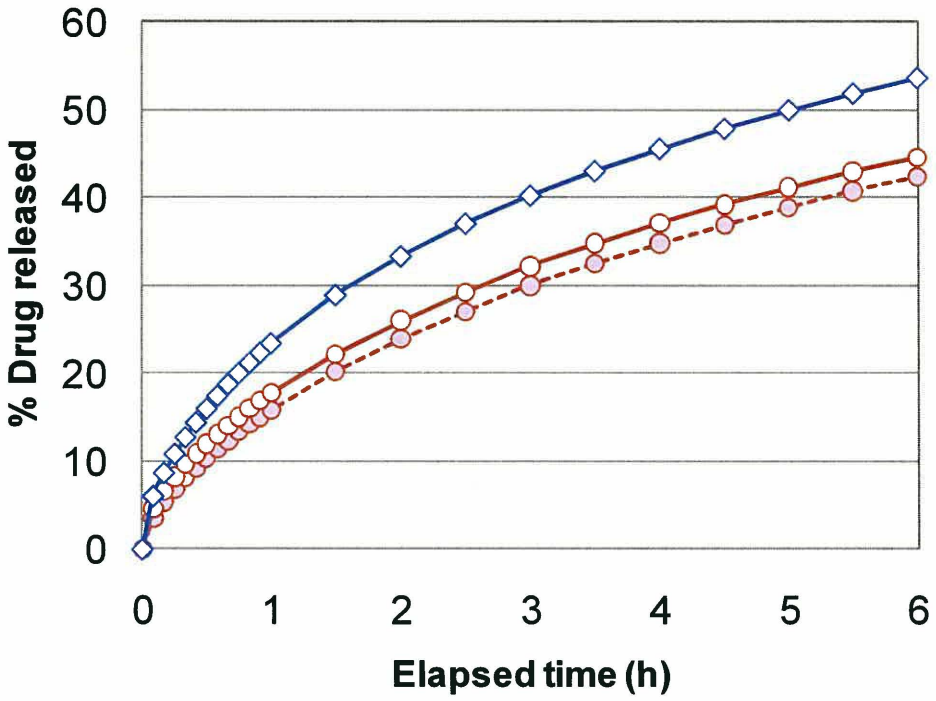

Figure 8. Accumulated percent drug-release profiles; hydrodynamic effect. Medium flow rate is dotted line: 4 mL·min^{-1} and solid line: 16 mL·min^{-1}, The type of flow-cell is ○: large cell and ◇: small cell.

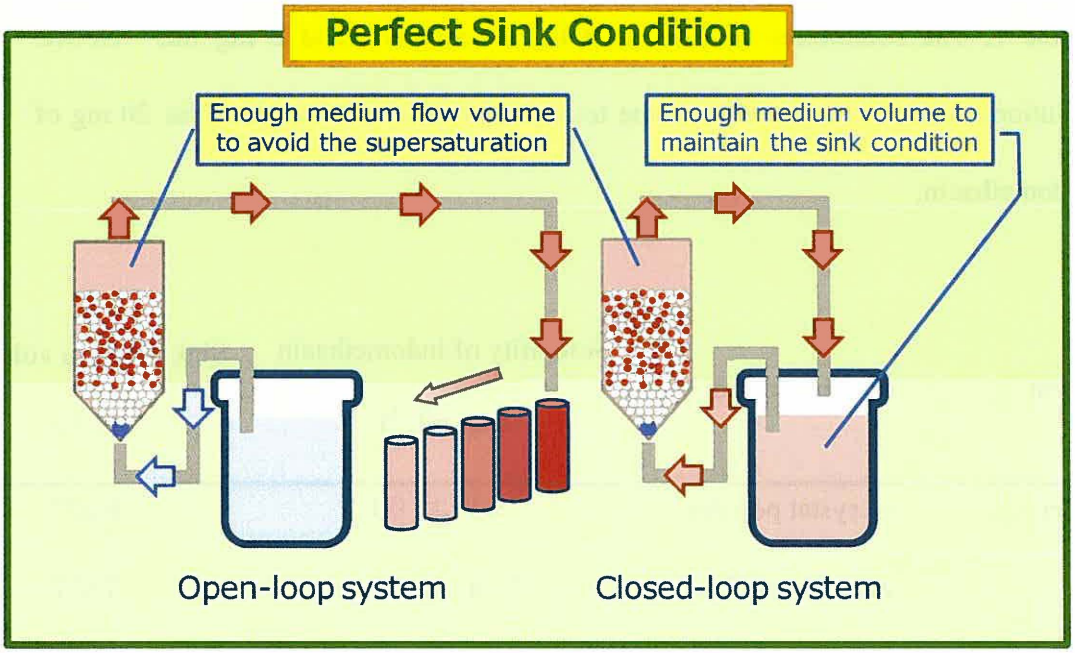

Figure 9. Schematic illustration of the critical factors in open and closed-loop configurations on flow-through cell.

Table 1. The solubilities of indomethacin in water, 0.5 and 2 $mg \cdot mL^{-1}$ HPMC solutions, and each necessary volume to maintain their sink condition for 20 mg of indomethacin.

Solvent	Sample state	Solubility of indomethacin ($\mu g \cdot mL^{-1}$)	Sink medium volume* (mL)
Water	γ-crystal powder	9.1 ± 0.1	6,577
	ethanol solution	15.6 ± 0.3	3,837
	solid dispersion	35.8 ± 0.4	1,675
0.5 $mg \cdot mL^{-1}$ HPMC solution	γ-crystal powder	11.6 ± 0.1	5,168
	ethanol solution	24.1 ± 0.3	2,486
	solid dispersion	37.7 ± 0.5	1,592
2 $mg \cdot mL^{-1}$ HPMC solution	γ-crystal powder	28.6 ± 0.1	2,097
	ethanol solution	40.8 ± 0.1	1,470
	solid dispersion	52.1 ± 0.7	1,151

*: Three times medium volume to dissolve 20 mg of indomethacin.

Table 2. Band assignments of infrared spectra of carbonyl stretching bands of indomethacin in γ-crystalline and solid dispersion.

Wavenumbers (cm^{-1})		Assignments
γ-crystalline IDM	IDM in solid dispersion	
-	1732	hydrogen bonded acid
1713	1716	cyclic dimer acid[42,43]
1689	1691	non-hydrogen bonded benzoyl[42,43]
-	1680	hydrogen bonded benzoyl

Chapter 4: Release Mechanism of Acetaminophen from Polyethylene oxide/polyethylene glycol Matrix Tablets utilizing Magnetic Resonance Imaging

Abstract

Release mechanism of acetaminophen (AAP) from extended-release tablets of hydrogel polymer matrices containing polyethylene oxide (PEO) and polyethylene glycol (PEG) were achieved using flow-through cell with magnetic resonance imaging (MRI). The hydrogel forming abilities are observed characteristically and the layer thickness which is corresponding to the diffusion length of AAP has a good correlation with the drug-release profiles. In addition, polymeric erosion contribution to AAP releasing from hydrogel matrix tablets was directly quantified using size-exclusion chromatography (SEC). The matrix erosion profile indicates that the PEG erosion kinetic depends primarily on the composition ratio of PEG to PEO. The present study has confirmed that the combination of *in situ* MRI and SEC should be well suited to investigate the drug-release mechanisms of hydrogel matrix such as PEO/PEG.

1. Introduction

In an effort to improve quality of life among patients, researchers have developed controlled-release technologies using hydrogel-forming polymers. Hydroxypropyl methylcellulose (HPMC) is the most common material as a hydrogel matrix for controlled-release tablets and capsules due to its safety, chemical stability, and compatibility with many drugs. The drug-release characteristics of HPMC matrices have been extensively investigated.[1–7] Recently, polyethylene oxide (PEO), which is highly soluble in water and has high gelability and low toxicity, has been proposed as an alternative hydrophilic polymer to HPMC for use in extended-release systems controlled by the drug self-diffusion and the polymeric matrix erosion.[8–13] Sako et al.[11] developed enhanced PEO hydrogel matrix tablets containing polyethylene glycol (PEG), which can be used as a hydrophilic component to promote the uptake of water into tablets and accelerate complete gelation within a few hours. They revealed that the combined use of PEO and PEG has enabled the stable, sustained release of drugs throughout the gastrointestinal tract, including the colon, where water availability is limited. Further, there has also been a number of studies on the drug-release behavior from PEO matrices.[14–16]

Evaluation of a drug-release mechanism generally involves characterization using drug-release profiles, which are determined by collecting fractions of the dissolution media and measurement using high-performance liquid chromatography (HPLC) or ultraviolet-visible (UV-VIS) spectroscopy. However, for more complex systems comprised of a number of functional polymeric excipients, thorough comprehension of the drug-release mechanism is difficult using drug-release profiles alone. In

particular, hydrogel matrix tablets are required a certain amount of time before the testing fluid reaches the tablet core, and subsequently they swell characteristically. Maggi et al.[17] reported that PEO matrices take approximately eight hours to reach the maximum swelling. Such previous findings have lent support to the belief that the kinetics of water ingress into tablets plays an important role in controlling drug-release from hydrogel matrices.

In recent years, magnetic resonance imaging (MRI) has been used to explore the hydration phenomenon in pharmaceutical products using hydrophilic polymer matrices such as HPMC and PEO.[18–25] Baumgartner et al.[19] used MRI to quantitatively describe the swelling process seen in HPMC and hydroxypropyl cellulose (HPC) hydrogels on the basis of the concentration and mobility of water and the polymer as functions of time and distance. Abrahmsén-Alami et al.[18] have developed a small release cell fitted in the MRI equipment, and revealed qualitatively and quantitatively the swelling and erosion behavior of PEO matrix tablet. Further, when MRI is combined with a flow-through cell apparatus for use in compendial analysis[26–28] (Fig. 1), the physical changes in solid dosage forms can be examined in a dissolution test.[20,29–31] Indeed, Fyfe et al.[20] used such a combined system to assess drug delivery devices and thereby obtain a better understanding of drug delivery systems based on diffusion, dissolution, and osmosis mechanisms. Further, Dorożyński et al.[29] and Kulinowski et al.[30] carried out the compendial flow-through cell dissolution method for a HPMC matrix using two different solutions; fasted state simulating gastric fluid (FaSSGF) and fed state simulating gastric fluid (FeSSGF), under the continuous flow conditions to simulate *in vivo*

conditions as closely as possible. However, the integrated investigation of the drug-release mechanism from PEO hydrogel matrix tablet among the cumulative drug-release profiles, the contribution of hydrogel matrix erosion and the conformation changes of the hydrogel under the compendial flow-through cell dissolution method have not been reported.

Here, to comprehensively examine the unique drug-release mechanisms from PEO/PEG hydrogel matrix tablets, I used the combination of flow-through cell equipped with an MRI device to simultaneously evaluate the cumulative drug-release profiles and internal states of tablets over time in a non-invasive and non-destructive manner. Further, the effect of polymeric erosion was assessed using size-exclusion chromatography (SEC), which was the most common way to obtain information about the molecular mass distribution of polymers.[18,32,33] Acetaminophen (AAP) was used as a water-soluble drug, thereby enabling me to ignore the rate-determining step and instead focus on examining the drug-release mechanism from PEO/PEG hydrogel matrices.

2. Experimental

2.1. Materials

AAP was purchased from API Corporation (Tokyo, Japan), and two kinds of PEO with average molecular weights of 7.0×10^6 (Polyox WSR 303, PEO-7M) and 2.0×10^6 g/mol (Polyox N60K, PEO-2M) were obtained from Dow Chemical (MI, USA). PEG with an average molecular weight between 7.3×10^3 and 9.3×10^3 g/mol (Macrogol 6000) was purchased from Sanyo Chemical Industries (Kyoto, Japan). All other chemicals used were of reagent grade.

2.2. Preparation of Testing Tablets

To avoid aggregation, the AAP and polymers (PEO and PEG) were passed through a sieve (355-μm aperture) before mixing. In total, six tablets were prepared with the concentration of AAP in each fixed at 10% (w/w). Polymer matrices of PEO and PEG mixtures were blended at weight ratios of 5:1, 1:1, and 1:5, respectively, and the tablets were designated A, B, C, D, E and F in Table 1. AAP was manually mixed with PEO and PEG in separate mortars for 5 min, and the resultant mixtures were compressed into 200-mg tablets in an autograph oil press (AGS-20kNG; Shimadzu, Kyoto, Japan) using 8 kN in applied force and a round-faced 8.0-mm diameter tooling.

2.3. Dissolution Test

The *in vitro* drug-release properties of the tablets were evaluated via the flow-through cell apparatus (DZ70; Pharma-Test AG, Hainburg, Germany) at a flow rate of 4 mL/min in a closed loop circuit containing 900 mL of dissolution test medium at 37 °C following the pharmacopoeia.[26–28] A flow-through cell was filled with 1-mm glass beads to create laminar flow, and a metal clip was used to hold the tablet in the original position. Distilled water was used as the medium, and was degassed by filtration in a vacuum before use, as described in the protocol.[28] Every two hours, the dissolution medium was withdrawn from the dissolution vessels and the amount of AAP released from the tablets was measured using UV-VIS spectroscopy at 280 nm (UV-2400PC; Shimadzu). In addition, the amounts of PEO

and PEG eroded from the matrices were quantified by SEC, using a HPLC system (1200 series; Agilent Technologies, CA, USA) equipped with a charged aerosol detector (Corona CAD; ESA Biosciences, MA, USA) and a SEC column (TSK-GEL Alpha-3000; Tosoh, Tokyo, Japan; 7.8 mm i.d. × 30 cm, 7 μm). Purified water was used as a mobile phase for HPLC analysis, and the flow rate was 0.75 mL/min.

2.4. Magnetic Resonance Imaging Scanning during the Dissolution Test

My experiment combining MRI with a flow-through cell method was conducted using a bench-top MRI system (MARAN-iP; Oxford Instruments, Oxfordshire, UK) equipped with a 0.5 tesla permanent magnet system stabilized at 37 °C and operating at 20.6 MHz for ^{1}H-NMR imaging. The testing conditions for flow-through cell were described in 2.3. MRI images were collected under the continuous medium flow conditions. To maintain the tablet in its original slice position for image acquisition, a plastic holder with a rubber retaining band was used instead of the original metal Pharmacopoeia clip, since a metal clip would have caused distortions in the magnetic field. T_1-weighted images were produced in the spin echo method. The signal intensity of the MRI pictures was defined as

$$S = M_0 \times \exp\frac{-\mathrm{TE}}{T_2} \times (1 - \exp\frac{-\mathrm{TR}}{T_1}) \quad (1)$$

where M_0 is magnetization, T_1 and T_2 are relaxation times, and TR and TE are repetition time and echo time, respectively. The imaging parameters were as follows: TR, 1 s; TE, 10 ms; the number of accumulations, 2; single image acquisition time, 4.3 min.; and temporal resolution of MRI data, 30 min. Resolution for the 128 × 128 pixel 2D images was 250 μm, with a slice thickness of 3 mm. In

the present study, the image processing and analysis were carried out as with previous works using Image analysis and ImageJ software.[22,23]

2.5. Fourier transform Infrared Spectroscopy

All IR spectra were measured at a resolution of 2 cm^{-1} using a FT-IR spectrometer (NICOLET 6700; Thermo Fisher Scientific, MA, USA) equipped with a diamond-ATR accessory and a deuterated triglycine sulfate detector. In order to acquire the IR spectra of both hydrogelling and non-hydrogelling parts, Tablet A was taken one hour after starting dissolution test. Tablet A was measured as a representative hydrogel matrix, because the two states are expected to be the same among six tablets. It was peeled and divided into the hydrogel layer and non-hydrogel core to understand the differences between the two states. A total of 64 scans were co-added to obtain spectra for each layer, the dried Tablet A, and water. All of the IR spectra were defined in absorbance units as

$$A = -\log_{10}\frac{R}{R_0} \tag{2}$$

where R and R_0 are the intensities of IR light from a sample and a reference compound, respectively.

3 Results

3.1. Dissolution Study by Flow-through Cell

Photos were taken every two hours during the flow-through cell dissolution test for Tablet A (Fig. 2). These photos clearly show gradual swelling of the tablet over time, due to gelling of the hydrophilic matrix, and complete gelling within approximately

four hours.

Cumulated drug-release curves for the tablets used in the present study indicated that the lower the concentration and molecular weight of PEO, the faster AAP released (Fig. 3). In particular, Tablet F showed much faster AAP releasing than the other tablets. These findings therefore suggested the possibility that the release mechanism of Tablet F differed from those of other tablets.

3.2. Infrared Spectra

I investigated the types of water and the interaction between water and PEO/PEG matrix in the hydrogel using FT-IR spectroscopy. Fig. 4a showed IR spectra in the 4000-750 cm^{-1} region of dried Tablet A, water as a dissolution medium, and the surface of both the hydrogel layer and non-hydrogel core of Tablet A which was taken one hour after starting dissolution test. Figures 4b and 4c depicted enlarged spectra in the 3700-2700 and 1200-980 cm^{-1} regions, respectively. A relatively intense O-H stretching band (3700-3000 cm^{-1}), due to water penetration, could be seen in the hydrogel layer (blue line) and appeared strikingly similar to that for bulk water (light-blue line), indicating that much of the free water existed in the hydrogel layer. Interestingly, this O-H stretching band can also be observed in the non-hydrogel core (red line), although not in the dried tablet (green line), in a higher wavenumber (approximately 3500 cm^{-1}) than that for bulk water (light-blue line). This observation suggests the presence of non-freezing water in the non-hydrogel core,[34,35] indicating incomplete hydrogelling transformation. Further, as the dissolution medium penetrated into a tablet, a C-O stretching band at 1102 cm^{-1} (red

line) shifted by approximately 20 cm^{-1} to a lower wavenumber (blue line) caused by the formation of hydrogen bonds between the C-O groups of PEO/PEG and water molecules (Fig. 4c). The C-O-C asymmetric stretching band at 1061 cm^{-1} assigned to a helical conformation of crystalline PEO/PEG[36] disappeared in the spectrum of the hydrogel layer (blue line), indicating that the crystalline hydrophilic matrices were completely altered to an amorphous state by water penetration.

3.3. Magnetic Resonance Imaging Monitoring

^{1}H-NMR images of each tablet during the flow-through cell dissolution test were shown in Fig. 5. In each image, non-hydrogelling layers were shown in black (extremely short T_2 relaxation time), hydrogelling layers in white (T_1 relaxation time: <1 s), and dissolution medium in gray (T_1 relaxation time: approximately 3 s). The high-intensity areas of the hydrogels in MRI images (white part, Fig. 5) had a smaller relaxation time (T_1) than bulk water (gray region, Fig. 5) due to the hydrogen bonds between the hydrophilic polymers and water,[37] as verified by IR study. Further, the IR study additionally indicated that the zero intensity region (black area) was a non-hydrogelling layer.

The time-dependence of the gelling process was quantified by plotting the changes in the non-hydrogelling regions (black area, Fig. 5) during the dissolution test (Fig. 6a). Changes in hydrogel thicknesses (white part, Fig. 5) during the dissolution test were shown in Fig. 6b. MRI studies suggest that the non-hydrogel area (black part) was reduced as the fluid was penetrated into a tablet (Fig. 6a). In the present study, all non-hydrogel portions of all tablets disappeared within approximately three hours,

indicating that all of the tablets' matrices were hydrated and gelled. Further, from a different viewpoint, the MRI data shown in Fig. 6a indicate the fluid ingress behavior. For both the PEO-2M and PEO-7M formulations, the greater the concentration of PEG in tablets, the faster the penetration of dissolution medium. However, no significant difference in penetration process is observed between the two formulations.

Evaluation of changes in hydrogel layer thickness during the dissolution test indicated that their thicknesses increase with time, except in Tablets C and F (Fig. 6b). The differing findings with Tablets C and F are believed to be due to the higher content of PEG in these tablets when compared with the other tablets, as water-soluble PEG tends to accelerate tablet erosion. Further, tablets containing PEO-7M retained a much thicker hydrogel portion than tablets with PEO-2M. Taken together, these results suggest that the greater molecular weight and tangled structure of PEO-7M will allow it to form a more rigid hydrogel structure than PEO-2M.

Given the MRI findings of the present study, I hypothesize that the hydrogelation kinetics of the tablets depends only on the composition ratio of PEG to PEO. However, the behavior of hydrogel formation was not completely controlled by the concentration of PEG, on the other hand, the shape retention capability were strongly affected by the concentration of PEG as well as the molecular weight of PEO.

3.4. Erosion Behavior of Hydrogel Matrices

Figures 7a and 7b show the erosion profiles of PEO and PEG quantified by SEC, respectively, for each formulation during flow-through cell dissolution study. These profiles appear to indicate that the accumulative erosion profiles of PEG depend primarily on the composition ratio of PEG to PEO, given that tablets with higher compositions of PEG showed quicker erosion of hydrogel matrices than those with lower compositions; similar patterns were also observed for PEO. Considering that PEG is more soluble and releasable than PEO, erosion of PEG should initiate and subsequently accelerate the erosion of PEO from the hydrogel.

Findings also showed that accumulative erosion profiles of PEO-2M exceeded those of PEO-7M, due to the differences in the molecular weight mentioned before. The characteristic erosion profiles observed for Tablet F may be explained by considering that the erosion effect of Tablet F's formulation, which included a relatively high concentration of PEG and the relatively low-molecular weight PEO-2M.

4. Discussion

4.1. Correlation between Fluid Ingress and Acetaminophen Release Behaviors

MRI findings in the present study suggest that the dissolution medium perfused the whole tablet within the first few hours (Fig. 6a), suggesting complete dissolution of AAP in the tablet within 3 hours. However, as shown in Figure 3, AAP was not fully released from the hydrogel matrices within the expected period, even though the tablet was completely infused with testing medium within the first few hours (see Fig. 2 and 6a). Indeed, the amount of drug-released from Tablets A-F range between

40% and 80% at the sampling point of 4 hours, indicating that there is no correlation between fluid ingress behavior and the cumulative drug-release profile. Therefore, the contributions of both the drug self-diffusion and the matrix erosion which are well known controlling factors will be discussed below.

4.2. Diffusion of Acetaminophen from Hydrogel Matrices

To discuss the diffusion mechanism of AAP from PEO/PEG matrices, the relationship between hydrogel layer thicknesses and cumulative AAP release profiles was evaluated, with results showing a good correlation between their accumulated layer thicknesses measured by MRI every 30 min. and the amount of drug-released (Fig. 8). In the early phase of dissolution test, up to around two hours after starting dissolution test, there were little differences in the amount of AAP released whose drug molecules were originally located near the surface of each tablet. On the other hand, after about four hours, the amount of drug-released decreases with increasing drug diffusion length corresponding to the thicknesses of their matrix layers, prompting the conclusion that hydrogel layer thickness may affect the cumulative AAP release profile. Thus, the hydrogel layer thickness is regarded as the primary factor of controlling drug-release by diffusion from the PEO/PEG matrices, except for in Tablet F, the erosion mechanism of which will be discussed below.

4.3. Erosion of Hydrogel Matrices

In the present study, I were able to precisely detect changes in hydrogel thicknesses

during the dissolution test using MRI (Fig. 6b). However, estimating the contribution of hydrogel erosion to the drug-release profile based solely on the MRI data proved difficult. Therefore, I used SEC to directly define the erosion profiles of each hydrophilic polymer over time in the dissolution test (Fig. 7).

Typically, hydrogel matrices constructed using high-molecular weight polymers do not show much erosion, particularly at early stages of dissolution, as their helical chains tend to form rigid interactions among polymer molecules. With regard to PEO, the crystalline portion was transformed into an amorphous (random) state, which improved the molecular and chain interaction when the compound was soaked in water (see Section 3.2). However, erosion and diffusion of both PEO and PEG were observed even for tablets with a high ratio of PEO to PEG (Fig. 7). SEC data suggest that once portions of PEO or PEG begin to erode, large pores form in the hydrogel matrix, possibly contributing to subsequent further erosion. The large amount of PEG and infusion of low-molecular weight PEO-2M in Tablet F may therefore explain the significantly faster release of not only AAP but PEO and PEG observed with this tablet in comparison with other tablets. These results indicate that SEC is useful for quantifying the amount of eroded matrices in discerning the release mechanism for controlled-release tablets.

4.4. Release Mechanisms on Poly(ethylene oxide)/Poly(ethylene glycol) Hydrogel Matrix Tablets

A schematic illustration of the release mechanisms of AAP from PEO/PEG matrix tablets was presented in Fig. 9. As with the MRI images, the dark gray areas

represent portions of the non-hydrogel core, while the white areas indicated portions of the hydrogel layer. Black, blue, and red particles represented non-dissolved AAP, dissolved AAP, and AAP released from the matrix, respectively.

Results from the present study indicate that the drug-release mechanism of Tablet F is strongly controlled by the erosion of its hydrogel matrix (depicted as "Erosion" in Fig. 9). For this tablet, the erosion of PEG and PEO-2M occurs when the testing solution begins to penetrate into the matrix, and the erosion profiles of their hydrophilic materials are completely consistent with the release profile of AAP. In contrast, the AAP release in the other tablets (A, B, C, D, and E) is faster than their matrix erosion, indicating that the release mechanism of AAP is not controlled by matrix erosion, and is primarily dominated by the self-diffusion of AAP through the hydrogel layers (depicted as "Diffusion" in Fig. 9). Further, the cumulative drug-release profiles are restrained with increasing hydrogel layer formation which is dependent on the composition of hydrogel matrices (depicted as "Fluid ingress" in Fig. 9).

With regard to Tablets A-E, I suspect that erosion of hydrogel matrices did indeed occur, as a measurable amount of PEO/PEG is found to be removed from the matrices (see Fig. 7). In the late stage of the dissolution test in particular, I suspect that the thinner the hydrogel layer becomes, the shorter the diffusion length for AAP. Thus, matrix erosion also affects the drug-release behavior indirectly.

5. Summary

The AAP release mechanism from Tablet F which contains high PEG ratio to PEO

and low molecular weight PEO is found to be strongly controlled by the erosion of the hydrogel matrix by SEC. On the other hand, the mechanism from the other tablets whose ratios of PEO to PEG is higher than that of Tablet F is not dominated by matrix erosion, and the contribution of the drug self-diffusion through the hydrogel layers is demonstrated by MRI.

Flow-through cell equipped with MRI and SEC are well suited to investigate the release mechanisms of hydrogel matrix tablets. With further development, this sort of combination study may aid in better understanding of the release mechanisms of pharmaceutical drug delivery system products.

6. References

1 Alderman, D. A. *Int. J. Pharm.* 1984, 5, 1–9.

2 Ford, J. L.; Rubinstein, M. H.; Hogan, J. E. *Int. J. Pharm.* 1985, 24, 327–338.

3 Ford, J. L.; Rubinstein, M. H.; Hogan, J. E. *Int. J. Pharm.* 1985, 24, 339–350.

4 Ford, J. L.; Rubinstein, M. H.; McCaul, F.; Hogan, J. E.; Edgar, P. J. *Int. J. Pharm.* 1987, 40, 223–234.

5 Ford, J. L.; Mitchell, K.; Rowe, P.; Armstrong, D. J.; Elliott, P. N. C.; Rostron, C.; Hogan, J. E. *Int. J. Pharm.* 1991, 71, 95–104.

6 Rao, K. V. R.; Devi, K. P.; Buri, P. *J. Control. Release* 1990, 12, 133–141.

7 Salomen, J. L.; Doelker, E.; Buri, P. *Pharm. Ind.* 1979, 41, 799–802.

8 Graham, N. B.; McNeill, M. E. *Biomaterials* 1984, 5, 27–36.

9 Kim, C. J. *J. Pharm. Sci.* 1995, 84, 303–306.

10 Kim, C. J. *Drug Dev. Ind. Pharm.* 1998, 24, 645–651.

11 Sako, K.; Nakashima, H.; Sawada, T.; Fukui, M. *Pharm. Res.* 1996, 13, 594-598.

12 Sako, K. *Pharm. Tech. Japan* 1998, 14, 85-98.

13 Yang, L.; Venkatesh, G.; Fassihi, R. *J. Pharm. Sci.* 1996, 85, 1085–1090.

14 Kojima, H.; Yoshihara, K.; Sawada, T.; Kondo, H.; Sako, K. *Eur. J. Pharm. Biopharm.* 2008, 70, 556-562.

15 Maggi, L.; Segale, L.; Torre, M. L.; Machiste, E. O.; Conte, U. *Biomaterials* 2002, 23, 1113-1119.

16 Wu, N.; Wang, L. S.; Tan, D. C. W.; Moochhala, S. M.; Yang Y. Y. *J. Control. Release* 2005, 102, 569-581.

17 Maggi, L.; Bruni, R.; Conte, U. *Int. J. Pharm.* 2000, 195, 229-238.

18 Abrahmsén-Alami, S.; Körner, A.; Nilsson, I.; Larsson, A. *Int. J. Pharm.* 2007, 342, 105-114.

19 Baumgartner, S.; Lahajnarb, G.; Sepeb, A.; Kristala, J. *Eur. J of Pharm. and Biopharm.* 2005, 59, 299-306.

20 Fyfe, C. A.; Grondey, H.; Blazek-Welsh, A. I.; Chopra, S. K.; Fahie, B. J. *J. Control. Release* 2000, 68, 73-83.

21 Kojima, M.; Nakagami, H. *Chem. Pharma. Bull.* 2002, 50, 1621-1624.

22 Malaterre, V.; Metz, H.; Ogorka, J.; Gurny, R.; Loggia, N.; Mäder, K. *J. Control. Release* 2009, 133, 31-36.

23 Metz, H.; Mäder, K. *Int. J. Pharm.* 2008, 364, 170-175.

24 Richardson, J. C.; Bowtell, R. W.; Mäder, K.; Melia, C. D. *Adv. Drug Deliv. Rev.* 2005, 57, 1191-1209.

25 Strübing, S.; Metz, H.; Mäder K. *J. Control. Release* 2008, 126, 149-155.

26 *European Pharmacopoeia, seventh ed.*, European Directorate for the Quality of Medicines, 2011, 266–275.

27 *The Japanese Pharmacopoeia 16th ed.*, Society of Japanese Pharmacopoeia, 2011, 116–120.

28 *The United States Pharmacopeia 34-National Formulary 29*, The United States Pharmacopeial Convention, 2011, 278–285.

29 Dorożyński, P.; Kulinowski, P.; Jachowicz, R.; Jasiński, A. *AAPS PharmSciTech* 2007, 8, art no. 15, E1-E4.

30 Kulinowski, P.; Dorożyński, P.; Jachowicz, R.; Weglarz, W. P. *J. Pharm.*

Biomed. Aanl. 2008, 48, 685-693.

31 Nott, K. P. *Eur. J. Pharm. Biopharm.* 2010, 74, 78-83.

32 Kuga, S. *J. Chromatgr.* 1981, 206, 449-461.

33 Laguna, M. T. R.; Medrano, R.; Plana, M. P.; Tarazona, M. P. *J. Chromatogr. A* 2001, 919, 13-19.

34 Morita, S.; Tanaka, M.; Ozaki, Y. *Langmuir* 2007, 23, 3750-3761.

35 Tanaka, M.; Mochizuki, A. *J Biomed. Mater. Res.* 2004, 68A, 684-695.

36 Brubach, J.B.; Ollivon, M.; Jannin, V.; Mahler, B.; Bourgaux, C.; Lesieur, P.; Roy, P. *J Phys. Chem. B* 2004, 108, 17721-17729.

37 Fyfe, C. A.; Blazek A.I. *Macromolecules* 1977, 30, 6230-6237.

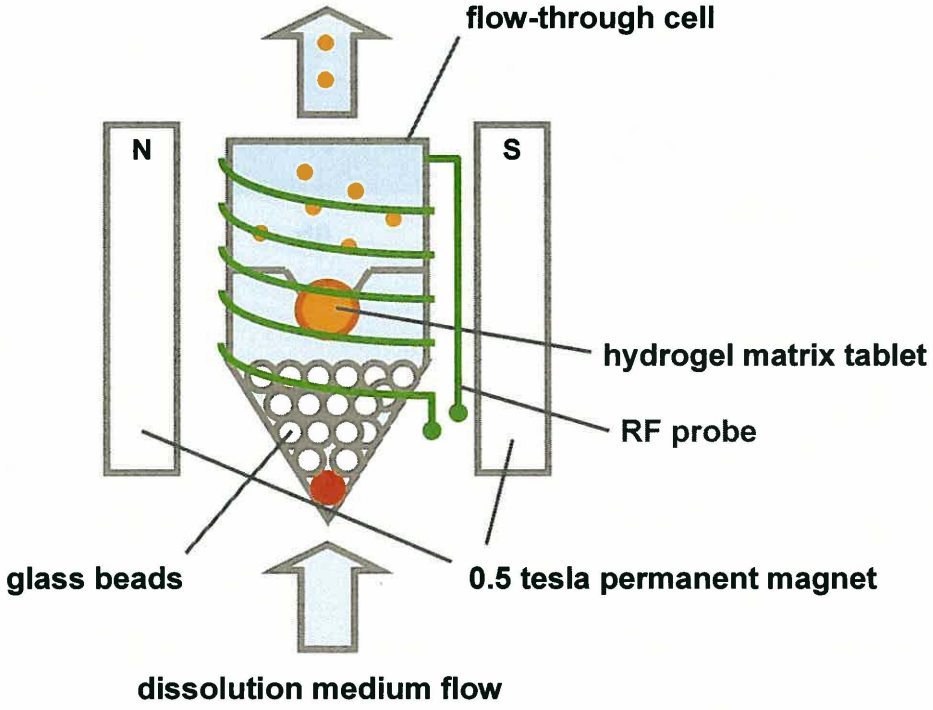

Figure 1. Schematic illustration of flow-through cell apparatus fitted with a MRI.

Figure 2. Hydrogelation progress of Tablet A; PEO-7M/PEG (5:1) during flow-through cell dissolution test.

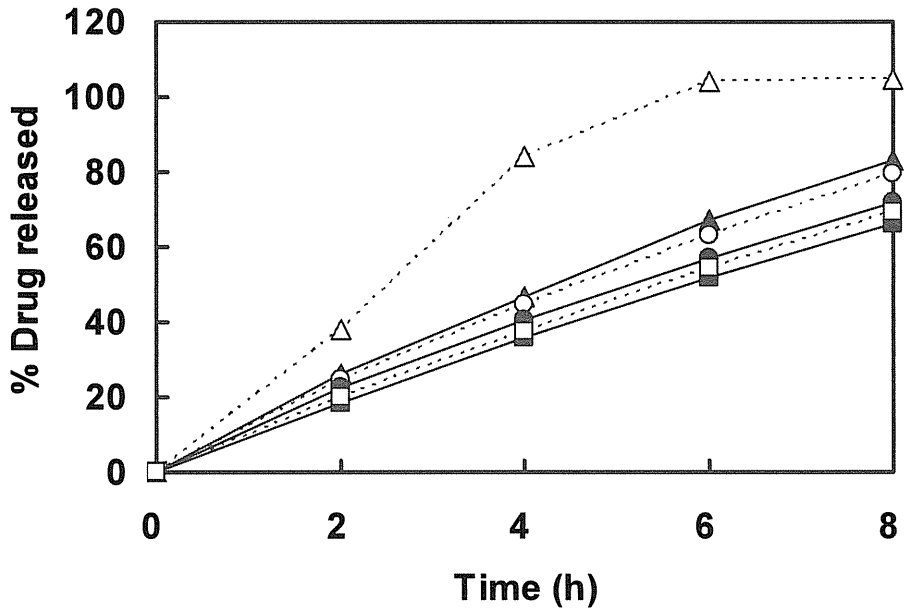

Figure 3. Release profile of AAP; ■: Tablet A: PEO-7M/PEG (5:1), ●: Tablet B: PEO-7M/PEG (1:1), ▲: Tablet C: PEO-7M/PEG (1:5), □: Tablet D: PEO-2M/PEG (5:1), ○: Tablet E: PEO-2M/PEG (1:1), Δ: Tablet F: PEO-2M/PEG (1:5).

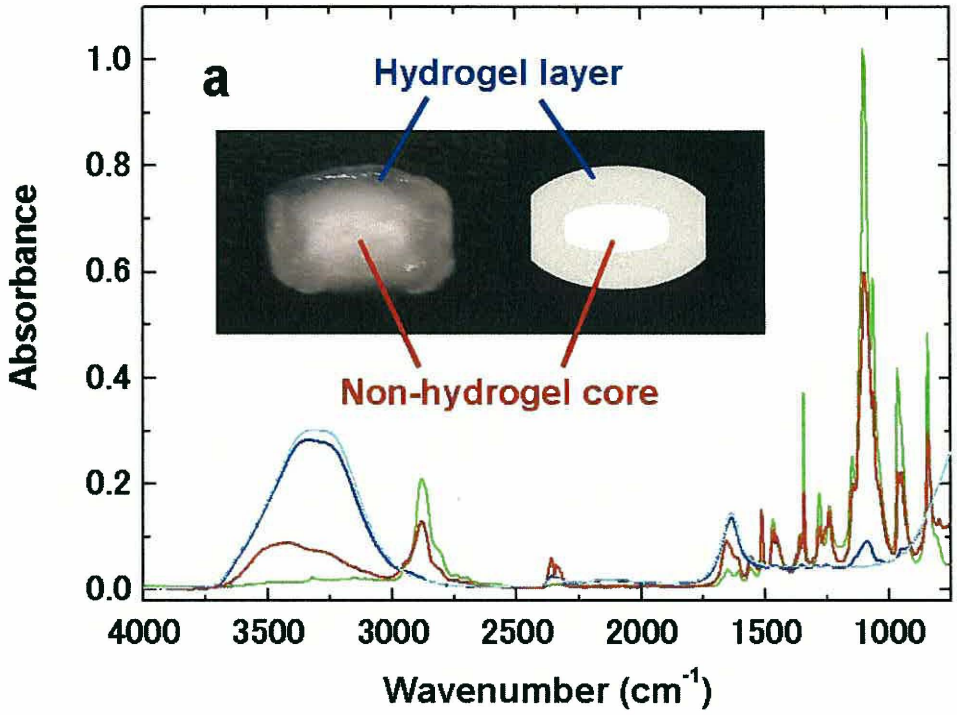
a
Hydrogel layer
Non-hydrogel core
Absorbance
1.0
0.8
0.6
0.4
0.2
0.0
4000
3500
3000
2500
2000
1500
1000
Wavenumber (cm-1)

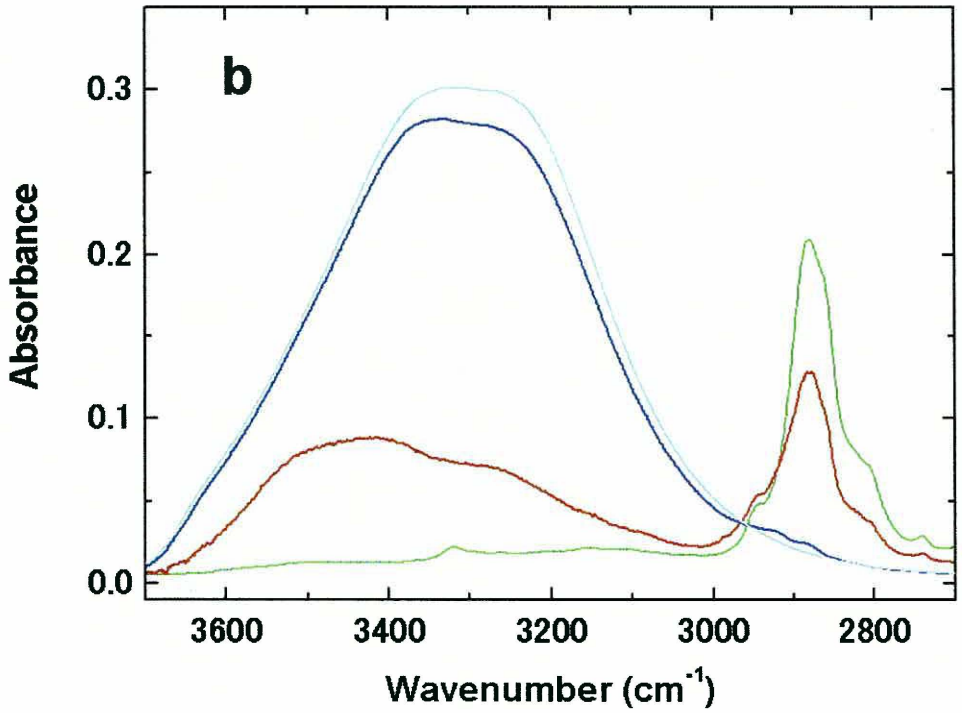
b
Absorbance
0.3
0.2
0.1
0.0
3600
3400
3200
3000
2800
Wavenumber (cm-1)

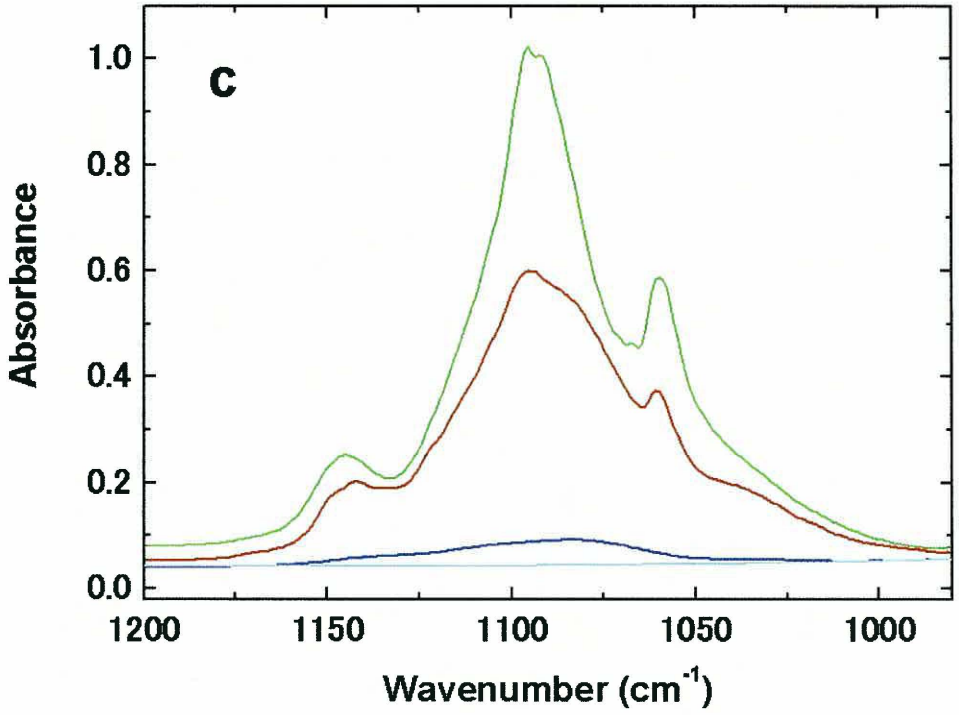

Figure 4. ATR-IR spectra of dried Tablet A, water, and the surface of the hydrogel layer and non-hydrogel core parts of Tablet A, at one hour after the dissolution test in the 4000-750 cm^{-1} region (a), close-up spectra in the O-H stretching region (b), and close-up spectra in the C-O stretching region (c). Green line: dried Tablet A, blue line: surface of the hydrogel layer, red line: surface of the non-hydrogel core part, and light blue line: water.

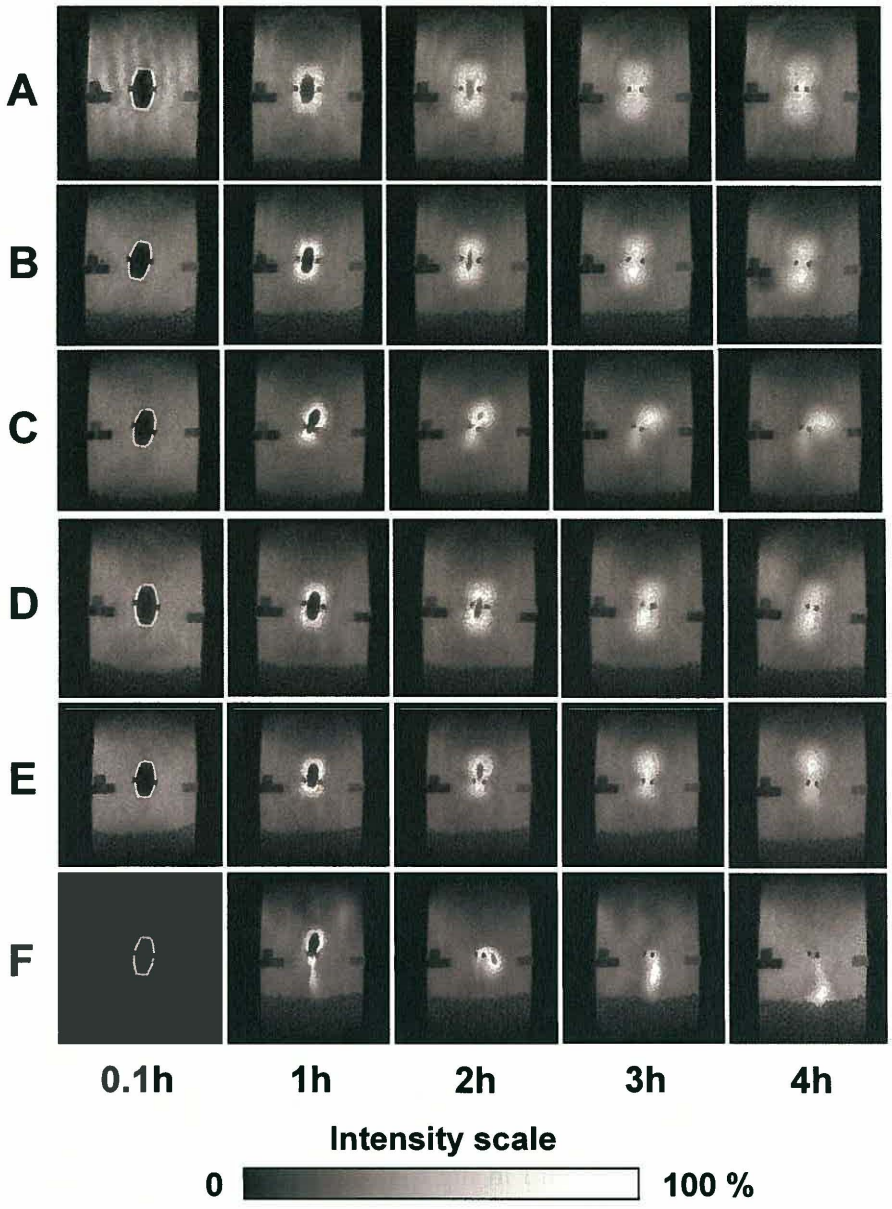

Figure 5. MRI images of each formulation during flow-through cell dissolution test, taken every hour. From the top: (A) Tablet A: PEO-7M/PEG (5:1), (B) Tablet B: PEO-7M/PEG (1:1), (C) Tablet C: PEO-7M/PEG (1:5), (D) Tablet D: PEO-2M/PEG (5:1), (E) Tablet E: PEO-2M/PEG (1:1), and (F) Tablet F: PEO-2M/PEG (1:5).

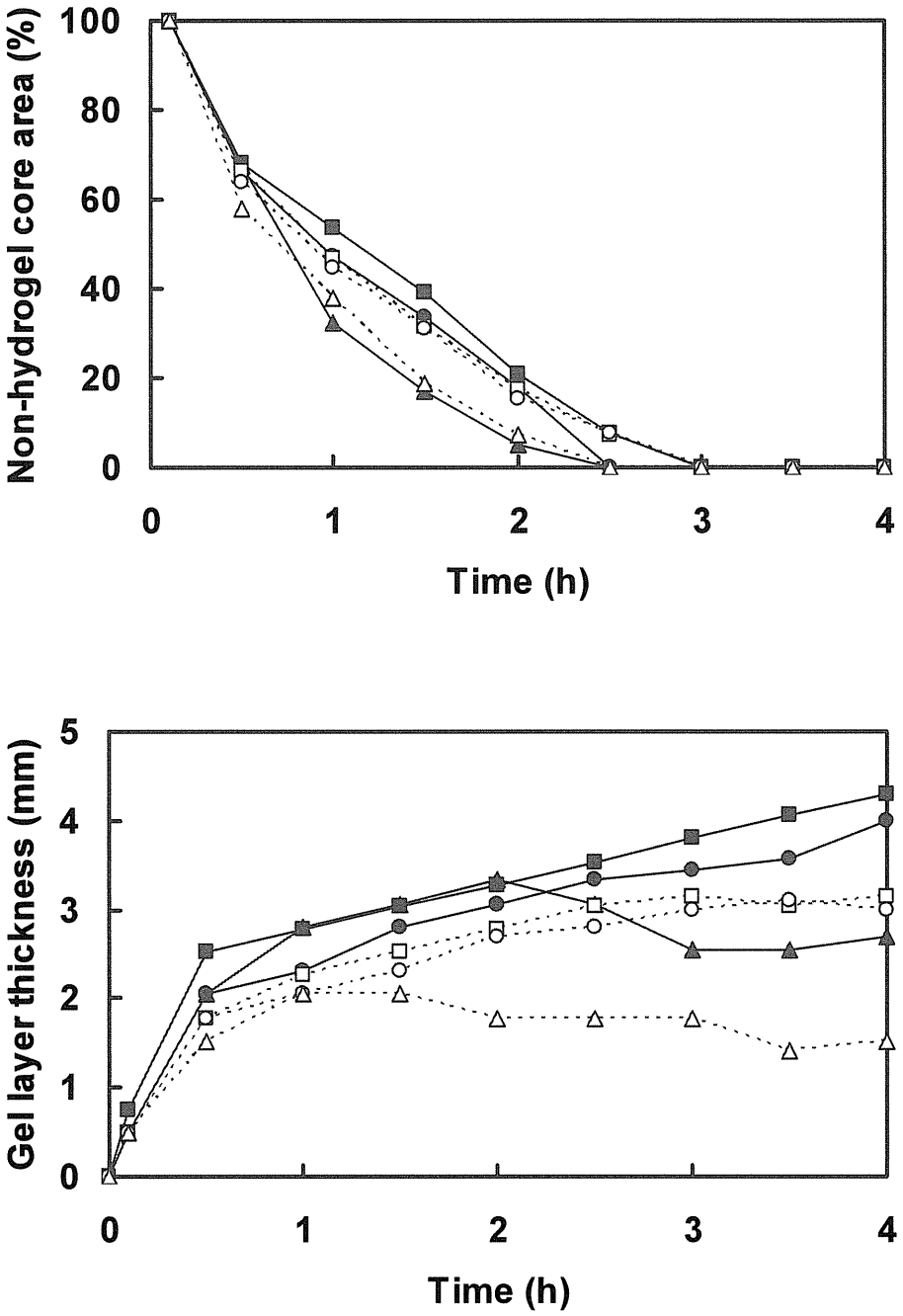

Figure 6. Analysis graphs for MRI images of each tablet in the dissolution study. (a): Ratios of remaining portions of the non-hydogelling core to each initial area, (b): gel layer thickness. ■: Tablet A: PEO-7M/PEG (5:1), ●: Tablet B: PEO-7M/PEG (1:1), ▲: Tablet C: PEO-7M/PEG (1:5), □: Tablet D:

PEO-2M/PEG (5:1), ○: Tablet E: PEO-2M/PEG (1:1), Δ: Tablet F: PEO-2M/PEG (1:5).

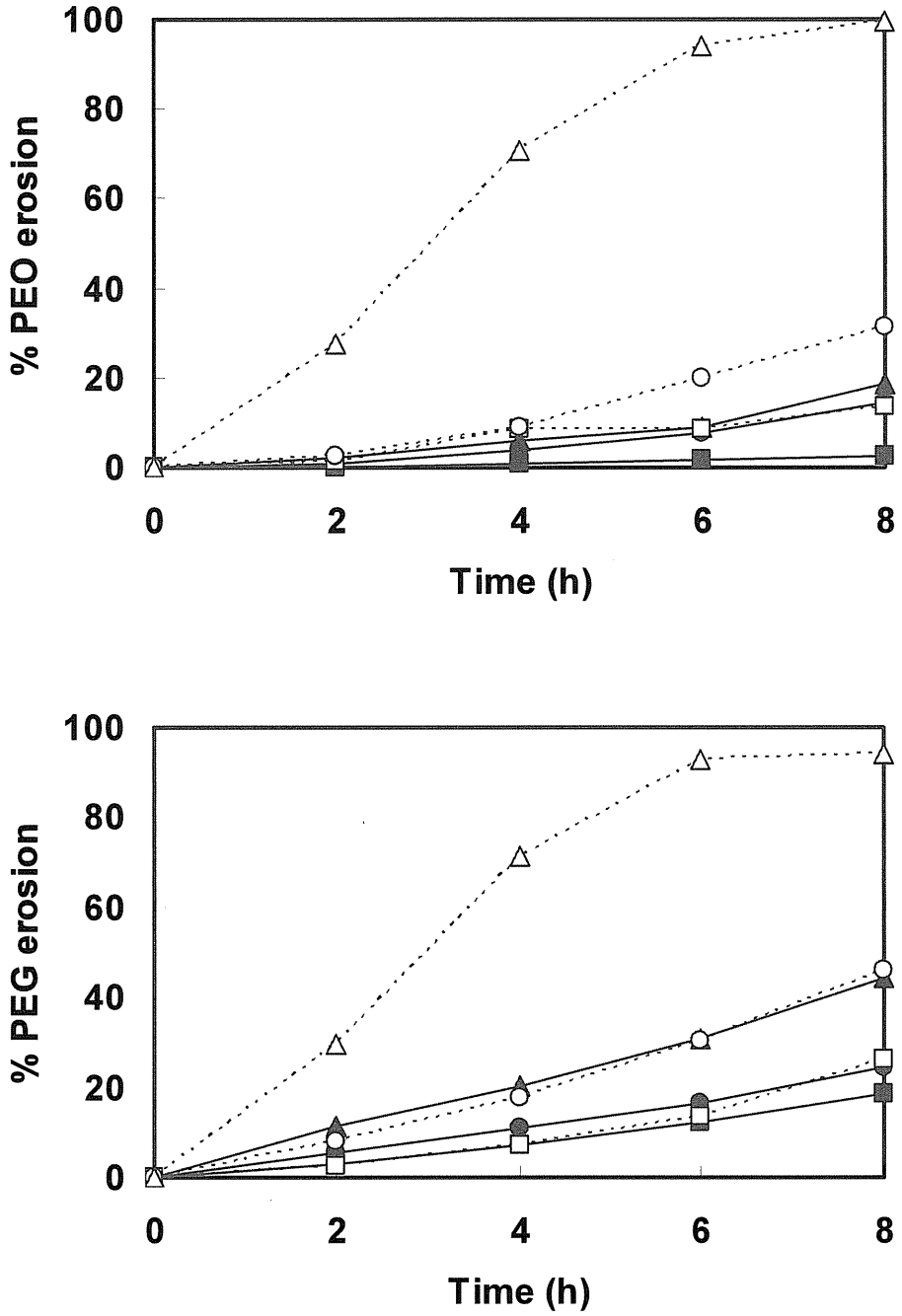

Figure 7. Erosion profile of hydrogel matrices. (a): PEO, (b): PEG. ■: Tablet A: PEO-7M/PEG (5:1), ●: Tablet B: PEO-7M/PEG (1:1), ▲: Tablet C: PEO-7M/PEG (1:5), □: Tablet D: PEO-2M/PEG (5:1), ○: Tablet E: PEO-2M/PEG (1:1), Δ: Tablet F: PEO-2M/PEG (1:5).

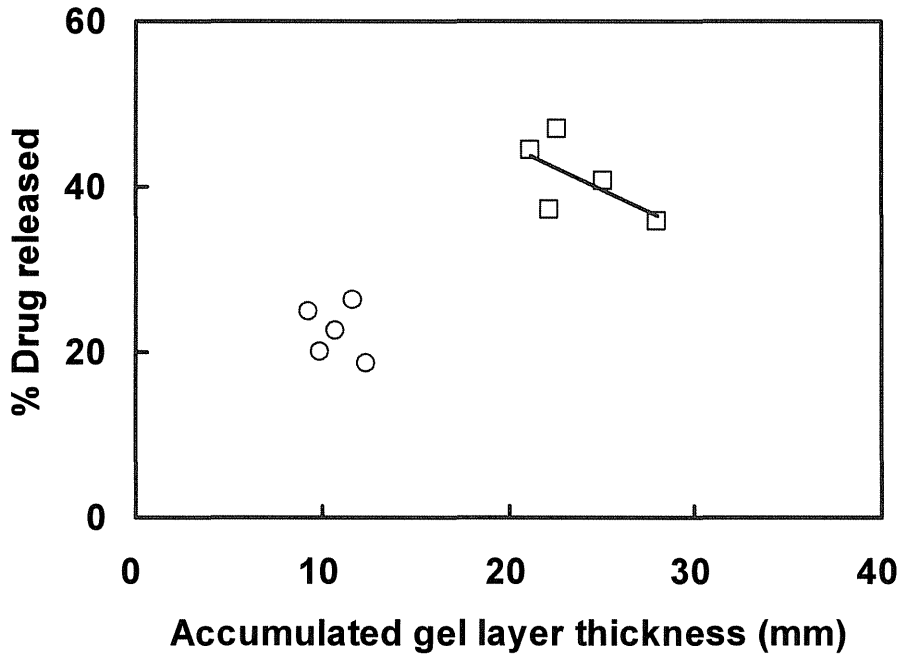

Figure 8. Diagram describing the correlation between changes in accumulated hydrogel layer thickness measured by MRI every 30 min. and the amount of AAP released. ○: after 2 hours, □: after 4 hours.

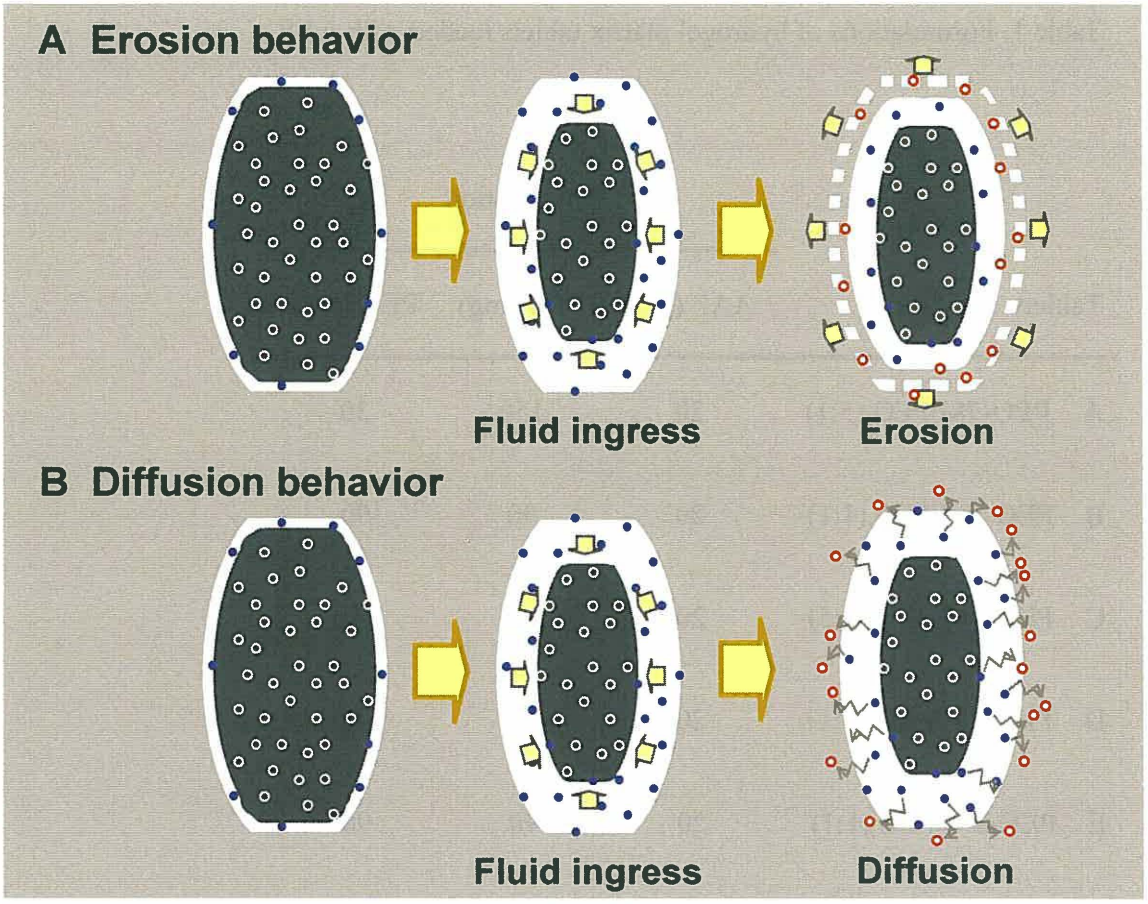

Figure 9. Schematic illustration of drug-release mechanism in PEO hydrogel matrix tablets. A: erosion behavior, and B: diffusion behavior.

Table 1. Formulations of hydrogel matrix tablets loaded with AAP.

Tablets	Formulation		
	AAP (mg)	PEO (mg)	PEG (mg)
A PEO-7M/PEG (5:1)	20	150	30
B PEO-7M/PEG (1:1)	20	90	90
C PEO-7M/PEG (1:5)	20	30	150
D PEO-2M/PEG (5:1)	20	150	30
E PEO-2M/PEG (1:1)	20	90	90
F PEO-2M/PEG (1:5)	20	30	150

Conclusion

In this investigation into the processes of hydrogelation of PMAA and PEO films using time-resolved *in situ* IR spectroscopy, new insights into the hydrogelation behaviors of their solids have been provided. Further, the calculated wavenumbers and interaction energies obtained by QCC using short chain models instead of actual polymers supported my estimation of the spectra-structure correlation of the hydrated PMAA and PEO. IR spectroscopy with a flow-cell is well suited to investigating hydration mechanisms of hydrophilic polymers. It seems reasonable conclude that water molecules in hydrogel play important roles to keep their hydrogel states. Conducting such a study as performed here may eventually allow me to understand the physical properties of pharmaceutical drug delivery products in water.

Further, the flow-through cell equipped with MRI and SEC are well suited to investigate the release mechanisms of hydrogel forming matrix tablets using hydrophilic polymers. With further development, this sort of combination study may aid in better understanding of the release mechanisms of pharmaceutical drug delivery system products.

Acknowledgements

During the course of the study, I have received a number of fruitful discussion, enlightening comments, and hearty encouragement from many people. First of all, I wish to express my sincere gratitude to Professor Yukihiro Ozaki (Kwansei Gakuin University) for his continuous instruction, discussion, and encouragements in carrying out this study. I am deeply indebted to Professor Shigeki Morita (Nagoya University) for precious advises, valuable discussion, and cordial encouragements.

I also give special thanks to Dr. Satoshi Kitamura (Astellas Pharma Tech Co., Ltd.) for his valuable advises and discussion. I owe my gratitude to Dr. Harumi Sato (Kwansei Gakuin University) for precious advices and useful discussion.

I express many thanks to all the members in Prof. Ozaki's laboratory of Kwansei-Gakuin University for their helpful discussion and technical supports. I am very much grateful to Mr. Hideaki Miyanishi and Ms. Mutsumi Ueshima (Astellas Pharma Inc.) for technical supports and warm encouragement during my work.

I am deeply grateful to Senior Manager Shigeaki Yamanashi of Astellas Pharma Inc., for having given me the chance that I do this Ph.D. study. Finally, I give whole heated thank to my parents for their encouragement.

List of Publications

Original Papers:

(1) Tomokazu Tajiri, Shigeaki Morita, Yukihiro Ozaki "Hydration Mechanism on a Poly(methacrylic acid) Film Studied by In Situ Attenuated Total Reflection Infrared Spectroscopy" *Polymer*, 2009, 50, 5765-5770.

(2) Tomokazu Tajiri, Shigeaki Morita, Ryosaku Sakamoto, Masazumi Suzuki, Shigeaki Yamanashi, Yukihiro Ozaki, Satoshi Kitamura "Release mechanisms of Acetaminophen from polyethylene oxide/polyethylene glycol matrix tablets utilizing magnetic resonance imaging" *Int. J. Pharm.*, 2010, 395, 147-153.

(3) Tomokazu Tajiri, Shigeaki Morita, Yukihiro Ozaki, "Time-resolved conformational analysis of poly(ethylene oxide) during the hydrogelling process" *Polymer*, *In press.*

(4) Tomokazu Tajiri, Shigeaki Morita, Ryosaku Sakamoto, Shigeaki Yamanashi, Yukihiro Ozaki, Satoshi Kitamura "Design of *in vitro* dissolution method for extended drug-release matrix containing poorly water-soluble indomethacin utilizing flow-through cell apparatus under perfect sink conditions" *Int. J. Pharm.*, *In preparation.*

Presentation

Invited Presentations:

(1) 田尻智計, PharmaSense を用いたゲルマトリックス製剤の溶出メカニズ

ムに関する研究，MRI セミナー，2009 年 10 月 30 日（東邦大学）

(2) Tomokazu Tajiri, "What are the desired PAT for QbD?", Setting Specifications, November 23-24, 2010, Amsterdam, the Netherlands.

(3) Tomokazu Tajiri, "Desirable sink condition for ext*ended release* m*atrix containing* poorly water-soluble indomethacin on flow-through cell dissolution", May 31, 2011, SOTAX dissolution conference, Tokyo, Japan.

Oral Presentations:

(1) 田尻智計，森田成昭，尾崎幸洋

『振動分光法を用いた医薬品製剤の物性研究 [1] Poly(Methacrylic acid –*co*– Ethylacrylate) film の含水過程時間分解赤外観察』日本分析化学会・第 56 年会，2007 年 9 月 19 日～21 日（徳島大学）

(2) 田尻智計，森田成昭，尾崎幸洋

『振動分光法を用いた医薬品製剤の物性研究 [2] Poly(Methacrylic acid –*co*– Methyl methacrylate) film の含水過程時間分解赤外観察』日本分析化学討論会，2008 年 5 月 15 日，16 日（名古屋国際会議場）

(3) 田尻智計，森田成昭，尾崎幸洋

『振動分光法を用いた医薬品製剤の物性研究 [3] 固体分散体製剤中の難水溶性薬物の存在状態赤外観察』日本分析化学会・第 57 年会，2008 年 9

月 10 日～12 日（福岡大学）

(4) 田尻智計，坂本良作，鈴木正純，山梨繁行，北村智

『フロースルーセル法－MRI を用いた徐放性ゲルマトリックス製剤の溶出メカニズム評価』日本薬剤学会・第 24 年会，2009 年 5 月 21 日～23 日（静岡コンベンションアーツセンター）

(5) 田尻智計，森田成昭，尾崎幸洋

『振動分光法を用いた医薬品製剤の物性研究 [4] Polyethylene oxide を用いたゲルマトリックス製剤のハイドロゲル化過程時間分解赤外観察』日本分析化学会・第 58 年会，2009 年 9 月 24 日～26 日（北海道大学）

Poster Presentations:

(1) Tomokazu Tajiri, Shigeaki Morita, Yukihiro Ozaki "Hydration Behavior of a Poly(methacrylic acid) Film Studied by ATR-IR Spectroscopy" The fifth International Conference on Advanced Vibrational Spectroscopy (ICAVS-5), June 12-17, 2009, Melbourne, Australia.

(2) 田尻智計，坂本良作，山梨繁行，北村智

『腸溶性製剤の最適な *in vitro* 溶出試験法の検討』日本薬学会・第 132 年会，2012 年 3 月 28 日～31 日（北海道大学），発表予定